

A REGIONAL MODEL FOR THE PREDICTION OF IONOSPHERIC DELAY FOR SINGLE FREQUENCY USERS OF THE GLOBAL POSITIONING SYSTEM

I. R. WEBSTER

April 1993



**TECHNICAL REPORT
NO. 166**

PREFACE

In order to make our extensive series of technical reports more readily available, we have scanned the old master copies and produced electronic versions in Portable Document Format. The quality of the images varies depending on the quality of the originals. The images have not been converted to searchable text.

**A REGIONAL MODEL FOR THE
PREDICTION OF IONOSPHERIC DELAY
FOR SINGLE FREQUENCY USERS OF THE
GLOBAL POSITIONING SYSTEM**

Iain Robert Webster

Department of Geodesy and Geomatics Engineering
University of New Brunswick
P.O. Box 4400
Fredericton, N.B.
Canada
E3B 5A3

April 1993
Latest Reprinting March 1996

© Iain Robert Webster, 1993

PREFACE

This technical report is a reproduction of a thesis submitted in partial fulfillment of the requirements for the degree of Master of Science in Engineering in the Department of Surveying Engineering, February 1993. The research was supervised by Dr. Alfred Kleusberg, and funding was provided partially by the Natural Sciences and Engineering Research Council of Canada. Energy, Mines and Resources Canada provided the data.

As with any copyrighted material, permission to reprint or quote extensively from this report must be received from the author. The citation to this work should appear as follows:

Webster, I.R. (1993). *A Regional Model for the Prediction of Ionospheric Delay for Single Frequency Users of the Global Positioning System*. M.Sc.E. thesis, Department of Surveying Engineering Technical Report No. 166, University of New Brunswick, Fredericton, New Brunswick, Canada, 124 pp.

Abstract

One of the major limitations to the accuracy attainable using single frequency Global Positioning System receivers is the propagation delay of the signals as they pass through the ionosphere, especially during times of high solar activity. Errors of several parts per million can be encountered on baselines where only one frequency has been observed. This thesis presents an approach for modelling the ionospheric delay, using phase measurements from dual frequency receivers to estimate corrections for single frequency users operating within the same region. A surface is used to approximate the spatial distribution of the delay, and temporal changes are also taken into account by the estimation of a new surface at every epoch.

To test the validity of the model, data were obtained from an experiment conducted near Ottawa, Canada, in October of 1990 by the Canada Centre for Remote Sensing and the Canada Centre for Surveying. Three dual frequency receivers on the ground are used to estimate ionospheric delay variations and to correct the observations from an airborne single frequency receiver moving in the vicinity of the other three receivers. It is shown that after the model has been applied, differences between three separate solutions for the position of the aircraft, computed with respect to different monitor stations, are at a level of one part per million (ppm). Before correction these differences were at two to three ppm, with periods of up to 50 ppm. It is felt that the model, although fairly simple in design, is effective in reducing the ionospheric bias sufficiently well for a broad range of applications, including remote sensing, for which the test data was obtained.

Table of Contents

	Page
Abstract	ii
Table of Contents	iii
List of Figures	vi
List of Tables	vii
List of Acronyms and Symbols	viii
Acknowledgements	ix
Chapter 1 Introduction	1
1.1 Objective of the Thesis	1
1.2 Motivation for the Research	1
1.3 Previous Investigations and Contribution of the Thesis.....	2
1.4 Investigative Approach.....	5
1.5 Outline of the Thesis.....	6
Chapter 2 The Global Positioning System.....	8
2.1 Introduction.....	8
2.2 System Description	9
2.2.1 Control Segment	9
2.2.2 Space Segment	10
2.2.3 User Segment.....	10
2.3 Signal Structure	10
2.4 Observables.....	12
2.4.1 Pseudoranges.....	12
2.4.2 Carrier Beat Phase Observations	13
2.4.3 Instantaneous Doppler Measurements	14
2.5 Biases and Errors	15
2.5.1 Orbital Biases.....	15
2.5.2 Clock Errors	16
2.5.3 Ionospheric Refraction	16
2.5.4 Tropospheric Refraction.....	17
2.5.5 Multipath	17
2.5.6 Carrier Cycle Ambiguity and Cycle Slips	18
2.5.7 Station Coordinates	18
2.5.8 Measurement Noise.....	18
2.5.9 Selective Availability.....	19
2.6 Linear Combinations of Observations.....	19
Chapter 3 The Ionosphere and GPS.....	22
3.1 Introduction.....	22
3.2 Formation of the Ionosphere	23
3.3 Causes of Electron Density Variation.....	25
3.3.1 Temporal Variations	26

3.3.2	Influence of Variations in Solar Radiation	28
3.3.3	Effects of Latitude and the Earth's Magnetic Field	30
3.4	Further Anomalous Conditions	31
3.4.1	Sporadic E	31
3.4.2	The Equatorial Ionosphere	31
3.4.3	The Polar and Auroral Ionosphere	32
3.4.4	Travelling Ionospheric Disturbances.....	34
3.4.5	Scintillations	34
3.5	Some Concluding Comments on the Ionosphere	35
3.6	The Refraction of GPS Signals in the Ionosphere	35
Chapter 4 Kinematic Positioning Software.....		42
4.1	Introduction.....	42
4.2	Corrections to Data	43
4.3	Linearization of the Observation Equations.....	43
4.4	Positioning Algorithm.....	45
4.4.1	Computation of Approximate Values and Pseudo-observations	46
4.4.2	A Priori Precisions of Observations	47
4.4.3	Solution for Parameters	47
4.4.4	Introduction of Constraints	50
Chapter 5 Model Description		51
5.1	Outline of the Model.....	51
5.2	Details of Model Formulation	53
5.2.1	Determination of Intersection Points.....	53
5.2.2	Mapping Ionospheric Delays to the Vertical	54
5.2.3	Bivariate Polynomials and the Determination of Coefficients.....	56
5.3	Shortcomings of Previous Investigations for Kinematic Positioning.....	58
5.3.1	The Need for Epoch by Epoch Delay Information	59
5.3.2	Rapid Changes in Delay.....	59
5.4	Improvements from this Research	60
5.4.1	Time Dependent	60
5.4.2	Satellite Specific	60
5.5	Procedural Details for Implementing the Model.....	61
5.5.1	Cleaning Static Data.....	61
5.5.2	Computation and Smoothing of Ionospheric Phase Delays.....	61
5.5.3	Setting Average Inter-station Offset to Zero.....	64
5.5.4	Computation of Surface Coefficients.....	65
5.5.5	Interpolating the Delay for the Single Frequency Receiver.....	66
5.5.6	Applying Corrections to the Data.....	67
5.6	Assumptions Made in the Model.....	67
5.6.1	Straight Signal Path.....	67
5.6.2	Infinitesimally Thin Ionosphere	68
5.6.3	Mapping Delays to the Vertical	69
5.6.4	Average Inter-station Offset is Zero	69
5.7	Redundancy and the Numerical Stability of the Surface Determination	70
Chapter 6 Test Data and Results.....		71
6.1	Test Data.....	71
6.2	Problems with the Data.....	74
6.2.1	Data Volume	74

6.2.2	Data Quality.....	75
6.2.3	Incorrect Ephemeris Data.....	76
6.3	Data Pre-processing.....	77
6.4	Static Baseline Computation.....	78
6.5	Computation of the Aircraft Trajectory and Model Validation.....	79
6.5.1	Difference Between the MA/FA and ME/FA Solutions.....	80
6.5.2	Difference Between the MA/FA and AL/FA Solutions	85
6.5.3	General Remarks.....	89
Chapter 7 Summary, Conclusions and Recommendations.....		91
7.1	Summary of the Research.....	91
7.2	Conclusions	92
7.3	Recommendations for Related Future Research.....	94
References		97
Appendix I	Plots of Ionospheric Phase Delays	102
Appendix II	Plots of Between-station Differences of Phase Ionospheric Delays ..	115
Appendix III	Plots of the Tracks of Sub-ionospheric Points for Each Satellite	119
Appendix IV	Polar Plot of Satellite Visibility	123

List of Figures

		Page
Figure 3.1	Formation of a layer of maximum electron density.....	24
Figure 3.2	Variation of electron density with height for a typical mid-latitude location during summer daytime.....	25
Figure 3.3	Total Electron Content for three consecutive days over Hawaii, 1986	27
Figure 3.4	Major regions of the ionosphere.....	33
Figure 3.5	Dispersion curve and phase velocity	37
Figure 5.1	Intersection points on the ionospheric layer	52
Figure 5.2	A surface describing the vertical delay fitted to the intersection points.	52
Figure 5.3	The zenith distance, z , at the intersection point	55
Figure 5.4	Comparison of the inverse of the obliquity factor, Q , at elevation angles from 0 to 90 degrees, and the cosine of the zenith distance at the corresponding ionospheric point for a shell at a height of 350 km. ...	56
Figure 5.5	Data flow for the interpolation of delays.....	62
Figure 5.6	Example of raw and smoothed ionospheric phase delays for SV12 at Mallorytown	63
Figure 5.7	Example of raw and smoothed ionospheric phase delays for SV13 at Mallorytown	64
Figure 5.8	The effect on the interpolated values of the delay offset between stations.....	65
Figure 6.1	Location of the survey area.....	71
Figure 6.2	Location of the GPS antenna on the aircraft.....	73
Figure 6.3	Observation sessions at all receivers	73
Figure 6.4	Trajectory of the aircraft and the locations of the monitor stations	74
Figure 6.5	Indication of signal to noise ratio of phase observations for SV 13 at station Metcalfe	76
Figure 6.6	Example of the correlation between the residuals and the ionospheric delay	79
Figure 6.7	Latitude differences between MA/FA and ME/FA solutions	82
Figure 6.8	Longitude differences between MA/FA and ME/FA solutions.....	83
Figure 6.9	Height differences between MA/FA and ME/FA solutions.....	84
Figure 6.10	Latitude differences between MA/FA and AL/FA solutions.....	86
Figure 6.11	Longitude differences between MA/FA and AL/FA solutions	87
Figure 6.12	Height differences between MA/FA and AL/FA solutions	88

List of Tables

	Page
Table 5.1	Characteristics of different surfaces 57
Table 6.1	Coordinates of Monitor Stations..... 72
Table 6.2	Statistics before and after using the model 81
Table 6.3	Statistics before and after using the model 85

List of Acronyms and Symbols

AS	Anti-Spoofing
MCS	Master Control Station
PPS	Precise Positioning Service
PRN	Pseudorandom Noise
SA	Selective Availability
SNR	Signal to Noise Ratio
SPS	Standard Positioning Service
SV	Space Vehicle
TEC	Total Electron Content
TID	Travelling Ionospheric Disturbance
WVR	Water Vapour Radiometer
p	Pseudorange observation
ϕ	Carrier phase observation (cycles)
Φ	Carrier phase observation (metres)
D	Instantaneous range rate measurement
ρ	Satellite-receiver range
dp	Orbital bias
dt	Satellite clock error
dT	Receiver clock error
d_{ion}	Ionospheric propagation delay
d_{trop}	Tropospheric propagation delay
η_p	Pseudorange multipath error
η_ϕ	Carrier phase multipath error
λ	Carrier signal wavelength
N_1	L1 ambiguity
N_2	L2 ambiguity
N	Electron density
N_m	Maximum electron density
$N_m E_s$	Maximum electron density of Sporadic E layer
$N_m F_2$	Maximum electron density of F2 layer
$f_0 F_2$	Critical frequency of F2 layer
n_p	Phase refractive index
n_g	Group refractive index

Acknowledgements

I would like to express my sincere appreciation for the assistance and support given by my supervisor, Professor Alfred Kleusberg. His guidance has been vital both in the research and writing of this thesis, and in the rest of my graduate studies. He has a natural ability to express complex ideas in easily comprehensible terms. I would also like to thank Dr. Yola Georgiadou. Her experience with the test data proved to be very valuable and undoubtedly saved much time in the initial stages of this research. My thanks also go to Professor Richard Langley, who also provided assistance in this project and my studies in general.

This research was made possible by financial support from the Natural Sciences and Engineering Research Council (NSERC) through operating grants. The data used in this thesis was provided by the Geodetic Survey Division of the Department of Energy, Mines and Resources in Ottawa.

Lastly, and certainly by no means least, are the thanks due to the other graduate students in the department who helped me in my studies and above all were there to keep my spirits up when things weren't looking so great. This task would have been immeasurably harder without their encouragement and support.

Chapter 1

Introduction

1.1 Objective of the Thesis

The object of this research was the development of a model which can be used to accurately predict the spatial variation in range errors caused by ionospheric refraction of signals from satellites of the Navstar Global Positioning System (GPS). In terms of applicability, it is intended that the model be used for differential positioning in a post-processing mode. There is no requirement for the remote receiver to be stationary. The estimates of the errors derived from the model can in turn be applied to carrier phase measurements to obtain more accurate estimates of the desired parameters, e.g., the position of the remote antenna.

It is shown that, by and large, this objective has been met. The resulting model can improve the agreement between two solutions for the position of the remote station, computed with respect to different monitor stations, by an order of magnitude.

1.2 Motivation for the Research

Even though it is still in the development stage, already many observation and processing campaigns have shown that GPS has the potential to revolutionize the way survey measurements are taken in the field, and the accuracies achievable of the parameters obtained from them. When the full constellation of 24 satellites becomes a reality later

this decade (21 space vehicles plus three active spares), users will have the benefits of a 24-hour, world-wide, all-weather, unified positioning system capable of producing relative positioning accuracies of the order of one part per million (ppm) and better (e.g., Wells et al. [1987]; Kleusberg et al. [1988]; Jones [1989]; Bagley and Lamons [1992]).

However, measurements of GPS signals are contaminated with a number of errors, both systematic and random, including ephemeris errors, satellite and receiver clock errors, propagation errors and random observation errors. Propagation errors are the effects of atmospheric refraction on GPS signals as they pass through the ionosphere and troposphere. Ionospheric propagation delay is a major source of concern to GPS users since it can reach extremal values of around 50 metres for satellites directly overhead at times of high solar activity, and up to three times this amount for satellites near the horizon [Wells et al., 1987]; indeed, Feess and Stephens [1986] state that this particular bias represents the largest range error for users that do not have access to some method of compensating for the delay. It is envisaged that the type of receiver used by the majority of civilian users will be of the less expensive, single frequency kind, which, as will be explained later, does not provide enough information to allow elimination of the delay. The consequence of this is a degraded estimation of the parameters, be they position, velocity, time, or some other quantity. For precise positioning applications some method of eliminating or reducing the effects of the ionospheric range errors is clearly highly desirable; this thesis proposes one method of accomplishing this objective.

1.3 Previous Investigations and Contribution of the Thesis

There are many methods presently available directed towards the elimination of ionospheric delay, ranging greatly in complexity, sophistication, cost and performance. They can basically be classified into two groups; those which use combinations of GPS measurements, and those which attempt to model the delay prior to subtracting it from observations. The method proposed here falls into the latter category, and is suitable for

use on a regional basis, as opposed to those models which attempt to globally predict ionospheric delay, or equivalently, total electron content/electron density profiles (Newby [1992] reviews three of these global models and compares them to the GPS broadcast model).

As will be explained in Chapter Three, due to the large number of variables which affect ionization of the earth's atmosphere it is impossible to give precise figures for the dimensions of the area for which this regional model would be useful; in other words, it is extremely difficult to give a definition of "regional" that will be correct in all locations and at all times. The situation is further complicated by the fact that the sophistication, and hence accuracy, of the model can be increased by the number of monitor stations used to drive it. Basically, the variation in the delay over the area enclosed by the monitor stations is approximated by a surface, the simplest case of which is a plane. Therefore, instead of giving definitive figures followed by a string of caveats, a more elegant (and, it is hoped, not too evasive) approach would be to say that the model is useful for areas over which the variation in ionospheric delay can be approximated closely enough by the surface used for the purposes of any particular user. It is hoped that after reading this thesis, particularly Chapter Three, the reader will have a better appreciation for the size of the area over which the model will prove useful for any particular application.

The test data used in this research were collected by three monitor stations forming a triangle that was roughly isosceles in shape, with longer sides of approximately 220 km and a short side of 90 km. However, it should be borne in mind that this area is in the relatively "quiet" mid-latitude region, albeit at a time of high solar activity, and that in regions where the variation of the delay over time and space is greater, e.g., the equator, the model should be used advisedly as results may well prove to be less encouraging.

The prediction model presented in this thesis is an extension of a method first proposed by Georgiadou and Kleusberg [1988a]. This research will be dealt with in greater detail in Chapter Five, but essentially the authors used the measurements from a dual frequency receiver located in the centre of a static network to estimate ionospheric delays for all the other receivers in the vicinity; these were actually dual frequency receivers so it was possible to compute the corrected L1 solutions with the L3 ionosphere-free solutions, which were used to represent the "truth". A bivariate polynomial was used to approximate the spatial variation in ionospheric delay over the area. This concept was extended to include any number of dual frequency receivers and to estimate the stochastic variation of the ionosphere [Wild et al., 1989] and further developed to use the stochastic information in a collocation process to improve the above deterministic model [Wild et al., 1990].

For each of the investigations, one polynomial was used for the entire observation session, with the consequence that the deterministic part of the model was incapable of changing over time and was therefore unable to cope with temporal changes in ionospheric delay. Additionally, the use of only one surface meant that there was little flexibility available to reflect the differing delays encountered by signals from different satellites. However, since all three of the above investigations used static data, it was the effect of the delays over the whole session that were of interest, and the limitations outlined above were of little concern.

In the case of kinematic positioning, however, we have to consider a new approach, due to factors which will be outlined in Chapter Five. In the meantime it is sufficient to outline the major changes implemented to the concept introduced above. Briefly, these improvements are:

- The model is time-dependent. A new set of model parameters is created for every epoch. This also means that an updated value for the differential delay is computed every epoch.
- For each epoch, a separate set of model parameters is computed for each satellite, i.e., the model could be termed satellite specific. This also means that if a change in the visible scenario occurs, e.g., a satellite disappears below the horizon, the interpolated delays for the remaining satellites will not be affected.

1.4 Investigative Approach

Once a concept for the model had been decided upon, software was written to implement it. In order to test the validity of the model, data were obtained from the Geodetic Survey Division of the Department of Energy, Mines and Resources, in Ottawa. These consisted of dual frequency data for three ground-based stations and single frequency data for an aircraft moving in and near the triangle defined by the monitor stations. Using the data from the ground stations to drive the model, estimates for the delays for the signals received by the aircraft were computed and applied as corrections to the data.

Unfortunately, there was no reference system available with which to compare the aircraft positions after applying the model. It was therefore impossible to obtain a direct evaluation of its performance. Instead, the location of the aircraft was calculated with respect to each of the monitor stations in turn, giving three solutions, both before and after applying the model. These solutions were then differenced to see the degree of agreement between them. The criterion for the model to have succeeded in improving the solutions was to have them in significantly better agreement after having applied it.

1.5 Outline of the Thesis

Chapter Two gives an outline of the Global Positioning System, including a description of the three constituent parts, namely, the control segment, the space segment, and the user segment. The signals transmitted by the satellites are also described, as are the various types of observables. An overview of the sources of systematic error and their effects on the signals and derived parameters follows, while the chapter is completed by a description of linear combinations of observables.

Chapter Three describes the ionosphere, including the causes of ionization, and the temporal and spatial variations associated with it. The effects of this medium on the signals from GPS satellites are also discussed in some detail. It is also shown how GPS measurements can be used to estimate the delays, and how these can affect the estimation of positional information.

Chapter Four is concerned with the positioning software used in this research, HIPPOS. It is felt that a brief description of the package is necessary since ultimately it is positions that will be compared in the analysis. The algorithm is described, including the observation and adjustment models, and the assumptions made.

Chapter Five goes into the details of the model developed to predict ionospheric delay, including the factors that have to be considered for it to be applicable to both static and kinematic positioning, the features of the model, and outlines the assumptions that have to be made for the model to work successfully.

Chapter Six gives a description of the test data which were used to validate the model. A summary of the problems found with the data, not the least of which was the sheer volume of it, is given. The implementation of the model is given in a step-by-step manner. This chapter also discusses and analyses the results before and after the application of the model.

Finally, the research is summarized and some conclusions from the results are drawn in Chapter Seven. Several recommendations are also made for further research to improve the model and therefore, it is hoped at least, to improve the results.

Chapter 2

The Global Positioning System

2.1 Introduction

The purpose of this chapter is to give an outline of the Global Positioning System, dealing with some aspects briefly, while more attention is given to those areas of more relevance to the subject of this thesis. It is therefore stressed that this is not intended as a detailed reference on the GPS; those readers requiring such a work are directed to examples such as Leick [1990], Ackroyd and Lorimer [1990] and Wells et al. [1987].

The Navstar Global Positioning System (GPS) is a satellite-based positioning and navigation system which is still in the developmental stage, but which is expected to be fully operational, with a constellation of 21 satellites and 3 active spares, by the middle of this decade. The United States Department of Defense (DoD) has the ultimate responsibility for implementing and maintaining the system and while many civilian individuals and organizations have and will use this system, the quality of data available to these users will be intentionally degraded; obviously this will affect the derived parameters. The current policy of the DoD is to restrict access by non-DoD approved users to the Standard Positioning Service (SPS). The Precise Positioning Service (PPS) will be available to authorized users [Langley, 1992a].

GPS development was instigated in 1973, in order to provide a space-based system that would allow passive navigation using signals received from satellites. The satellites are being launched in three successive groups, or blocks, the first of which consisted of prototypes for testing and evaluation. The final constellation will have the satellites in six orbital planes, each inclined at 55° to the equator. They will be in nominally circular orbits, at an altitude of approximately 20,200 km, giving an orbital period of 12 sidereal hours. When fully operational, it is planned that at least four satellites will be visible at all locations on the earth's surface at any time; the consequence of this will be the ability to obtain three-dimensional positioning information in all types of weather, 24-hours a day, worldwide, using a unified coordinate system.

2.2 System Description

The system can be conveniently divided into three units: the space segment, the control segment, and the user segment. A brief description of each will be given in the following sections.

2.2.1 Control Segment

Five ground-based stations comprise the tracking and control segment of the system. These are located at nearly even intervals around the globe, and with the exception of the Master Control Station (MCS) at Colorado Springs, are within 20° of the equator. Such a distribution allows continuous tracking of all satellites by one or more stations. The coordinates of each are very accurately known and dual frequency receivers connected to cesium clocks are used to track the signals from the satellites; these are then sent to the MCS where they are used to calculate and predict orbits and satellite clock errors. The MCS, along with several other tracking stations, can also transmit commands for satellite movement and upload new ephemerides and clock correction information.

2.2.2 Space Segment

This segment is composed of the satellites in orbit and is therefore presently incomplete; orbital details have already been given in section 2.1. The SVs essentially act as beacons sending signals in a one-way ranging mode with which users can calculate their position/velocity etc. In order to do this the satellites must perform several basic functions; on board processing of data; maintenance of very accurate time; transmission of information; and manoeuvre on demand from the ground control stations [Wells et al., 1987].

2.2.3 User Segment

This is the ultimate segment in the chain of system components. It is a receiver consisting of an antenna, signal tracking circuitry, user interface, power supply, and a microprocessor to control the operation of the receiver and to compute satellite and user coordinates on the WGS 84 geodetic datum [Langley, 1991]. There are many receivers now commercially available ranging from cheap (<\$1,000), low-accuracy sets to expensive (>\$50,000) dual frequency devices with internal data-logging and communications ports for a variety of applications. The former are often single channel devices (capable of tracking one satellite at a time) although the use of software channels, i.e., multiplexing, allows the receiver to track four or more SVs. The latter are commonly multi-channel devices with a dedicated channel for tracking each satellite in view.

2.3 Signal Structure

Each satellite carries four atomic clocks set to a **fundamental frequency**, f_0 , of 10.23 MHz (in reality they are offset slightly to account for special and general relativistic effects) [Ackroyd and Lorimer, 1990]. It is from one of these oscillators, chosen by the MCS, that all signals transmitted by the satellite are derived. Two coherent microwave radio signals are created, termed **L1**, at a frequency of 1.57542 GHz ($154f_0$),

and L2, at 1.2276 GHz ($120f_0$); these are the **carrier signals** and are simple sinusoidal waves. The L1 signal is modulated by two pseudorandom noise (**PRN**) codes (the P and C/A-codes), and a message segment which includes the ephemeris data for the SV transmitting the signal, system time, SV clock behaviour data, status messages, and C/A to P-code handover information [ARINC, 1991]. Almanac data are also included which allow approximate satellite positions to be calculated, enabling the receiver to search only for those satellites in view. The L2 signal is modulated with the P-code and the message. Each of the codes consists of a binary series which, although appearing random, is actually deterministic in nature and repeats after a specific time period — hence the term pseudorandom.

The **C/A-code** (Coarse/Acquisition) code is 1,023 binary digits (chips) long, which repeats every millisecond and therefore gives a wavelength of around 300 m [Langley, 1990]. The **P-code** has a wavelength of only 30 m, with the chip rate being 10.23 million per second, or 10 times higher than the C/A-code. A technique known as binary biphasic modulation is used to superimpose the codes onto the carrier signals. Essentially, the phase of the carrier is modulated, or changed, by 180° whenever the binary sequence of a particular code changes from 0 to 1 or vice versa; the same effect is achieved by multiplying the carrier phase by -1 when the code state changes. Since only the P-code is modulated onto the L2 carrier, the process is simple. However, the L1 carrier has both the P-code and C/A-code superimposed, and phase quadrature is employed to avoid complications; this involves creating a second L1 signal, phase shifted by 90° from the original, and modulating it with the C/A-code, while the original is modulated with the P-code. The two are then recombined. In reality the codes are modulo 2 added to the navigation message before being applied to the carrier signals. This message is transmitted at 50 bits per second, and it takes 12.5 minutes for all the information to be sent. Spilker [1980] gives a detailed account of the signal characteristics, while van Dierendonck et al. [1980] deal with the navigation message.

2.4 Observables

As shown in the previous section, two composite signals at differing frequencies are transmitted from the satellite. Some receivers can extract one or both of the codes to provide one type of observable, the pseudorange, while measuring the phase of the pure carrier signal provides another observable. Both have relative merits and drawbacks. A third possibility is measurement of the instantaneous Doppler shift of the carrier signals.

2.4.1 Pseudoranges

If we momentarily assume that there are no errors present, the travel time of the signal can be found by cross-correlating the code on the incoming signal with an exact replica generated within the receiver. Since both versions of the code are referenced to the same time system, the time delay needed to produce maximum correlation is a measure of the travel time. Multiplying this by the speed of light in a vacuum gives a range to the satellite. Unfortunately, the clocks in both the satellite and the receiver are prone to drifting from the GPS time scale, which results in an error in the range — hence the term “pseudorange”. The equation relating the observable to the unknown parameters can be written [Wells et al., 1987]

$$p = \rho + d\rho + c \cdot (dt - dT) + d_{\text{ion}} + d_{\text{trop}} + \eta_p + \epsilon_p, \quad (2.1)$$

where	p	is the pseudorange observation (m);
	ρ	is the geometric satellite–receiver range (m);
	$d\rho$	is the range error due to incorrect ephemeris data (m);
	c	is the speed of light in a vacuum (m/s);
	dt	is the satellite clock offset (s);
	dT	is the receiver clock offset (s);
	d_{ion}	is the ionospheric range error (m);
	d_{trop}	is the tropospheric range error(m);

η_p is the error caused by code signal multipath (m);
 ϵ_p are random measurement errors (m).

The coordinates of the receiver are actually disguised by the geometric range, since

$$\rho = \sqrt{(x_S - x_R)^2 + (y_S - y_R)^2 + (z_S - z_R)^2}, \quad (2.2)$$

where x_R, y_R, z_R are the coordinates of the receiver;
 x_S, y_S, z_S are the coordinates of the satellite.

Since the receiver antenna intercepts signals from all visible satellites, it is necessary to differentiate between them; this is accomplished by using unique codes for each satellite that are nearly orthogonal, i.e., cross-correlation between codes from different satellites is low, although not zero.

With analogue receivers, measurements can be made to approximately 0.01 of the wavelength of the signal [Wells et al., 1987] so that the noise on C/A-code measurements is 3 m, while that on the P-code is 30 cm. More recently, with the development of digital receivers, noise levels of as low as 1.5 cm (using 120 s averaging) for the P-code on L1 have been reported [Meehan et al., 1992]. Essentially, this observable gives an absolute but relatively noisy measure of the range.

2.4.2 Carrier Beat Phase Observations

This type of observation is obtained by differencing the signal generated by the receiver oscillator, and the incoming Doppler-shifted carrier signal from the satellite. The equation relating it to the unknowns can be written

$$-\lambda\phi = \rho + d\rho + c \cdot (dt - dT) - d_{ion} + d_{trop} + \eta_\phi + \lambda N + \epsilon_\phi, \quad (2.3)$$

where λ is the wavelength of the carrier signal (m);

ϕ	is the carrier beat phase measurement (cycles);
N	is the cycle ambiguity (cycles);
η_ϕ	is the error caused by phase signal multipath (m);
ϵ_ϕ	are random measurement errors (m),

and the other symbols are exactly the same as those in equation (2.1).

The carrier beat phase observable is a measure of the number of cycles (integer and fractional parts) that have elapsed since the receiver last locked onto the signal, plus some arbitrary integer number of cycles. Equation (2.3) is directly comparable to that for the pseudorange, except for the **cycle ambiguity** term; this is the (unknown) integer number of cycles between the satellite and receiver at the epoch when the receiver locked onto the signal. The noise on these measurements for analogue receivers is commonly around 2 mm and 3 mm for L1 and L2 respectively; however, digital technology has again improved the situation and figures as low as 0.13 mm and 0.11 mm (10 s averaging) have been claimed [Meehan et al., 1992]. Phase observations are more precise than pseudoranges, but can only be considered relative measures of the range due to the unknown, constant ambiguity term.

2.4.3 Instantaneous Doppler Measurements

Measurement can be made of the instantaneous Doppler shift of the frequency of the incoming carrier signal. This shift is the result of the relative motion of the receiver and satellite and is a measure of the range rate between the two; it is therefore contaminated by the rate of change of the biases and errors over time:

$$D = \frac{d}{dt} \rho + \frac{d}{dt} (d_\rho - d_{\text{ion}} + d_{\text{trop}} + c \cdot (dt - dT) + \eta_\phi) + \epsilon_D, \quad (2.4)$$

where D is the instantaneous range rate (m/s);
 ϵ_ϕ are random measurement errors (m/s),

and the other symbols are as for equation (2.1).

2.5 Biases and Errors

Biases can be defined as those undesirable effects that can be “removed or at least suppressed, by an attempt to model them” [Wells et al., 1987]. Examples are clock offsets, biases in the broadcast ephemeris and station coordinates, atmospheric refraction, and the carrier beat phase ambiguity. In other terminology the same effects are called **systematic errors**. **Errors** are the residual biases that have not been modelled or differenced out, and other effects which are still present in the data, often due to the fact that they vary in a complex or unpredictable fashion in time and/or space. Uncorrected cycle slips, multipath and measurement noise are examples of errors.

2.5.1 Orbital Biases

Orbital biases result from situations where the satellite is not at the exact position dictated by the broadcast ephemeris. At present, orbits derived from the broadcast ephemeris are accurate to about 4–5 parts in 10^7 [Spofford et al., 1992], the uncertainty being a consequence of the inability to completely model the forces acting on a satellite, and degradation due to Selective Availability (see section 2.5.9). If left uncorrected, such errors will be apparent as position errors of similar magnitudes. Differencing observations from one particular satellite between receivers reduces the error, with more effect on shorter baselines; a well known rule-of-thumb giving the error in differential positioning is [Beutler et al., 1984]:

$$db/b = d\rho/\rho, \tag{2.5}$$

where	db	is the error in the baseline;
	b	is the baseline length;
	$d\rho$	is the ephemeris error;

ρ is the satellite–receiver range.

With an ephemeris error of 20 m, the resulting (worst–case) error is 1 ppm which, on a baseline of length 100 km, gives an error of 10 cm. Another option for reducing the error is to relax the orbit and estimate a number of orbital parameters along with the baseline components, although networks extending over large areas are more useful for this approach.

2.5.2 Clock Errors

Clock errors occur in both the satellites and the receivers. The GPS control segment monitors the behaviour of the satellite clocks and models the corrections for drift by a quadratic polynomial, the coefficients of which are uplinked to the satellite, and are in turn broadcast as part of the message. Any residual effects can be eliminated by differencing between receivers which are operating simultaneously. The magnitude of this error can reach 1 ms, depending on when the clock was last reset. Receiver clock errors are generally of larger magnitude than the satellite clock errors, due to the lower quality of the (quartz) oscillators. Differencing, this time between satellites, can again eliminate this clock error. An alternative approach, often used in navigation, is to leave the receiver clock offset as an unknown to be solved in the parameter estimation.

2.5.3 Ionospheric Refraction

Since the reduction of this error is the subject of this thesis, it will be dealt with in some detail in the next chapter. However, it is important to remember that this error can be quite large, reaching values of 50 m for a vertically propagating signal.

2.5.4 Tropospheric Refraction

The troposphere is the lowest part of the atmosphere, extending up to between 9 and 16 kilometres in altitude although the neutral atmosphere can extend up to several tens of kilometres. For frequencies of less than 30 GHz, refraction in this region is not dependent on the frequency of signals passing through it [Langley, 1992b], and typical values for range errors are 1.9–2.5 m for a satellite directly overhead [Leick, 1990]. The total delay can be separated into dry and wet components [Hopfield, 1971]. The dry component, constituting about 90% of the total, is a function of pressure and temperature and is easier to determine than the wet component; this is primarily due to the fact that water vapour distribution is difficult to predict from surface measurements. Hence the correlation over time and space is low.

Various models have been developed to estimate refractivity profiles which may be used to evaluate delays. Also, water vapour radiometers (WVRs) may be used to measure water vapour and liquid water content along lines-of-sight; however, these instruments are quite expensive. Current tactics commonly employed to reduce tropospheric delay are to apply a local vertical refractivity profile model driven by surface measurements or standard meteorological data, and difference observations between stations, relying on the assumption that the troposphere is spatially positively correlated. Reviews of tropospheric refraction are given by Elgered [1992], and Brunner and Welsch [1993].

2.5.5 Multipath

Multipath occurs when signals reach an antenna along more than one path, i.e., besides the direct line-of-sight path, signals reflected from nearby surfaces are also received. Carrier phase measurements are affected less than code measurements [Georgiadou and Kleusberg, 1988b]. This error is dependent on the environment around the antenna, and will repeat on a diurnal basis (minus approximately four minutes each time) due to the

orbital period of the satellites. Suppression of multipath can be achieved by careful site selection, away from reflective surfaces and the use of antennae with gain patterns which will be less likely to pick up reflected signals.

2.5.6 Carrier Cycle Ambiguity and Cycle Slips

Although carrier phase observations are characterized by low noise, they do not provide absolute measurements of the satellite–receiver range; this is because there is an unknown constant to be determined in equation (2.3), namely the carrier cycle ambiguity. Every time the receiver loses lock on the signal, the ambiguity is set to a new arbitrary (integer) value, and a **cycle slip** is said to have occurred. The value remains constant as long as loss of lock is avoided. Many methods have been proposed to detect and correct cycle slips — Lichtenegger and Hoffmann–Wellenhof [1989] provide a good overview. Resolving this ambiguity will provide the most precise observable available, and is the subject of much attention currently.

2.5.7 Station Coordinates

Among other factors, Santerre [1989] investigated the effect of offsets in master station coordinates on baseline components. The result is a slowly changing bias that is dependent on the size and direction of the offset, the baseline length and satellite geometry.

2.5.8 Measurement Noise

Wells and Kleusberg [1989] define measurement noise as “...those errors that remain after all propagation errors, clock errors, and errors related to the physical properties of the antenna have been taken into account.” It has already been shown in sections 2.4.1 and 2.4.2 that measurement type has a significant influence on the noise; it is important to realise that the dynamics acting on the antenna also have an effect. The greater the

accelerations affecting the antenna, the wider the tracking loop bandwidth has to be in order to keep a lock on the incoming signal (due to the greater change in the Doppler shift on the signal). However, this has the drawback of increasing the noise on the received signal. Also of importance is whether the receiver is of the code correlating or codeless type; the use of the latter has consequences which will be discussed in Chapter Six. Finally, the quality and noise suppression of the receiver circuits will play a role; this is one of the reasons why it is claimed that some of the more expensive receivers available have remarkably low levels of noise on zero baseline tests [Meehan et al., 1992].

2.5.9 Selective Availability

The DoD is intentionally degrading the accuracy of positional information to unauthorized users; this policy is Selective Availability (S/A) and is justified by the DoD in the interests of national security. The two possible methods of implementing S/A are by including errors in the broadcast ephemeris, and by dithering the satellite clock. The effect is to restrict accuracies for absolute horizontal coordinates to 100 m (2 d.r.m.s., i.e., twice the r.m.s. of the horizontal error) and for vertical coordinates to 156 m at a 95% confidence level for users of the SPS [Georgiadou and Doucet, 1990]. However, differential positioning has been seen as a method of overcoming S/A without posing a security risk, and is now used by most individuals requiring precise positioning.

2.6 Linear Combinations of Observations

Because of difficulties in accurately modelling satellite orbits, clock errors and propagation delays, it is now very common to use GPS observations in a differential mode. The motive for this is that these biases will be correlated to some extent between observations, and creating differences of the measurements will either totally cancel the biases or lessen their effect, depending on the type of differencing operator used. Three such operators are:

- ∇ between-satellite differencing operator;
- Δ between-receiver differencing operator;
- δ between-epoch differencing operator.

Using any one of these operators will create a **single difference**; obviously, three types of single difference can occur. Between-satellite differences have the advantage that the common receiver clock error is eliminated. Properties of between-receiver differences include cancellation of common satellite clock errors and mitigation of orbit and atmospheric delay errors (assuming the receivers are observing simultaneously). Finally, between-epoch differences cause the ambiguity term to disappear.

Further differencing of these single differences will, logically, create **double differences**. The observations in this investigation are formed into receiver-satellite double differences. The respective equations for pseudorange, carrier beat phase and instantaneous range rate observations are:

$$\nabla\Delta\rho = \nabla\Delta\rho + \nabla\Delta d\rho + \nabla\Delta d_{\text{ion}} + \nabla\Delta d_{\text{trop}} + \nabla\Delta\eta_p + \nabla\Delta\epsilon_p, \quad (2.6)$$

$$\nabla\Delta\Phi = \nabla\Delta\rho + \nabla\Delta d\rho - \nabla\Delta d_{\text{ion}} + \nabla\Delta d_{\text{trop}} + \nabla\Delta\eta_\Phi + \lambda \cdot \nabla\Delta N + \nabla\Delta\epsilon_\Phi, \text{ and} \quad (2.7)$$

$$\nabla\Delta D = \frac{d}{dt} \nabla\Delta\rho + \frac{d}{dt} \nabla\Delta [d\rho - d_{\text{ion}} + d_{\text{trop}} + c \cdot (dt - dT) + \eta_\Phi] + \nabla\Delta\epsilon_D. \quad (2.8)$$

Note that the term $-\lambda\phi$ is now denoted by the symbol Φ , in units of metres. The maximum value for $(d/dt)\nabla\Delta d_{\text{ion}}$ for the dataset used in this research (found from computing the triple differences of ionospheric delay for the static baselines) was found to be approximately 2 mm/s for a 220 km baseline and 1 mm/s for a 90 km baseline. It is to be expected that $(d/dt)\nabla\Delta d_{\text{ion}}$ and $(d/dt)\nabla\Delta d_{\text{trop}}$ will exhibit larger values for longer baselines since spatial correlation will generally decrease with distance. It should be remembered that these data were collected at stations in the ionospherically quieter mid-latitude zone, and that the temporal change of the ionospheric delay may be considerably

greater outside this zone, especially in the auroral and polar regions during ionospheric storms [Langley et al., 1991]. Héroux and Kleusberg [1989] give results for a 20 km baseline in the Canadian arctic at a solar minimum (1986) where double differences of ionospheric delay showed changes of 0.5 mm/s to 1 mm/s. The clock parameters in equation (2.8) will drop out when differenced. The magnitude of the multipath term, $(d/dt)\nabla\Delta\eta_{\Phi}$, will be independent of baseline length except for some of the shortest baselines (some metres in length) where the environment is similar for both antennae. However, due to the slowly changing geometry of the situation, it is expected that values will be well under 1 mm/s. To give an estimate of the total magnitude of these errors, it is useful to consider an example. Langley et al. [1991] show sets of ionosphere-free residuals for a 109 km baseline where the maximum variation rarely exceeds 2 mm/s; some of the residuals exhibited periodic variations which the authors suggested may be due to incorrect broadcast ephemerides. Combining this with the figure for $(d/dt)\nabla\Delta d_{ion}$ above, the total error is certainly less than 1 cm/s and more likely to be under 5 mm/s. Indeed Kleusberg and Georgiadou [1991a] state that the combined magnitudes of these biases are negligibly small since they usually exhibit a slow change over time. Considering this to be the case, equation (2.8) can now be written:

$$\nabla\Delta D = \frac{d}{dt} \nabla\Delta\rho + \nabla\Delta\epsilon_D . \quad (2.9)$$

We now have the final form of the equations relating the three types of observation to the desired parameters. In Chapter Four we will see how the parameters are obtained from the observation equations above.

Chapter 3

The Ionosphere and GPS

3.1 Introduction

Despite the beneficial aspects of the earth's atmosphere, not the least of which is the need for it for life to exist, it is the cause of several problems for geodesists using electromagnetic radiation to measure geophysical parameters. In the context of this thesis, two types of biases are introduced into the range and range rate measurements that are made using GPS; these are due to the ionosphere and troposphere. It is the geometric straight line distance between the satellite and receiver that is desired, and therefore the removal of these biases is of some importance. The effects due to the troposphere will not be considered here.

The ionosphere has been defined as “that region of the earth's atmosphere in which ionizing radiation (principally from ultraviolet and x-ray emissions) causes electrons to exist in sufficient quantities to affect the propagation of radio waves” [Langley, 1992b]. As will be shown, the dimensions of this layer of ionized material vary both spatially and temporally, but general guidelines are 50–60 km and 1000 km for the lower and upper limits respectively; above this threshold the earth's atmosphere is practically totally ionized [Baker, 1967], although the **electron density** (the number of electrons per cubic metre, symbolised here by the letter **N**) decreases. In reality, the ionized part of the atmosphere extends into interplanetary space and merges with the plasma — the upper

limit of the ionosphere therefore really depends on the application in mind. It should also be stressed that while the ionosphere can occasionally be relatively stable, there are times when ionospheric activity is so unpredictable as to make any attempt at modelling it virtually useless.

3.2 Formation of the Ionosphere

The primary driving forces of ionospheric formation is energy radiated from the sun at extreme ultraviolet (EUV) and X-ray wavelengths. A "packet" of EUV light (called a **photon**) encountering gaseous atoms and molecules in the atmosphere can impart enough energy for **photoionization** to occur, producing positively charged ions and negatively charged free electrons; it is the latter that respond to the oscillations caused by radio waves, causing refraction, and are therefore of interest in this context [McNamara, 1991]. A number of different gases constitute the atmosphere and each requires a different level of energy, called the **ionization potential**, to become ionized. If the number of photons is not adequate for this, the energy will be absorbed by the gases and they will expand [Bugoslavskaya, 1962]. A secondary ionizing force, of much lesser importance except at low altitudes, is **cosmic radiation**, which consists of charged particles from the sun and outer space; these are characterized by very high levels of energy and can penetrate to the earth's surface.

Another process that occurs in the ionosphere is **recombination**, in which the ions and free electrons join again, producing neutral atoms and molecules. Additionally, although only really of importance in the lower region of the ionosphere, free electrons can combine with neutral molecules and atoms to produce negatively charged ions, an act called **attachment**. However, like their positively charged cousins, these ions have little effect on electromagnetic waves, due to their relatively high mass and consequent inability to oscillate when exposed to an electromagnetic wave.

While recombination and attachment happen in a continuous manner (the latter depending on the presence of neutral molecules), it is obvious that photoionization will only happen in the presence of incoming EUV energy from the sun, i.e., when it is above the horizon. The net effect of these three processes is a continuous change in electron density, which is a function of time, location, and solar and geomagnetic activity.

Although photoionization does not occur at night, not all free electrons are lost to recombination and attachment, especially at higher altitudes where the mean free path between collisions of particles is greater (10 μm at 50 km [Bugoslavskaya, 1962]). At lower altitudes, where atmospheric density is greater, and the mean free path is smaller (0.1 μm at the earth's surface [ibid.]), electron density tends to decrease to a larger extent at night.

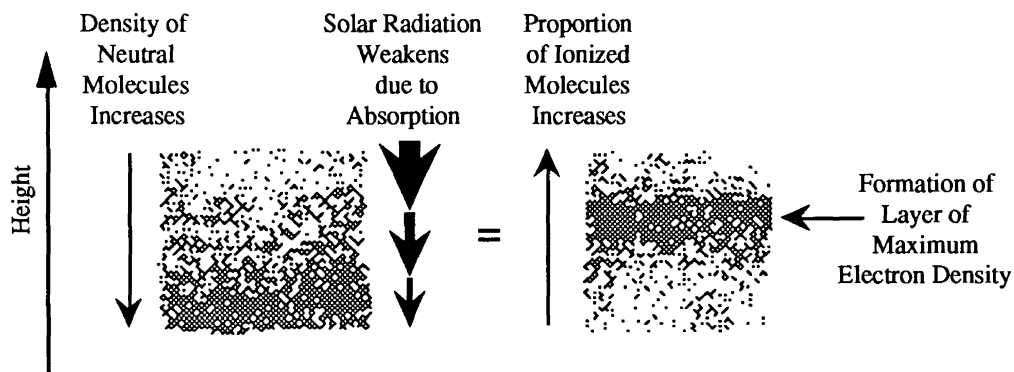


Figure 3.1 Formation of a layer of maximum electron density

During the day, absorption of EUV light increases as altitude decreases and the net result of this and decreasing atmospheric density with altitude is the formation of a layer of maximum electron density, N_m (see Figure 3.1). Actually, due to the mixture of molecules and atoms in the atmosphere, their differing ionization potentials, and their differing rates of absorption of the various wavelengths of EUV, a series of distinct regions or layers of electron density can exist. These are denoted by the letters D, E and F; indeed, at times of high insolation, e.g., daylight in midsummer, the F region splits

into two more distinct layers, called F1 and F2 (see Figure 3.2). The F2 layer is usually where N_m occurs, and the electron density decreases at an approximately exponential rate until it merges with the solar wind.

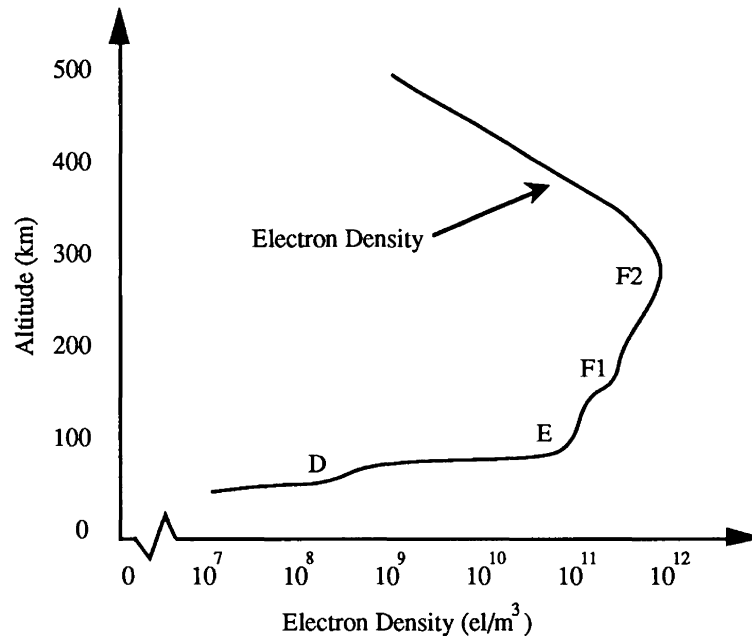


Figure 3.2 Variation of electron density with height for a typical mid-latitude location during summer daytime. The letters refer to the distinct regions and layers of the ionosphere (After McNamara [1991])

Each region has its own **critical frequency**, denoted by f_0 , which is the maximum frequency which can be reflected from the layer at vertical incidence, ignoring the effect of the earth's magnetic field [McNamara, 1991]; e.g., signals at higher frequencies than f_0F2 , the critical frequency of the F2 layer, will pass through it.

3.3 Causes of Electron Density Variation

This section gives a necessarily brief description of the temporal and spatial variations which can occur in the ionosphere. It is impossible to give a definitive account of all the causes and effects here, not only due to the limitations of space, but also because some of

them are not yet fully understood. Hence, it is on the main variations that this overview will concentrate; these can be divided into three categories; temporal, including diurnal, seasonal and longer period cycles; spatial variations; and those due to variations in solar activity. However, it should be borne in mind that ultimately it is solar energy that is the driving force behind ionization.

3.3.1 Temporal Variations

On a diurnal timescale, the D, E and F1 layers largely disappear at night, due to recombination and attachment (the latter being of more importance in the D region), while electron density in the F2 layer is reduced (although not reaching zero) due to recombination, reaching its lowest value just prior to dawn; it then increases rapidly with the rising sun and consequent incoming EUV. Since the F2 layer is at a height of several hundred kilometres, ionization in this layer over a point on the earth's surface actually extends for some time before sunrise and after sunset for the point. The F2 layer is renowned for its not infrequent unpredictable behaviour and the characteristics described above are very general. Much of what is observed of this layer is the result of a combination of processes and it is difficult to isolate their effects [Rishbeth and Garriot, 1969]. Some of the anomalies associated with this layer will be outlined as the chapter progresses.

Throughout the day, the **Total Electron Content (TEC)** at a location is dependent on the local time, with the density reaching a maximum between 12h00 and 16h00; TEC is the total number of electrons in a column of 1 m² cross section through the ionosphere. This temporal variation can be seen in Figure 3.3. Around April, the F2 layer often exhibits a diurnal anomaly, with the f_0F2 reaching a maximum just before and/or just after midday; this phenomenon is reversed in autumn. It is supposed that this is due to quantitative changes in solar radiation, to which the ionosphere is very sensitive at these times [Bugoslavskaya, 1962].

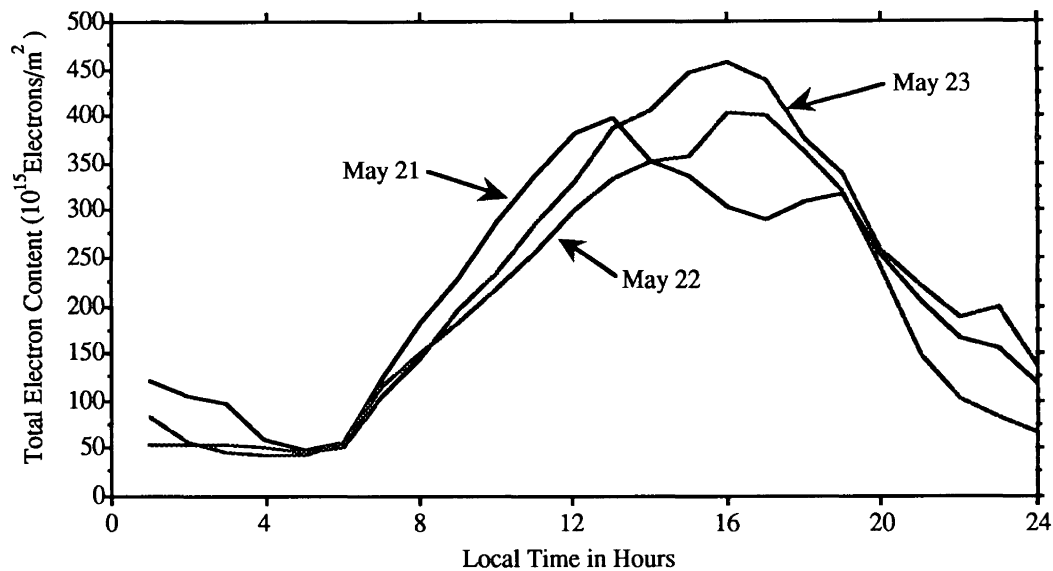


Figure 3.3 Total Electron Content for three consecutive days over Hawaii, 1986
(After Henson and Collier [1986])

Variations in electron density in the D, E and F1 layers from season to season are due primarily to the changes in the elevation angle of the sun. For either hemisphere, radiation strikes the earth and its atmosphere less obliquely in the summer than in the winter causing a lower rate of absorption and a consequent increase in ionization. In winter for the same hemisphere, the daytime F1 layer disappears, while the E layer is reduced. The F2 layer exhibits a rather contrary characteristic however, known as the **mid-latitude seasonal anomaly**, which shows up as an increase in the ionization (by up to 20% [Rishbeth and Garriot, 1969]) for the daytime in the winter. This is due to changes in the proportions of the various gaseous elements and molecules present between the seasons. A further anomaly in this layer is the occasional increase in ionization at night over the polar region that is in winter; this can last for several weeks at a time.

The causes of variations from day to day are not completely understood, but are generally thought to be fluctuations in solar activity (see section 3.3.2) and high altitude winds

redistributing the neutral particles from which the ionosphere is created. Figure 3.3 shows the TEC for three consecutive days over Palehua, Hawaii, at a time of low solar activity.

3.3.2 Influence of Variations in Solar Radiation

From section 3.2 it is perhaps obvious that variations in the quantity of EUV light being emitted by the sun will have an effect on the levels of ionization present in the earth's atmosphere. The periods of these variations range from minutes to years.

Coronal holes are sources of **high speed solar wind streams (HSSWSs)** and are most common in periods of declining solar activity. Charged particles are always being ejected from the sun in the form of the **solar wind**, at speeds of up to 300 km/s; HSSWSs are streams of particles travelling at 500 km/s, and together with the rotation of the sun form spiral shapes in which the earth is occasionally immersed; the occurrence of this is quite predictable since the sun rotates with an approximate period of 27 days. They are also a cause of **ionospheric storms**.

Solar flares are localized rapid increases of energy on the surface of the sun, lasting up to several minutes. This energy is then ejected from the sun, often accompanied by charged particles [Ratcliffe, 1970]. They happen most frequently during periods of high solar activity and range greatly in size and duration, although it is only the largest which affect the ionosphere. The expelled energy, in the form of X-rays, takes about eight minutes to reach the earth and can penetrate as far as the D region, causing increased levels of ionization (up to a tenfold increase); these are called **sudden ionospheric disturbances (SIDs)** and the E and F layers remain largely unaffected. The duration of a SID is often around an hour. Obviously, only the side of the earth in daylight will be affected and locations where the sun is highest in the sky will be more affected since the incident energy will be spread over a smaller area. Protons, actually positively charged hydrogen

ions, can also be emitted when a flare occurs. Their arrival time can be anything from ten minutes to two days after their ejection. As they reach the earth they are guided along the force lines of the geomagnetic field towards the poles where they can descend as far as the D region increasing ionization (see section 3.4.3). Since the force lines are nearly horizontal near the equator most of the particles are guided away from this region which is therefore unaffected. A third type of emission is the plasma cloud which can cause ionospheric storms, and have a particularly strong effect (either a decrease or increase in ionization) in the F2 layer; the D, E and F1 layers are largely untouched. Again, higher latitudes are more prone to the effects of the clouds.

Sunspots can last for periods of days to weeks, and appear as dark regions relative to the normal brightness of the sun. They are surrounded by brighter regions, called **plages**, which emit higher than normal levels of EUV. The 27-day rotational period of the sun is evident when these features are studied since, if they last long enough, they take approximately 13.5 days to traverse the visible portion of the sun, and then disappear, returning after a similar period on the opposite edge from which they disappeared.

A final periodic variation is again due to the phenomenon of sunspots, this time to the approximate **11-year cycle** of the increase and decrease in their number. The sunspot number is calculated by multiplying the number of spot groups by 10 and adding the number of individual spots [McNamara, 1991]. Since this index of solar activity is quite subjective in that it is highly dependent on the observers' levels of experience and their idea of what a sunspot group is, a weighted average of sunspot numbers is calculated from an international network of observatories; the stability of the atmosphere over these observatories is also a factor to be considered, as well as the fact that each will have a different view of the solar disc. The solar flux at a wavelength of 10.7 cm is highly correlated with the sunspot number and can therefore provide another indication of how solar activity will affect the ionosphere.

3.3.3 Effects of Latitude and the Earth's Magnetic Field

Variation in latitude has a direct effect on the level of radiation falling upon an area of the earth. Outside the tropics, the minimum zenith angle of the sun is never zero, and it decreases towards the poles, which are in darkness for prolonged periods during winter. Although a gross generalization, mid-latitude regions are considered relatively free of ionospheric anomalies, while equatorial regions are characterized by high levels of electron density, and polar regions are very unpredictable; these will be discussed later.

The geomagnetic field can be approximated by a bar magnet centred in the earth with its axis tilted at an angle of 11° to the geographic axis. The geomagnetic equator is the plane which is perpendicular to the geomagnetic axis and which cuts the earth in a great circle. In reality, the solar wind compresses the force lines on the side of the earth facing the sun, while on the dark side the lines are extended into a tail. The strength of the geomagnetic field is greater at the poles, with an intensity of 75,000 nanoteslas (nT) compared to 25,000 nT at the equator (at the surface of the earth); variations caused by geomagnetic storms can reach over 240 nT in the auroral zone, although this is small compared with the ambient field. The lines of geomagnetic force (going from southern to northern geomagnetic hemispheres) cause the charged particles in the atmosphere to rotate around them at a rate dependent on the strength of the field, the mass of the particles and their charge. At the equator this **gyrofrequency** is around 1 MHz, and 1.6 MHz at the poles. The **dip angle** is the angle between the horizontal and the direction of the line of magnetic force at a point on the earth; this allows us to define a third "equator", the **dip equator** which is the line around the earth where the dip angle is zero; note that this does not coincide with the geomagnetic equator since the magnetic field of the earth is not exactly similar to that of a bar magnet. At low latitudes the dip angle has a large effect on the ionosphere such that the equatorial anomalies straddle the dip equator rather than the geographic equator. Differences in ionization between two points

at the same geographic latitude in the mid–latitude zone can often be attributed to the fact that the dip angle is different for the two locations [Bugoslavskaya, 1962]. The effects of geomagnetism on variations in electron density are covered in sections 3.4.2 and 3.4.3.

3.4 Further Anomalous Conditions

3.4.1 Sporadic E

Occasionally, a thin layer of high electron density appears at E region heights and this phenomenon has been named sporadic E, or E_s ; unfortunately its appearance is rather unpredictable. At mid–latitudes, E_s appears as clouds of electrons some hundreds of kilometres across and up to 10 km thick, and occur most often during daytime in summer; $N_m E_s$ (maximum electron density in E_s) can reach $1.2 \cdot 10^{12}$ el/m³. One explanation for the existence of E_s is high altitude winds compressing debris from meteors into a narrow layer [McNamara, 1991]. At low latitudes, E_s is again a daytime occurrence, varying little with season, although towards the equator electron densities in the layer tend to fall off — this is connected with the fountain effect (see section 3.4.2).

3.4.2 The Equatorial Ionosphere

Electron density on and around the equator is a result of high radiation levels from the sun, and the electric and magnetic fields of the earth. As electrons are freed at the equator by photoionization they tend to rise due to the combined effect of the fields, and then move along the horizontal force lines of the geomagnetic field away from the equator; this is the so–called **fountain effect** [Ratcliffe, 1970]. They descend to the altitude of the F region at geomagnetic latitudes of between 10° and 20°, causing a high concentration of electrons in two bands straddling the dip equator, which are often termed the **equatorial anomalies** (see Figure 3.4); values of $N_m F2$ can reach $5 \cdot 10^{12}$ el/m³. As might be expected, N_m reaches a maximum in the afternoon, at times of solar maximum and at the equinoxes. One of the problems encountered at low latitudes is the sharp

gradient of N_m both temporally, in an east–west direction in conjunction with insolation differences, and spatially, in a north–south direction due to the effects of poleward electron transfer. An example of the former is the change from $4.4 \cdot 10^{11}$ el/m³ to $2.4 \cdot 10^{12}$ el/m³ in one hour (between 06h00 and 07h00 local time) over Manila in January 1958 (high solar activity) [McNamara, 1991]. The latitudinal gradient can change quite rapidly and is rather unpredictable.

3.4.3 The Polar and Auroral Ionosphere

The ionosphere in the polar regions is undoubtedly the most unpredictable of all and is very variable both spatially and temporally. The major cause of this is the near verticality of the geomagnetic field lines in these regions, which lead the charged particles associated with the solar wind and solar flares to lower than normal altitudes. These particles can collide with and ionize the neutral atmospheric gases in a process known as **collisional ionization**.

It is obvious that the degree of ionization depends on the position of the sun and the condition of the solar wind, i.e., whether it is quiet or strong due to the presence of coronal holes. An interesting feature is the **auroral oval** (see Figure 3.4), a ring of high ionization circling each of the magnetic poles; these areas are where the northern and southern “lights” can be seen most regularly, as the charged particles from space interact with the atmosphere.

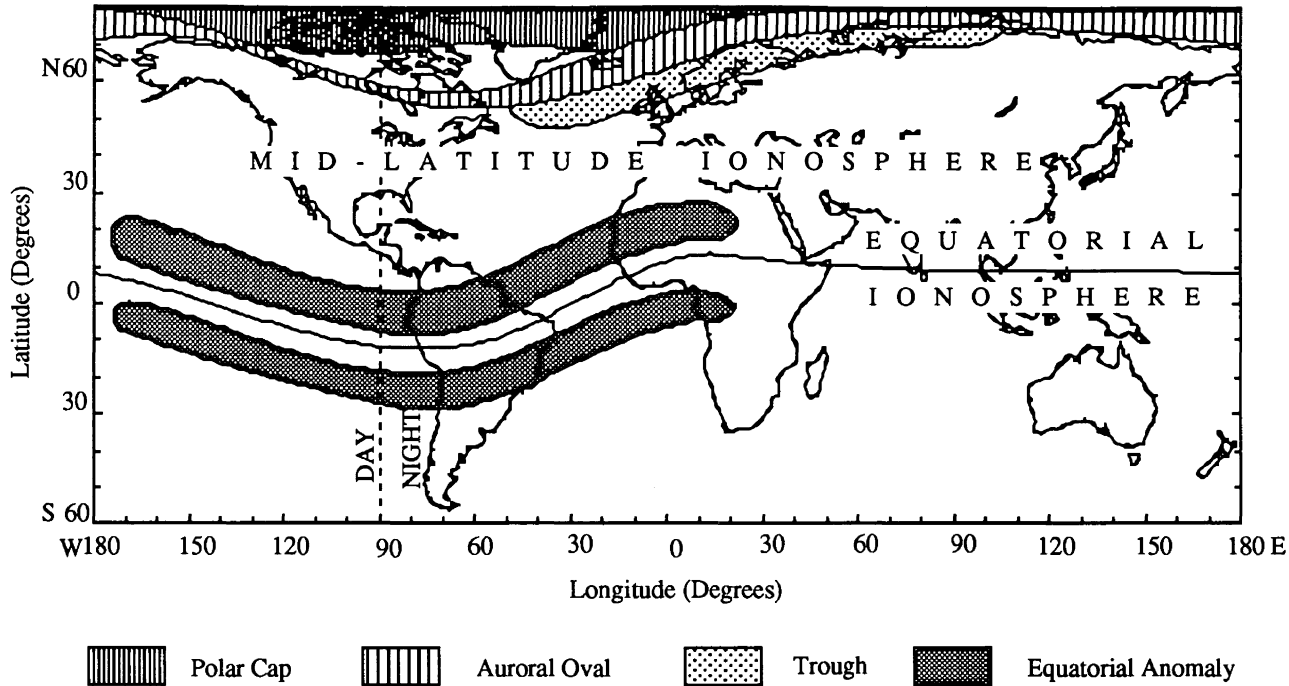


Figure 3.4 Major areas of the ionosphere (After Bishop et al. [1991])

Changes in the solar wind directly affect the size of the ovals. During quiet times, the ovals are centered at around 20° from the geomagnetic poles, while their width is a few degrees [Clynch et al., 1989]. At times of high solar activity the ovals expand poleward and towards the equator and can reach as far south as New York and as far north as Tasmania [McNamara, 1991]. A further feature is the **mid-latitude trough**, a region on the edge of the oval and only two or three degrees wide which is characterized by low levels of free electrons; this occurs essentially at nighttime.

3.4.4 Travelling Ionospheric Disturbances

Travelling Ionospheric Disturbances (TIDs) are caused by the interaction of wave-like motions in the neutral atmosphere with the ionosphere. They appear as ripple-like structures in the existing ionization with wavelengths of anywhere between 50 km and 500 km and travel horizontally at up to 10 km/min over distances of 3000 km [Rishbeth and Garriot, 1969]. Changes in any or all of phase, frequency, amplitude and polarization of a signal can occur due to the moving wavefronts of ionization; the changes are also a function of time due to the mobile nature of TIDs. Typically, variations in N are less than 15%. Since electrons cannot cross the field lines of the geomagnetic field, the occurrence of TIDs is strongly dependent on the direction of the neutral atmospheric waves.

At longer wavelengths, atmospheric tidal effects and the coriolis force can affect TIDs such that rotational atmospheric systems, known as Rossby waves, are produced which are similar to amphidromes found in ocean circulation.

3.4.5 Scintillations

Rapid fluctuations in phase and amplitude of a transionospheric radio signal are called scintillations and are analogous to the atmospheric refraction of visible light from stars. The polar and equatorial regions are the areas where scintillations are most common, and

they appear as periodic fading of the received signal as the ionosphere acts as a diffraction screen on the signal [Héroux, 1988]. The depth of fading can sometimes be so intense that the signal strength drops below the noise level and can result in the loss of lock of the transionospheric signal, particularly at solar maximum.

3.5 Some Concluding Comments on the Ionosphere

We have seen that the ionosphere can be classified by both its degree of ionization and its unpredictability into three general regions; the mid-latitudes which are relatively undisturbed; the equatorial region which has a trough along the dip equator and two anomalous regions of high ionization straddling it in the mid-afternoon and early evening; and the polar and auroral region which can be very unpredictable with the large spatial and temporal gradients of TEC causing problems for GPS users. It should be noted that although a GPS receiver may be sited under the relatively quiet mid-latitude region of the ionosphere, the signal paths from the satellites often travel through the more ionized equatorial region or the more disturbed polar and auroral areas. In addition, the signal may travel through ionospheric regions in both the night and day hemispheres of the earth, [Bishop et al., 1991]. Users should also be aware of the 11-year solar cycle when they are observing, bearing in mind the effects of high solar activity.

The accuracy of the model presented in this thesis depends on how closely the estimated surface model approximates the true spatial variations in TEC; e.g., when a linear surface is used it is assumed that the TEC changes linearly between stations. Obviously, the more the real TEC gradient deviates from the model, the less accurate will be the results.

3.6 The Refraction of GPS Signals in the Ionosphere

When radio waves, such as those from a GPS satellite, pass through an ionized medium, two effects are observed; the ray path is curved and the signal is delayed [Gu and Brunner, 1990]. As noted previously it is the free electrons in the ionosphere which are

the cause of these phenomena, the combined effect of which is called **refraction**. The process of refraction has been defined as “...the change in direction which radiation, especially light, or sound experiences on passing obliquely from one medium to another in which its velocity of propagation is different” [Considine, 1983] and can be expressed by Snell’s law:

$$n_1 \cdot \sin i_1 = n_2 \cdot \sin i_2, \quad (3.1)$$

where

- i_1 is the angle of incidence of the wave at the media interface;
- i_2 is the angle of the refracted wave;
- n_1 is the refractive index in the first medium;
- n_2 is the refractive index in the second medium.

The **refractive index** of a medium, n , is the ratio of the speed of propagation of radiation in free space to the speed of propagation of the same radiation in the medium. In a vacuum, $n = 1$, while in other media it may be either greater or smaller. For the ionosphere, n can be found by the Appleton–Hartree formula which in general terms can be written [Kleusberg, n.d.]:

$$n^2 = 1 - F(f, f_p, f_h, \nu, \theta), \quad (3.2)$$

where

- f is the carrier frequency (Hz);
- f_p is the plasma frequency (Hz);
- f_h is the gyrofrequency of free electrons (Hz);
- ν is the collision frequency (Hz);
- θ is the angle between signal and the magnetic field vector.

Equation (3.2) can be expanded as an infinite series, but it is often convenient to just take the first two terms:

$$n = 1 - \frac{1}{2} \cdot \frac{f_p^2}{f^2} \quad (3.3)$$

and since, for any point, $f_p^2 = 80.6 \cdot N \text{ Hz}^2$, (the constant being in units of m^3/s^2 and N being the electron density at the point in units of $1/\text{m}^3$) we can write equation (3.3) as:

$$n = 1 - 40.3 \cdot \frac{N}{f^2} \quad (3.4)$$

for a pure carrier signal. An important point to note is that n is a function of the square of the frequency of the signal, i.e., the ionosphere is a dispersive medium. The specific type of dispersion that we are interested in is **refractive dispersion** which is the separation of a set of signals due to the fact that the velocity of electromagnetic radiation (and hence the refractive index) in an ionized medium is dependent on frequency. A dispersion curve, as shown in Figure 3.5, can be drawn which shows the dispersion characteristics of the ionosphere.

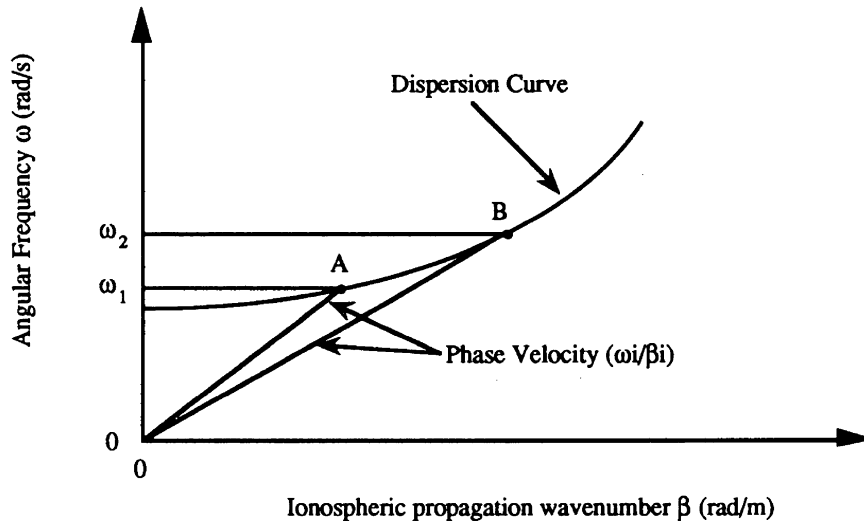


Figure 3.5 Dispersion curve and phase velocity (After Wells et al. [1987])

The curve in Figure 3.5 will change if the electron density changes due to processes already discussed in this chapter. The **phase velocity** for a signal is given by the gradient

of the line joining the origin with the point on the curve corresponding to the frequency of the signal (points A and B above for two different frequencies — note that $\omega = 2\pi f$); it is clear how the velocity changes with frequency. The **group velocity**, which is the propagation velocity of the code information impressed onto the GPS carrier signals, is given by the gradient to the curve at the point where the phase velocity line intercepts it. An interesting feature is that the point where the curve cuts the vertical axis is the critical frequency, in which case a group or pulse of radio waves will have no velocity (the curve is horizontal); if the frequency is raised, the pulse will continue to travel, confirming what was written in section 3.2. We now have a phase velocity, $v_p = \omega/\beta$, and a group velocity, $v_g = \partial\omega/\partial\beta$, with a corresponding phase index of refraction, $n_p = c/v_p$, and group index of refraction, $n_g = c/v_g$.

For the ionosphere we can write

$$n_p = 1 - 40.3 \cdot \frac{N}{f^2} \quad (3.5)$$

where N is the electron density in el/m^3 at the point of interest — note the equivalence to equation (3.4); and for the group refractive index

$$n_g = 1 + 40.3 \cdot \frac{N}{f^2} \quad (3.6)$$

It is the electromagnetic, rather than geometric, distance between the satellite and receiver that is actually measured. Symbolised by S , it can be written (ignoring other biases)

$$S = \int_{\text{Satellite}}^{\text{Receiver}} n \, ds. \quad (3.7)$$

Substituting equation (3.5) into (3.7) we obtain

$$S = \rho - 40.3 \cdot \frac{1}{f^2} \int_{\text{Satellite}}^{\text{Receiver}} N \, ds = \rho - 40.3 \cdot \frac{\text{TEC}}{f^2} \quad (3.8)$$

where TEC (total electron content) is the integrated electron density along the signal path and ρ is the range. The equivalent expression for a modulated signal is

$$S = \rho + 40.3 \cdot \frac{\text{TEC}}{f^2} \quad (3.9)$$

Note that S in equation (3.8) will always be shorter than the true distance, due to the advance of the phase, while equation (3.9) will always give the distance as longer than the true distance, since the signal is delayed.

If we write equation (2.3) for each of the two carrier frequencies, $L1$ and $L2$ and difference and rearrange these equations, we can obtain an expression for the **ionospheric delay** on $L1$ in metres:

$$d_{\text{ion}1} = \frac{f_2^2}{f_1^2 - f_2^2} (\Phi_1 - \Phi_2) + \frac{f_2^2}{f_1^2 - f_2^2} (\lambda_2 N_2 - \lambda_1 N_1) + \varepsilon \quad (3.10)$$

The second term on the right hand side will remain constant as long as the receiver remains locked onto the incoming signal. However this term cannot be determined and we can therefore only derive values of ionospheric delay up to a constant when using phase measurements i.e., we can examine the change in delay over time, but not its absolute value (unless other information such as dual frequency P-code data is used).

Assuming a constant frequency for any particular signal, we can see that the actual size of this bias is dependent solely on the TEC along the signal path. Unfortunately TEC is a constantly varying quantity in time and space and consequently the delays to the signals are extremely hard to model accurately.

It is now common practice to use the satellite-receiver double differences as written in equation (2.7) as input to any estimation process; the positioning software used in this investigation is no exception. Through the operation of double differencing, any

common part of the ionospheric delay between satellites and stations will be eliminated, and we are left with a residual delay, $\nabla\Delta d_{\text{ion}}$.

In static differential positioning, estimates are made for three groups of parameters: the baseline components; $\nabla\Delta N$; and residuals to the double differences. Since one of the inherent properties of a least squares estimation is that the sum of the residuals over the whole session will equal zero, it is therefore impossible for them to absorb any constant offset. Therefore, any constant part of the residual delay will be absorbed by the baseline components and $\nabla\Delta N$, both of which remain constant over the whole session, assuming that no cycle slips occur, and provided $\nabla\Delta N$ is not restricted to becoming an integer [Kleusberg, 1986b]. The proportion that each absorbs is dependent on the geometrical configuration of the satellites and receivers, and the constraints applied to each, i.e., the weighting that is given to each in the estimation process. A convenient method of dealing with this constant part of the delay would therefore seem to be to give the ambiguities a lower *a priori* weight than the baseline components, thus allowing the ambiguities to absorb the majority of the error. However, this has the inherent disadvantage of precluding the use of GPS in its highest accuracy mode, i.e., fixing the ambiguities to integer values, leaving only the baseline components as the unknowns, and therefore providing a stronger, more redundant solution. Any non-constant part of $\nabla\Delta d_{\text{ion}}$ will again be absorbed by the baseline components and the residuals of the adjustment.

In kinematic positioning, estimates are again sought for $\nabla\Delta N$, the baseline components, and the residuals. However, it is only the ambiguities which will generally remain constant from epoch to epoch, again assuming no cycle slips are present in the data. Since estimates are obtained on an epoch by epoch basis, the condition that the sum of the residuals equals zero will only hold true for any one epoch, and will generally not be the case for a summation over the whole observation session. At a single epoch, it is

plausible to suppose that since there is no information regarding the magnitude of the constant part of the ionospheric bias for the whole session, this constant can be absorbed by the residuals as well as the ambiguities and baseline components. However, since the residuals of the double differences are unimportant in this application, this is of little consequence.

In this research it is the residual ionospheric delay, $\nabla\Delta d_{ion}$, in equation (2.7) which is the subject of attention. An adjustment model is used in which the ambiguities are not fixed, therefore allowing part of the delay to be absorbed by them. In order to deal with the remaining part, the model which is the subject of this thesis is used; this is described in Chapter Five.

Chapter 4

Kinematic Positioning Software

4.1 Introduction

In order to appreciate the effects of the corrections from the model on the observations it is necessary to employ a program to compute positions. This chapter describes the algorithm in the positioning package **HIPPOS** which was used in this research. The algorithm is a development of that first proposed by Kleusberg [1986a] and has been improved and documented by Kleusberg and Georgiadou [1991a]. The package operates in a differential mode using the double differences of observations made at one monitor station and a remote receiver. It uses equations (2.6), (2.7) and (2.9) to estimate the position and velocity vectors of the remote receiver. These are rewritten below:

$$\nabla\Delta\rho = \nabla\Delta\rho + \nabla\Delta d\rho + \nabla\Delta d_{\text{ion}} + \nabla\Delta d_{\text{trop}} + \nabla\Delta\eta_p + \nabla\Delta\epsilon_p, \quad (2.6)$$

$$\nabla\Delta\Phi = \nabla\Delta\rho + \nabla\Delta d\rho - \nabla\Delta d_{\text{ion}} + \nabla\Delta d_{\text{trop}} + \nabla\Delta\eta_\phi + \lambda \cdot \nabla\Delta N + \nabla\Delta\epsilon_\phi, \text{ and} \quad (2.7)$$

$$\nabla\Delta D = \frac{d}{dt} \nabla\Delta\rho + \nabla\Delta\epsilon_D. \quad (2.9)$$

The positional information is contained in the term $\nabla\Delta\rho$ in equations (2.6) and (2.7), while the velocity information is to be found in the time derivative of this term in equation (2.9). All quantities are computed on the World Geodetic System 1984

(WGS 84) datum which is in accord with GPS philosophy, since the orbits of the satellites are computed with respect to this datum.

4.2 Corrections to Data

By differencing between stations and satellites it is hoped that a significant portion of the atmospheric refraction in the measurements is eliminated due to positive spatial correlation. However, some residual atmospheric effects will inevitably remain, and these must be accounted for to obtain reliable estimates of the unknowns.

In an attempt to model the double difference of the tropospheric delay, data are used in Hopfield's model [Hopfield, 1971]; in this research, since no meteorological readings were available, default values for all stations of 1013.25 mb (pressure), 5° C (temperature) and 50 % relative humidity were used to drive the model. The ionospheric delay is dealt with as described in the last section of the preceding chapter.

We can now write equations (2.6) and (2.7) in the form:

$$\nabla\Delta p = \nabla\Delta\rho + \nabla\Delta\epsilon_p, \quad (4.1)$$

$$\nabla\Delta\Phi = \nabla\Delta\rho + \lambda\cdot\nabla\Delta N + \nabla\Delta\epsilon_\Phi, \quad (4.2)$$

where the last term in each equation now includes residual atmospheric delays (those which haven't been eliminated by differencing or modelling), orbital errors, multipath errors and measurement noise; since the latter two are generally uncorrelated between stations and satellites, differencing actually will double their significance.

4.3 Linearization of the Observation Equations

We now have the final non-linear observation equations (equations (2.9), (4.1) and (4.2)).

We can write, for example, equation (4.1) as:

$$l = f(x) + v, \quad \text{or,} \quad l - f(x) = v, \quad (4.3)$$

where l is the vector of observations;
 $f(\bullet)$ is a vector of known functions mapping x to l ;
 x is the vector of unknown parameters;
 v is the vector of residuals, or corrections to the observations.

Before a least squares adjustment can be performed these equations must be linearized with respect to the unknowns. Linearization of equation (4.3) can be accomplished by replacing the non-linear functions with their Taylor series linear approximations expanded about an initial value of the solution vector, x^0 (the Taylor point), and retaining only the first order terms:

$$l - f(x^0) = \frac{\partial f}{\partial x} dx + v \quad (4.4)$$

or

$$w = A \cdot dx + v, \quad (4.5)$$

where w is the misclosure vector ($l - f(x^0)$);
 A is the design matrix of partial derivatives (evaluated using x^0);
 dx is the vector of corrections to x^0 ;
 v is the vector of residuals (corrections to observations).

In more explicit terms, if $\nabla \Delta p$ in equation (4.1) is expanded in a Taylor series about an initial point, x_R^0 , we obtain

$$\nabla \Delta p - \nabla \Delta p^0 = \nabla \Delta \frac{\partial p}{\partial x_R} dx_R + \nabla \Delta \epsilon_p \quad (4.6)$$

where x_R is the position vector of the receiver;

$$\begin{aligned}
d\mathbf{x}_R &= \mathbf{x}_R - \mathbf{x}_R^0 \text{ (i.e., a correction to the initial estimate, } \mathbf{x}_R^0\text{);} \\
\nabla\Delta\rho^0 &= \nabla\Delta \|\mathbf{x}_S - \mathbf{x}_R^0\|; \\
\mathbf{x}_S &\text{ is the position vector of a satellite.}
\end{aligned}$$

Note that this is the form of equation (4.5).

Similarly, linearization of the carrier phase observation equation gives

$$\nabla\Delta\Phi - \nabla\Delta\rho^0 = \nabla\Delta \frac{\partial\rho}{\partial\mathbf{x}_R} d\mathbf{x}_R + \lambda \cdot \nabla\Delta N + \nabla\Delta\epsilon_\Phi \quad (4.7)$$

Equation (2.9) is linearized around an initial value for the velocity of the remote receiver, $\dot{\mathbf{x}}_R$:

$$\nabla\Delta D - \frac{d}{dt}\nabla\Delta\rho^0 = \nabla\Delta \frac{\partial\left(\frac{d}{dt}\rho\right)}{\partial\dot{\mathbf{x}}_R} d\dot{\mathbf{x}}_R + \nabla\Delta\epsilon_D \quad (4.8)$$

where $d\dot{\mathbf{x}}_R = \dot{\mathbf{x}}_R - \dot{\mathbf{x}}_R^0$;

and equation (4.8) is evaluated using \mathbf{x}_R^0 and $\dot{\mathbf{x}}_R^0$. Notice that the left hand side of equations (4.6), (4.7) and (4.8) is the misclosure term.

4.4 Positioning Algorithm

At any epoch when we are observing n satellites, a total of $(n-1)$ independent double difference pairs may be formed for each of the types of observable available; we therefore must be observing at least four satellites at any epoch to estimate the parameters. We can write a system of linear equations for each of the doubly differenced code, phase and Doppler measurements:

$$\mathbf{w}_p = \mathbf{A} \cdot d\mathbf{x}_R + \mathbf{v}_p; \quad (4.9)$$

$$\mathbf{w}_\Phi = \mathbf{A} \cdot d\mathbf{x}_R + \mathbf{B} \cdot \mathbf{N} + \mathbf{v}_\Phi; \quad (4.10)$$

$$\mathbf{w}_D = \mathbf{A} \cdot d\dot{\mathbf{x}}_R + \mathbf{v}_D; \quad (4.11)$$

where the left hand side represents the double difference misclosure vector, i.e., observation minus the value computed from approximate values. \mathbf{A} is the first design matrix and contains the partial derivatives of the range double difference with respect to the receiver coordinates (equations (4.9) and (4.10)) and the partial derivatives of the range rate double differences with respect to the receiver's velocity (equation (4.11)); the two are actually identical [Kleusberg and Georgiadou, 1991a]. \mathbf{B} is a second design matrix for the ambiguity parameters.

4.4.1 Computation of Approximate Values and Pseudo-observations

Values of \mathbf{x}_R^0 and $\dot{\mathbf{x}}_R^0$ for any epoch, say t_i , are found by simply linearly extrapolating the estimates of the position and velocity from the previous epoch, t_{i-1} :

$$\mathbf{x}_R^0(t_i) = \hat{\mathbf{x}}_R^0(t_{i-1}) + \hat{\dot{\mathbf{x}}}_R^0(t_{i-1}) \cdot (t_i - t_{i-1}), \quad (4.12)$$

$$\dot{\mathbf{x}}_R^0(t_i) = \hat{\dot{\mathbf{x}}}_R^0(t_{i-1}). \quad (4.13)$$

The circumflex denotes a least squares estimate, while (t_{i-1}) indicates the value is from the previous epoch. While the position and velocity of the remote receiver will most probably change over time, the ambiguity term will remain constant as long as the receiver retains lock on the signals from the satellites. In this way we can use the estimate for \mathbf{N} at epoch t_{i-1} as *a priori* information for the estimate at epoch t_i ; additionally, the HIPPOS software takes the estimates of the corrections to the coordinates from the previous epoch and uses them as a set of pseudo-observations:

$$d\hat{\mathbf{x}}_R(t_{i-1}) = d\mathbf{x}_R(t_i) + \boldsymbol{\varepsilon}_R. \quad (4.14)$$

$$\hat{\mathbf{N}}(t_{i-1}) = \mathbf{N} + \boldsymbol{\varepsilon}_N. \quad (4.15)$$

These estimates are given *a priori* weight matrices, $\mathbf{P}_{dx}(t_{i-1})$ and $\mathbf{P}_N(t_{i-1})$, which are simply the inverses of the *a posteriori* covariance matrices from the previous epoch, i.e., $\mathbf{C}_{dx}(t_{i-1})$ and $\mathbf{C}_N(t_{i-1})$. In its present state, if the software detects a cycle slip (caused by loss of lock on the carrier signal), the element of $\mathbf{P}_N(t_{i-1})$ describing the weight of the affected ambiguity double difference is set to zero.

4.4.2 A Priori Precisions of Observations

A priori information concerning the uncertainty in the observations is contained in the covariance matrix for each type of observable. Assuming no correlation exists, for code, phase and Doppler measurements these are, respectively:

$$\mathbf{C}_p = \sigma_p^2 \mathbf{I}; \quad (4.16)$$

$$\mathbf{C}_\phi = \sigma_\phi^2 \mathbf{I}; \quad (4.17)$$

$$\mathbf{C}_D = \sigma_D^2 \mathbf{I}. \quad (4.18)$$

In the usual manner, the weight matrices for each, \mathbf{P}_p , \mathbf{P}_ϕ , and \mathbf{P}_D , are taken as the inverses of the above.

4.4.3 Solution for Parameters

A least squares algorithm is used for the solution of the parameters, i.e., a criterion is imposed on the solution such that it minimizes $\hat{\mathbf{v}}^T \mathbf{P} \hat{\mathbf{v}}$ (e.g., Cross [1983]; Vaníček and Krakiwsky [1987]). Equations (4.9), (4.10) and (4.11) are combined so that we now have the following linear system of equations:

$$\begin{bmatrix} \mathbf{w}_p \\ \mathbf{w}_\Phi \\ d\hat{\mathbf{x}}_R(t_{i-1}) \\ d\hat{\mathbf{N}}(t_{i-1}) \end{bmatrix} = \begin{bmatrix} \mathbf{A} & \mathbf{0} \\ \mathbf{A} & \mathbf{B} \\ \mathbf{I} & \mathbf{0} \\ \mathbf{0} & \mathbf{I} \end{bmatrix} \begin{bmatrix} d\hat{\mathbf{x}}_R(t_i) \\ \hat{\mathbf{N}}(t_i) \end{bmatrix} + \begin{bmatrix} \mathbf{v}_p \\ \mathbf{v}_\Phi \\ \mathbf{v}_{dx} \\ \mathbf{v}_N \end{bmatrix} \quad (4.19)$$

and we now have a design hypermatrix, \mathbf{A}_H . Note that the range rate observations are not included — they are used solely for the velocity computation. The weight hypermatrix, \mathbf{P}_H , takes the form

$$\mathbf{P}_H = \begin{bmatrix} \mathbf{C}_p^{-1} & \mathbf{0} & \mathbf{0} & \mathbf{0} \\ \mathbf{0} & \mathbf{C}_\Phi^{-1} & \mathbf{0} & \mathbf{0} \\ \mathbf{0} & \mathbf{0} & \mathbf{C}_{dx}^{-1} & \mathbf{0} \\ \mathbf{0} & \mathbf{0} & \mathbf{0} & \mathbf{C}_N^{-1} \end{bmatrix} \quad (4.20)$$

The solution for the unknowns is given by

$$\begin{bmatrix} d\hat{\mathbf{x}}_R(t_i) \\ \hat{\mathbf{N}}(t_i) \end{bmatrix} = \mathbf{M}^{-1} \mathbf{U} \quad (4.21)$$

where

$$\mathbf{M} = \mathbf{A}_H^T \mathbf{P}_H \mathbf{A}_H \quad (4.22)$$

and

$$\mathbf{U} = \mathbf{A}_H^T \mathbf{P}_H \mathbf{w}_H \quad (4.23)$$

where \mathbf{w}_H is the left hand side of equations (4.19).

In more explicit terms, we can write

$$\mathbf{M} = \begin{bmatrix} (\sigma_p^2 + \sigma_\Phi^2) \mathbf{A}^T \mathbf{A} + \mathbf{P}_{dx}(t_{i-1}) & \sigma_\Phi^2 \mathbf{A}^T \mathbf{B} \\ \sigma_\Phi^2 \mathbf{B}^T \mathbf{A} & \sigma_\Phi^2 \mathbf{B}^T \mathbf{B} + \mathbf{P}_{\hat{\mathbf{N}}}(t_{i-1}) \end{bmatrix} \quad (4.24)$$

$$\mathbf{U} = \begin{bmatrix} \sigma_p^2 \mathbf{A}^T \mathbf{w}_p + \sigma_\phi^{-2} \mathbf{A}^T \mathbf{w}_\phi + \mathbf{P}_{d\hat{\mathbf{x}}(t_{i-1})} d\hat{\mathbf{x}}(t_{i-1}) \\ \sigma_\phi^2 \mathbf{B}^T \mathbf{w}_\phi + \mathbf{P}_{\hat{\mathbf{N}}(t_{i-1})} \hat{\mathbf{N}}(t_{i-1}) \end{bmatrix} \quad (4.25)$$

Note that the weight matrices of the observations have been replaced by the inverses of the variances of the observations; this is possible due to the diagonal nature of the matrices. The estimate of the position for epoch t_i is then given by:

$$\hat{\mathbf{x}}_R(t_i) = \mathbf{x}_R^0(t_i) + d\hat{\mathbf{x}}_R(t_i). \quad (4.26)$$

The *a posteriori* covariance matrix of the parameters is given by the inverse of matrix \mathbf{M} .

However, this should be scaled by the unit variance, computed from:

$$\sigma_0^2 = (\hat{\mathbf{v}}_p^T \mathbf{P}_p \hat{\mathbf{v}}_p + \hat{\mathbf{v}}_\phi^T \mathbf{P}_\phi \hat{\mathbf{v}}_\phi + \hat{\mathbf{v}}_{dx}^T \mathbf{P}_{dx}(t_{i-1}) \hat{\mathbf{v}}_{dx} + \hat{\mathbf{v}}_N^T \mathbf{P}_N(t_{i-1}) \hat{\mathbf{v}}_N) / 2n \quad (4.27)$$

Using equation (4.11) normal equations for the velocity of the moving receiver can be formed and inverted to give corrections to the approximate value:

$$d\hat{\mathbf{x}}(t_i) = [\sigma_D^2 \mathbf{A}^T \mathbf{A}]^{-1} [\sigma_D^2 \mathbf{A}^T \mathbf{w}_D] \quad (4.28)$$

and hence

$$\hat{\mathbf{x}}_R(t_i) = \mathbf{x}_R^0(t_i) + d\hat{\mathbf{x}}_R(t_i) \quad (4.29)$$

with the unit variance given by

$$\sigma_0^2 = (\hat{\mathbf{v}}_D^T \mathbf{P}_D \hat{\mathbf{v}}_D) / (n - 3) \quad (4.30)$$

and the covariance matrix of the estimated velocities by

$$\hat{\mathbf{C}}_{\hat{\mathbf{x}}} = \sigma_0^2 [\sigma_D^2 \mathbf{A}^T \mathbf{A}]^{-1} \quad (4.31)$$

While the covariance matrices are statistically rigorous in their derivation, it should be stressed that the estimated standard deviations of the parameters (taken as the square root

of the variances, lying on the diagonals of the matrix) only represent the sensitivity of the scenario at any particular epoch to random errors of the magnitude described in equations (4.16), (4.17) and (4.18). The *a posteriori* covariance matrices (before scaling by the variance factor) will depend only upon the geometry and assumed precision of the measurements and will therefore give an indication of the precision, (otherwise known as the internal accuracy) of the results of the adjustment.

4.4.4 Introduction of Constraints

An option in the software is the ability to incorporate estimates of the initial position of the remote receiver, if it is felt that these are known to a high enough accuracy to be useful in the adjustment.

Furthermore, if we can fix the ambiguities estimated in equations (4.21) to integers (i.e., their real number estimates lie close enough to integers so that we can say we have unambiguously determined them) we can introduce infinitely small error terms into equation (4.15) (the last term on the right hand side below):

$$\hat{N}_{(i,j)} = N + \epsilon_{\infty}. \quad (4.32)$$

so that the weight matrix for the ambiguities in equations (4.24), (4.25) and (4.27) will contain infinitely large values, which are applied in reality with some large numerical value. In this research, no effort was made to constrain the ambiguities. As outlined in Chapter Three, this was because the ambiguity parameter was “used” in that it was left unconstrained so that it could absorb some of the double difference of ionospheric delay.

The necessary background information has been presented in Chapters Two, Three and Four. The following chapter describes the model developed in this research, while Chapter Six evaluates its performance using a test data set.

Chapter 5

Model Description

5.1 Outline of the Model

This chapter describes the model developed to predict ionospheric range errors for a single frequency receiver. Its purpose is to estimate ionospheric phase delays at the L1 frequency from values of phase delays obtained in the vicinity of the single frequency receiver, which may or may not be moving. The estimated corrections are then applied to the L1 phase measurements to obtain what is hoped to be a better solution for parameters relating to the receiver.

The concept behind the model is essentially very simple. If we assume an infinitesimally thin ionosphere at a certain altitude above the earth's surface, and compute the positions of the points where signal paths to a number of dual frequency ground-based receivers (at least three in number) cut this layer, we have a set of positions (the **intersection points**), each of which is associated with a value of ionospheric delay (see Figure 5.1). When projected vertically onto the earth's surface, these points are termed the **sub-ionospheric points**; obviously the horizontal geographic coordinates of each pair of one intersection point and its corresponding sub-ionospheric point will be identical. We can then find the coefficients of a simple bivariate algebraic polynomial fitted through these points (see Figure 5.2). It is then a matter of finding where the signal path to a single frequency

receiver in the same area cuts the layer, and using the coordinates of this point together with the coefficients from the polynomial to obtain the delay for that receiver.

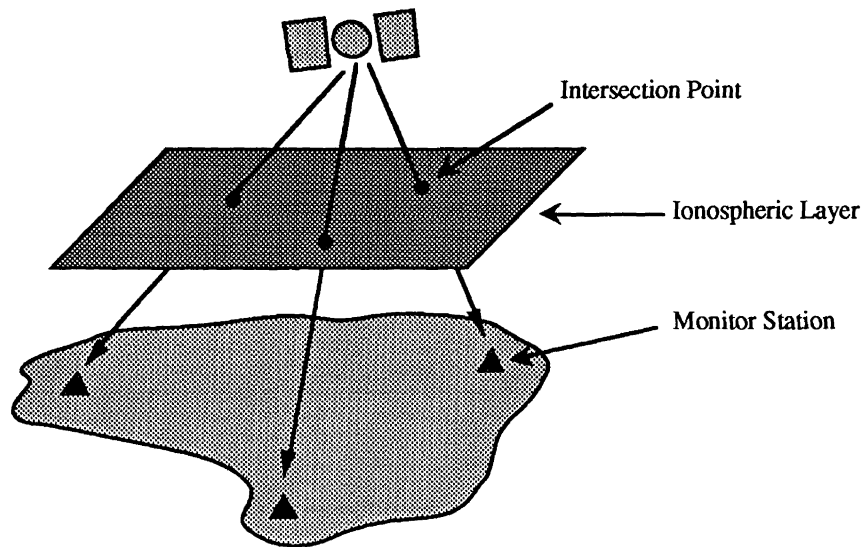


Figure 5.1 Intersection points on the ionospheric layer

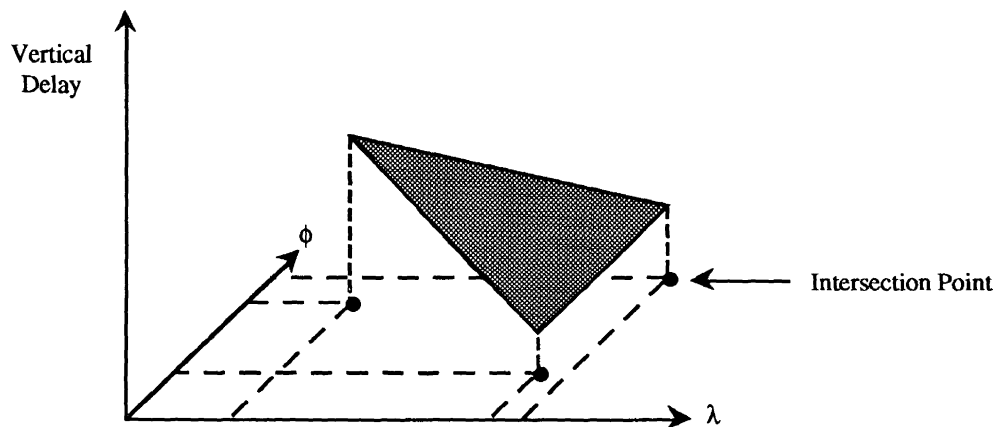


Figure 5.2 A surface describing the vertical delay fitted to the intersection points

It is hoped that this conceptual explanation has given the reader a framework which will enable the more detailed description that follows to be more easily and quickly understood.

5.2 Details of Model Formulation

The following three sections give more details, including some mathematical background, on three aspects of the above model, namely, the procedure for finding the intersection points, mapping delays to the vertical, and finding the coefficients of the surface.

5.2.1 Determination of Intersection Points

It is first of all assumed that the ionosphere is compressed vertically into an infinitesimally thin surface, or shell, at a specified altitude between 300 km and 400 km above the earth. It is also commonly assumed that the peak of electron density is at an altitude of 350 km and thus the altitude of the shell is set to this value (e.g., Klobuchar [1986], Bishop et al. [1991]). The shell can be approximated by a sphere over the area in question. The equation of this sphere can be written (e.g., Kindle [1950]):

$$x^2 + y^2 + z^2 = (R + h)^2, \quad (5.1)$$

where x, y, z are the coordinates of any point on the sphere;
 R is the radius of the earth;
 h is the altitude of the layer.

If we now have a satellite with position vector $\mathbf{r}_s = (x_s, y_s, z_s)^T$ and a dual frequency receiver with position vector $\mathbf{r}_r = (x_r, y_r, z_r)^T$, we can derive the equation of the line in space joining the two points [Kindle, 1950]:

$$\frac{x - x_r}{x_s - x_r} = \frac{y - y_r}{y_s - y_r} = \frac{z - z_r}{z_s - z_r}, \quad (5.2)$$

where x, y, z are the coordinates of any point on the line.

It is now possible to solve for the intersection points of the line and the sphere (with position vector, $\mathbf{r}_p = (x_p, y_p, z_p)^T$) by rewriting y and z in equation (5.2) in terms of x , substituting these expressions into equation (5.1), and solving a quadratic equation for x_p . The y_p and z_p coordinates can be found by substituting the value for x_p into equation (5.2). If the two solutions of the quadratic are imaginary, the line does not intersect the sphere; this is not possible in our case. If both solutions are identical, the line is tangential. If there are two real solutions, one is the point of ingress of the line and the other is the point of egress; the correct desired solution is that lying between the receiver and the satellite.

5.2.2 Mapping Ionospheric Delays to the Vertical

The next step is to map the slant ionospheric delays obtained directly from the phase measurements to the vertical. This is done using the relation:

$$\text{dion}_v = \text{dion} \cdot \cos(z), \quad (5.3)$$

where dion_v is the delay mapped to the vertical;
 dion is the slant delay;
 z is the zenith distance of the ray at the intersection point.

The zenith distance can be found from:

$$z = 180 - \alpha, \quad (5.4)$$

where α is the angle shown in Figure (5.3), and units are degrees.

The angle α can be found by employing the cosine rule in the following form:

$$\alpha = \cos^{-1} \left(\frac{|\mathbf{r}_p|^2 + |\mathbf{r}_s - \mathbf{r}_p|^2 + |\mathbf{r}_s|^2}{2 \cdot |\mathbf{r}_p| \cdot |\mathbf{r}_s - \mathbf{r}_p|} \right), \quad (5.5)$$

where $|\mathbf{r}|$ is the magnitude of vector \mathbf{r} .

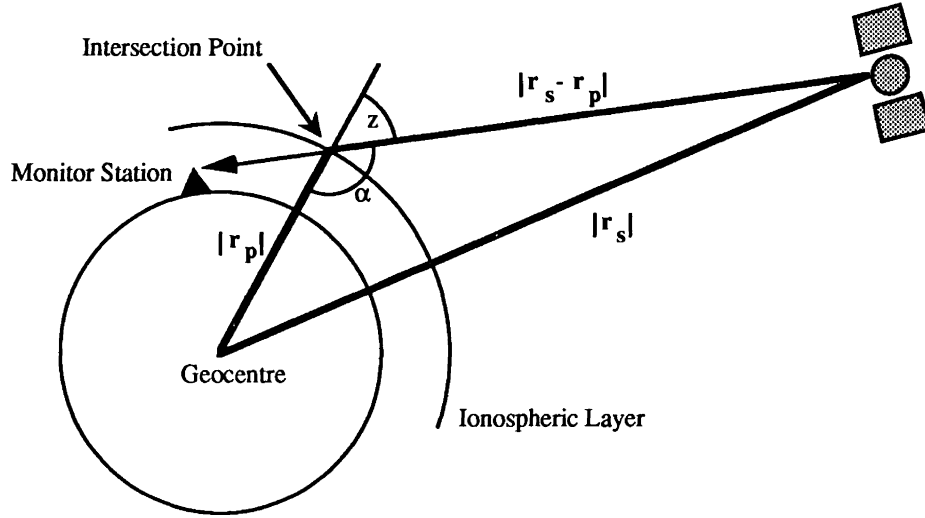


Figure 5.3 The zenith distance, z , at the intersection point

The cartesian coordinates of the intersection point are now converted to geographic coordinates, (ϕ, λ, h) , which can be done using:

$$\phi = \sin^{-1}((R + h)/z_p), \quad (5.6)$$

$$\lambda = \tan^{-1}(y_p/x_p), \quad (5.7)$$

with h being the altitude of the layer and known already. We now reach the point where we can fit a surface through the data points available.

Another method for converting slant delays to the vertical is described by Newby [1992] and Clynch et al. [1989], among others. The slant delays are divided by an obliquity factor computed from

$$Q = \sum_{j=0}^3 a_j x^{2j}, \quad \text{where} \quad x \equiv 1 - \frac{2}{\pi} \psi \quad (5.8)$$

where a_j are coefficients and ψ is the elevation angle of the satellite in radians. The relationship between ψ and z is given by [Georgiadou and Kleusberg, 1988a]:

$$z = \sin^{-1}\left(\frac{R \cdot \cos\psi}{R + h}\right) \quad (5.9)$$

As shown in Figure 5.4, the differences between using this factor and multiplying by the cosine of the corresponding zenith angle at the ionospheric point are slight.

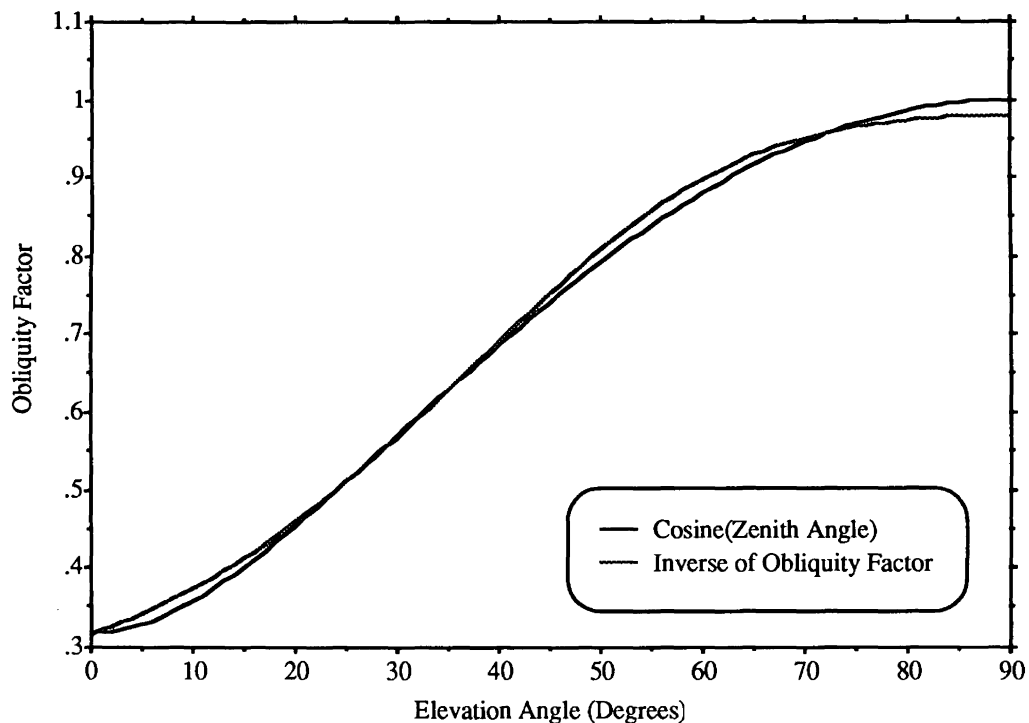


Figure 5.4 Comparison of the inverse of the obliquity factor, Q , at elevation angles from 0 to 90 degrees, and the cosine of the zenith distance at the corresponding ionospheric point for a shell at a height of 350 km.

5.2.3 Bivariate Polynomials and the Determination of Coefficients

This section introduces the bivariate polynomial, or polynomial in two variables. These functions are extremely important to surface modelling, with the two variables being the horizontal coordinates of a point, and the result of the evaluated polynomial being the

value for the third “dimension”, whatever this is intended to represent. Table 5.1 lists some of the classes of surfaces that may be produced and the corresponding basis functions that would be included in the expression for the surface.

Surface	No. of Terms	Basis Functions	Class
Constant	1	1	P_0
Linear	3	1 x y	P_1
Quadratic	6	1 x y x^2 xy y^2	P_2
Cubic	10	1 x y x^2 xy y^2 x^3 x^2y xy^2 y^3	P_3

Table 5.1 Characteristics of different surfaces

A vertical section through a linear surface will produce a straight line, while a section through a quadratic surface will give a quadratic curve (although this may be a degenerate curve, i.e., a straight line) and so on.

From inspection, it can be seen that to solve for the coefficients of any of the above surfaces, the number of data points must be at least equal to the number of basis functions used to define the surface; e.g., a P_2 surface requires six points and so on. Of course we are not restricted to the combinations listed in Table 5.1; we can use any grouping of basis functions to describe a surface, the selection of the functions depending on the choice of the user. For example, the functions {1, x, y, xy} could be chosen (incidentally, termed a bilinear surface), needing four data points to estimate the coefficients.

A linear surface is used in this investigation since there are three monitor stations, and therefore three data points for each satellite at any epoch. For each point we can write an equation of the form:

$$a\phi + b\lambda + c = \text{dion}_v, \quad (5.10)$$

where a, b, c are the coefficients of the plane;
 ϕ, λ are the coordinates of any point on the plane;
 dion_v is the vertical ionospheric delay at the data point,

and with three equations, values can be found directly for a, b and c . It is then possible to interpolate the vertical delay for any other point by inserting the horizontal coordinates of the point into the equation above, with the coefficients now known.

5.3 Shortcomings of Previous Investigations for Kinematic Positioning

The above concept was originally published by Georgiadou and Kleusberg [1988a], who used a dual frequency receiver to obtain one set of coefficients for the whole observation session, making use of redundant observations by fitting the surface in a least squares sense. Wild et al. [1989] further developed the idea to include any number of dual frequency receivers. In addition, the results from this deterministic part of the model were subtracted from the L4 observations ($L1 - L2$, in metres) and the result interpreted as stochastic variations of the ionosphere. In a further step, Wild et al. [1990] introduced correlation functions in time and space for the electron content and showed that it was possible to use the stochastic information in a collocation process to improve the above deterministic model.

In each case, one set of surface coefficients was estimated for the entire observation session i.e., a time-invariant model was produced with which the delays for signals received by single frequency receivers could be interpolated. In addition the same set of

coefficients was used for all the satellites observed in the session. Since all cases were concerned with static differential positioning the time-invariance of the model was of no great concern. This was due to the fact that the stations were not moving and it was therefore the *average* of the effect of the differential ionospheric delay at the unknown point(s) over the whole observation session that was important. Also, again due to the static nature of the receivers, the change in delay would only be a function of the temporal change in the TEC, and the change in the measurement path due to the motion of the satellite.

When we consider kinematic positioning, however, we have to look at a new approach, due to factors outlined in the following sections.

5.3.1 The Need for Epoch by Epoch Delay Information

Instead of using all the information gathered in an observation session to simultaneously compute one set of baseline components for each pair of stations, we often use the information gathered at a single epoch to compute a position for that epoch, say t_i . We are therefore not interested in the average of the ionospheric delay over the whole observation period; rather, we must correct the observations for epoch t_i and compute the position of the receiver before proceeding to epoch t_{i+1} .

5.3.2 Rapid Changes in Delay

The motion of the single frequency receiver means that the satellite-receiver vector will be changing more rapidly than in the static case. Therefore the rate of change of the delay along the measurement path will be greater than if the single frequency receiver were stationary. It should be noted, however, that in extreme cases (e.g. in polar regions during a severe magnetic storm) the maximum rate of change can be of the order of 1 km/s for very short periods.

5.4 Improvements from this Research

The model developed here again uses a surface to describe the variation in ionospheric delay over the area; the parameters of the surface are derived from dual frequency measurements taken at the monitor stations. However, in contrast to the previous investigations it has the following features.

5.4.1 Time Dependent

A new set of model parameters is created for every epoch so that the more rapid change in delay described in section 5.3.2 can be accommodated. This also means that an updated value for the differential delay is computed every epoch, in accord with the epoch by epoch position computation.

5.4.2 Satellite Specific

For each epoch, a separate set of model parameters is computed for each satellite. This is necessary due to spatial sampling considerations. For any one epoch, the points where the satellite–receiver vectors cut the ionospheric shell will often be poorly distributed for the estimation of the coefficients of a surface for the whole sky. To provide a better conditioned solution a separate polynomial is used for each satellite to provide a more accurate representation of the delay in the sector of the sky which the satellite occupies at that epoch. This is not such a great concern when one polynomial is used for the whole session since the spatial distribution of the points will be more even. Outside the sector for each satellite, estimated delays may be unreliable due to lack of information.

A further advantage of the independence of the model for each satellite is that if a satellite drops out of view, the entire interpolation process remains unaffected for the other satellites still visible.

5.5 Procedural Details for Implementing the Model

Several steps must be completed between obtaining the raw measurement data, and correcting the measurements. The overall data flow can be seen in Figure 5.5, while each of the steps is detailed below.

5.5.1 Cleaning Static Data

The dual frequency data at each monitor station are pre-processed to remove noisy data and correct any cycle slips that remain. More details about the pre-processing done in this research can be found in section 6.3. It should be stressed that data from code or codeless receivers may be used.

5.5.2 Computation and Smoothing of Ionospheric Phase Delays

The phase ionospheric delays are computed using equation (3.10) for each satellite-station combination. Therefore, with m stations and n satellites we would have $m \cdot n$ time series of delays. With some types of observations, particularly those from codeless receivers, which square the signal to retrieve the carrier and consequently square the noise of the measurements, it is often judicious to apply some kind of filter. Filtering has been defined as automatic smoothing which in turn can be regarded as a method of separating signal from noise [Vaníček and Krakiwsky, 1987]. Obviously, the definitions of noise and signal will vary from application to application. The data in this research included codeless L2 observations which had been obtained via squaring the incoming L2 signal.

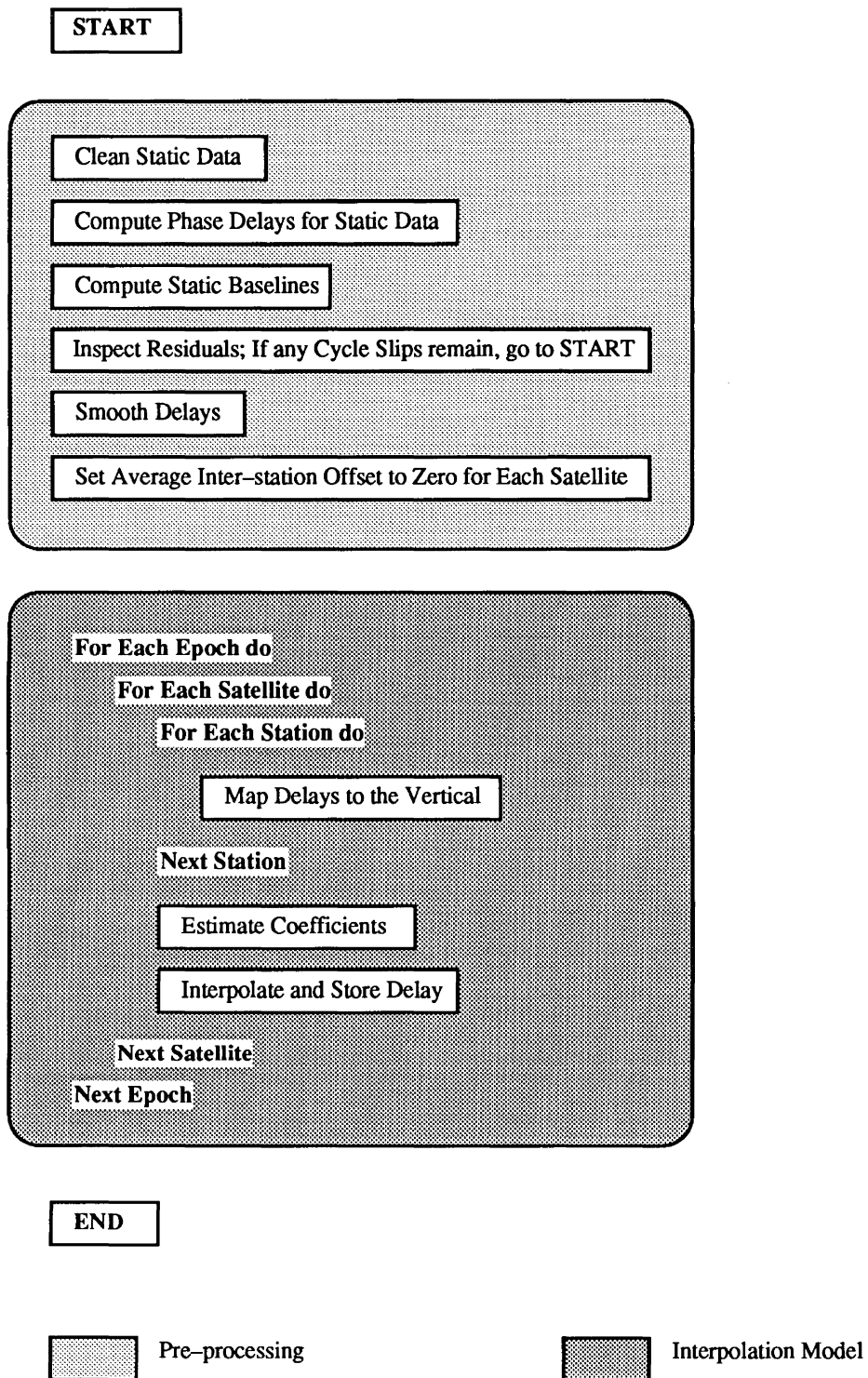


Figure 5.5 Data flow for the interpolation of delays

To dampen the effect of the noise a symmetric normalised filter (also known as a moving average) with a window of 180 s was applied to the phase delays. This kind of filter can be written

$$y = \mathbf{g}^T \cdot \mathbf{x} \quad (5.11)$$

where \mathbf{g}^T is the vector of weights describing the filter (sum of elements = 1);
 \mathbf{x} is the vector of raw data points;
 y is the filtered value at the midpoint of the window.

It has the property that it induces neither amplitude nor phase distortion in the filtered time series [ibid.] (see Figures 5.6 and 5.7).

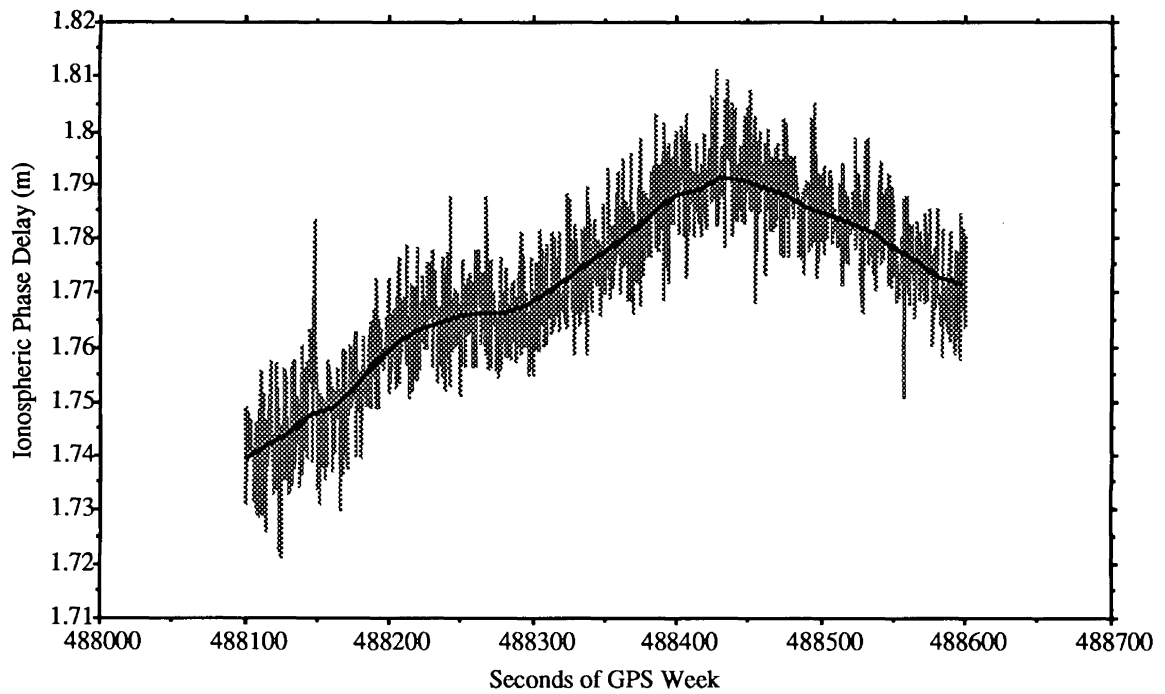


Figure 5.6 Example of raw (grey) and smoothed (solid) ionospheric phase delays for SV12 at Mallorytown

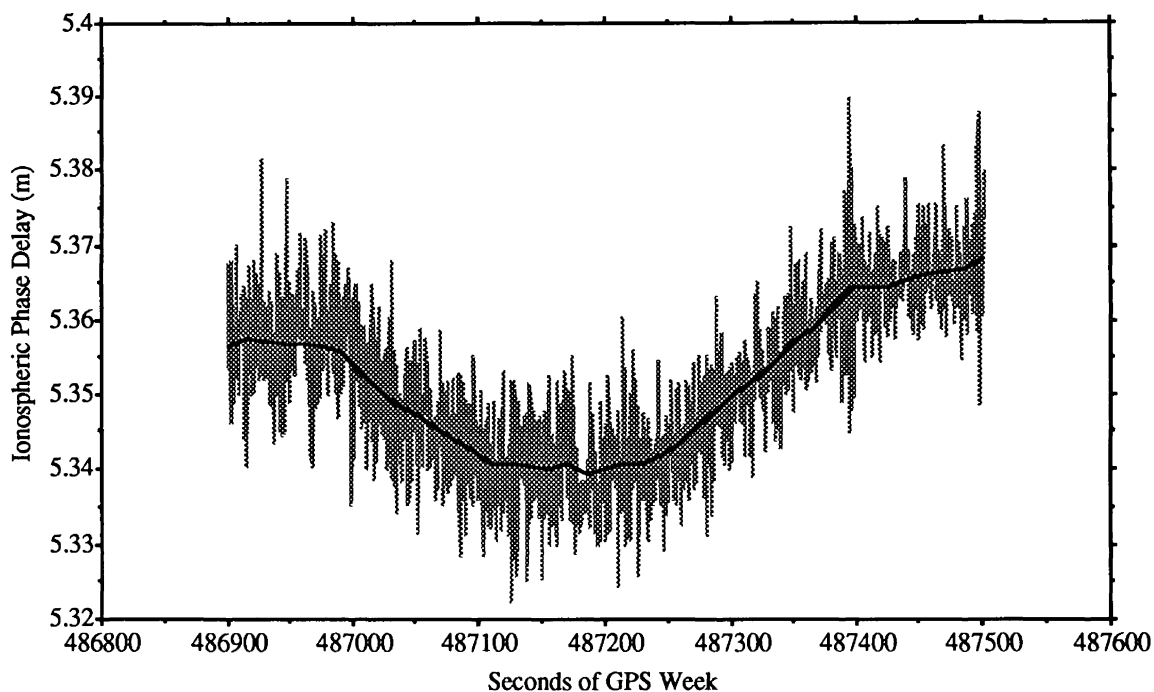


Figure 5.7 Example of raw (grey) and smoothed (solid) ionospheric phase delays for SV13 at Mallorytown

5.5.3 Setting Average Inter-station Offset to Zero

It is assumed that over the entire observation session the differential delay between the monitor stations for any one satellite is, on average, equal to zero. The reason for this follows. It has been mentioned already that delays calculated with equation (3.10) have an unknown constant associated with them, related directly to the unknown phase ambiguities at each station. A value for the phase delay for a single epoch is therefore meaningless, since the ionospheric delay for the first epoch at the last lock-on would be set to some arbitrary value. This presents a problem when we want to interpolate delays between stations since we have an unknown constant offset between the delays at two stations for any one satellite due to the fact that the ambiguities (or their double differences with the moving station) for each station will generally be different. Consider the case when we have two dual frequency ground stations, M_1 and M_2 , each with a time

series of ionospheric delays, which, for the purpose of illustration, are constant over the time interval in question.

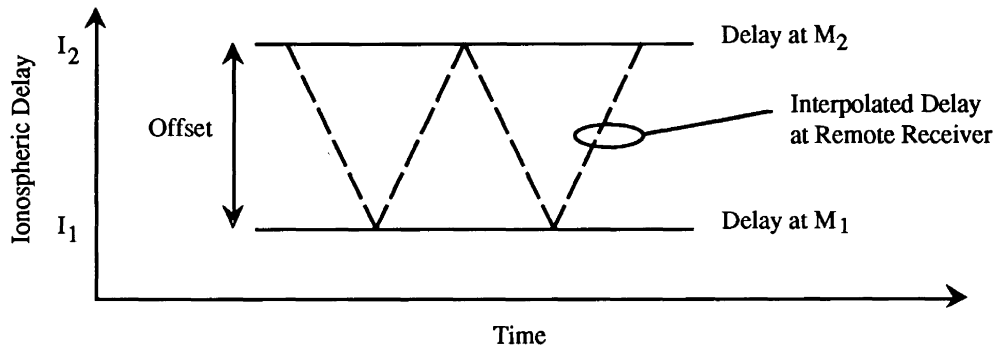


Figure 5.8 The effect on the interpolated values of the delay offset between stations.

The (arbitrary) initial values for the stations are I_1 and I_2 (see Figure 5.8). If the moving receiver were to trace a simple path back and forth between M_1 and M_2 we would end up with an interpolated delay for this receiver which contains artificially induced variations, the result of the arbitrary offset between the delays of M_1 and M_2 . The problem is therefore one of removing the effects of this offset, which is solved here by setting it to zero when averaged over the whole session. If there was some method of evaluating the absolute delay at each station e.g., by using dual frequency P-code data, this problem could be avoided.

5.5.4 Computation of Surface Coefficients

For each satellite, we now have, for every epoch, m delays. The delays are mapped to the vertical using equation (5.3). The height of the ionospheric layer is set to 350 km in this investigation, which is an approximate height for $N_m F_2$, the peak of electron density; this should therefore give reasonable locations for the sub-ionospheric points. There are three stations in this investigation and therefore a plane is fitted through the points. For each measurement we can rewrite equation (5.10) as:

$$a(\phi - \phi_0) + b(\lambda - \lambda_0) + c = \text{dion}_v, \quad (5.12)$$

where ϕ_0, λ_0 is the origin of a local coordinate system;
 ϕ, λ are the coordinates of the intersection point;
 a, b, c are the coefficients;
 dion_v is the vertical delay at ϕ, λ .

With three such equations the unknown coefficients, a, b and c , can be found. The local origin is defined in this investigation as the point defined by the average of the coordinates of the monitor stations.

5.5.5 Interpolating the Delay for the Single Frequency Receiver

Finding the delay for the remote receiver is now simply a case of finding the coordinates of the intersection point of the satellite–receiver vector with the ionospheric layer, reducing these to the local origin and substituting them into equation (5.12). This gives the vertical delay which is transformed to the delay along the measurement path by:

$$\text{dion} = \text{dion}_v \cdot \secant(z) \quad (5.13)$$

where z is again the zenith distance at the ionospheric layer. The temporal variation in delay is described by the fact that a new surface is found at every epoch. Therefore at each epoch we have n surfaces, one for each satellite.

The procedures in sections 5.5.4 and 5.5.5 are executed for every epoch, in the form of a loop as can be seen from Figure (5.5). The interpolated delays are stored in an output file and are applied to the data as detailed below.

5.5.6 Applying Corrections to the Data

Now that delays have been estimated for the observations at the single frequency receiver, they must be applied as corrections to the observations. The corrections are actually the variable part of the ionospheric term in equation (3.10), and if this term can be predicted exactly, obviously the effect of the variable part of the ionosphere will be eliminated. As explained in section 3.6, it is assumed that any constant part of the delay will be absorbed in the position computations by the ambiguity parameter.

Since the input file to the program HIPPOS contains double differences of the observations between one master station and the single frequency receiver, it is necessary to create double differences of the corrections and apply these to the file. Obviously, the same differences must be created as those that exist in the observation file, and the differencing must be in the same sense.

The result of this stage is a file containing corrected observation double differences for one master station and the single frequency receiver. This file can now be used as input to the HIPPOS software.

5.6 Assumptions Made in the Model

The following sections outline the assumptions necessary for the model to work in its present state. In making assumptions, limitations are imposed on the conditions under which the model will give useful results, and it should be realised that under certain conditions the model may perform poorly.

5.6.1 Straight Signal Path

It is assumed here that the signal from a satellite propagates along a straight line to the receiver. However, in reality, the path of the signal from the satellite is a curved line, resulting from angular refraction in the ionosphere. The effect of this on the model is to

cause the actual intersection point of the signal with the ionospheric layer to be in a slightly different location than is found using the straight line approximation. Brunner and Gu [1991], investigated, among other things, the magnitude of the deviation of the path from a straight line. For a value of $TEC = 1.38 \cdot 10^{18} \text{ m}^{-2}$, which is “typical for high N_m (maximum electron density) values which are frequently observed” [Brunner and Gu, 1991], the maximum deviation for the L1 frequency was 92.73 m for an elevation angle of 7.5° . At 15° , the deviation decreased to 55.53 m. The error in the position of the intersection point will therefore cause an error in the estimated coefficients. However, even if the maximum deviation occurred at the height of the layer, it would be negligible in comparison to the distances between the monitor stations. The straight line signal concept is therefore a valid approximation in this context.

5.6.2 Infinitesimally Thin Ionosphere

The concept of a shell-like ionosphere is used in order to give a convenient way of being able to assign the measured delay to a point, i.e., where the ray cuts the layer. Essentially this implies that all of the ionization along the signal path is concentrated at the height of the imaginary layer, and is negligible at all other heights. If it is the case that a major portion of the electron density along the path is in reality at a quite different height, the model is effectively assigning the delay to a wrong location. The magnitude of this error depends on both how distant the ionization is from the layer, and how obliquely the path intersects it; the greater the zenith distance, the greater will be the error.

Another consequence of this concept is that it is entirely possible for a point on the layer to have two or more different values of delay assigned to it. A situation such as this would occur when signals from two satellites passed through areas of differing electron density, but intersected the imaginary layer at the same point. Of course, if the electron density was really compressed into a shell, both signals would be delayed by the same amount.

5.6.3 Mapping Delays to the Vertical

In mapping measured slant delays to vertical by equation (5.3) and vice versa by equation (5.13), there is an implicit assumption made that the electron density profile along the slant and vertical paths is the same, i.e., the same electron density is encountered at the same height for each path. Again, the more oblique the slant path, the greater the distance between it and the vertical profile it is supposed to represent, and therefore the more likely the assumption is invalid due to differences in electron density along the paths.

5.6.4 Average Inter-station Offset is Zero

This assumption is made necessary here by the type of data used in this research; it is also the most likely to be proved fallacious. Its validity depends on both the behaviour of the time series of delays at each monitor station and the location of the remote receiver. Let us consider the case where the slant delays at one of the monitor stations, say M_1 , are in reality offset from those at the other stations by a constant, k . When the data are preprocessed, k is set to zero which in turn introduces an error into the coefficients of the surface; in general, the effect of this error will vary over time, since the model uses vertical delays, and the offset between these will not remain constant. The error in the interpolated delay is therefore a function of time and the position of the remote receiver; the closer it is to M_1 , the greater will be the error, and it will be greatest when the receiver lies on the signal path to M_1 , since it is at this location that the error has been induced.

To avoid the errors caused by this assumption, or at least reduce them to a negligible level, it is necessary to select monitor stations which are close enough to ensure that the value of the offset will never exceed the specifications of the project. In reality the offset may prove significant for stations separated by 30 – 40 km or more, especially when the signal path to each station passes through differing physical environments, e.g., night and

day, or auroral and mid-latitude ionospheric regions. Since the offset will not be known without access to absolute measurements of ionospheric delay or TEC values, which in turn would eliminate the need for this assumption anyway, it is necessary to plan the location of the monitor stations with this in mind.

5.7 Redundancy and the Numerical Stability of the Surface Determination

A few remarks should be made concerning the reliability of the solution for the coefficients. The best-conditioned solution will be provided if the data points are evenly spread over the area in question, e.g., if there are three points, they should form an equilateral triangle. There is, of course, the pathological case of all the points being colinear, resulting in no solution. However, perhaps of more concern are those cases where the points are nearly, but not quite, colinear, giving a solution, but which is poorly-conditioned. Care should be taken to avoid situations such as this.

Additionally, caution should be used when the minimum number of data points is used to determine a particular kind of surface, i.e., an exact solution is obtained. In this case there are no residuals available to provide a check on the reliability of the data points. One way of circumventing this problem is to examine the time series of delays for each satellite-station pair and ensure that each shows a smooth change over time; any discontinuities should be investigated as to their cause. Of course, this does not exclude the possibility that the entire time series is biased by some error.

Chapter 6

Test Data and Results

6.1 Test Data

To test the model described in the previous chapter, data were obtained from an experiment undertaken jointly by the Canada Centre for Remote Sensing (CCRS) and the Canada Centre for Surveying (CCS), on day 278 (5th October) of 1990, in Ontario near the Canada/U.S.A. border (see Figure 6.1).

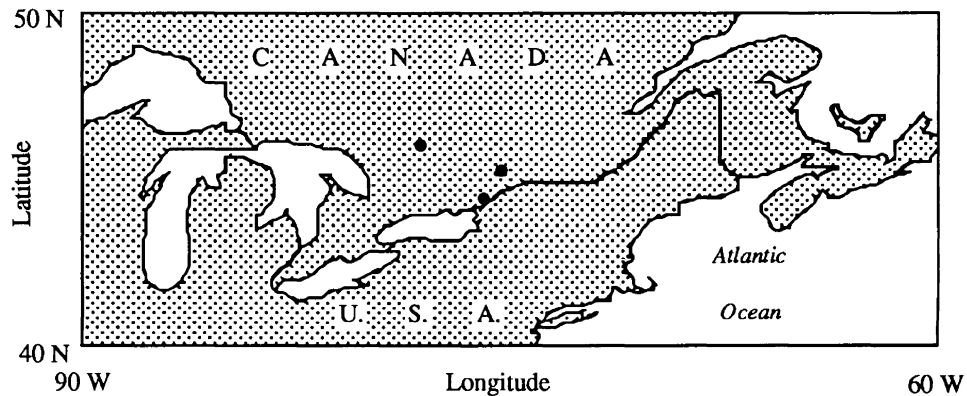


Figure 6.1 Location of the survey area — the three monitor stations are shown

As shown in Fig 6.2, the remote receiver was mounted on an aircraft (station name Falcon, or FA) which was taking part in a Remote Sensing experiment using the Multi-element Electro-optical Imaging Sensor (MEIS). The receiver was a dual frequency Ashtech MD-XII receiver, but the L2 antenna input was being used for other purposes —

therefore, only L1 carrier phase data, C/A-code pseudoranges and instantaneous Doppler measurements (L1 cycles/second) were available from the aircraft. A Litton LTN-51 inertial navigation system was also mounted on board. Before the aircraft took off, the aircraft-mounted antenna was placed as close as possible to a known control point on the ground, and an azimuth and distance were measured from the point to the antenna in order to calculate the offsets from the point to the receiver. In this way, reasonable estimates for the initial position of the antenna were obtained.

Three monitor stations were employed (Mallorytown (MA), Metcalfe (ME), and Algonquin (AL)), each with an Ashtech MD-XII receiver, recording C/A-code pseudoranges, dual frequency carrier phases and instantaneous Doppler measurements (see Table 6.1 for station coordinates). These stations had been fixed prior to the above experiment by GPS observations. At all three monitor stations, data were collected at an interval of 0.5 seconds between approximately 13h20 UT and 16h30 UT. The sampling interval for the aircraft was also 0.5 s, but the receiver was not switched on until 14h00 UT (see Figure 6.3). The trajectory of the aircraft and the positions of the monitor stations can be seen in Figure 6.4.

Station	Latitude	Longitude
Mallorytown	N44° 28' 20"	W75° 52' 05"
Metcalfe	N45° 14' 34"	W75° 27' 30"
Algonquin	N45° 57' 21"	W78° 04' 17"

Table 6.1 Coordinates of Monitor Stations

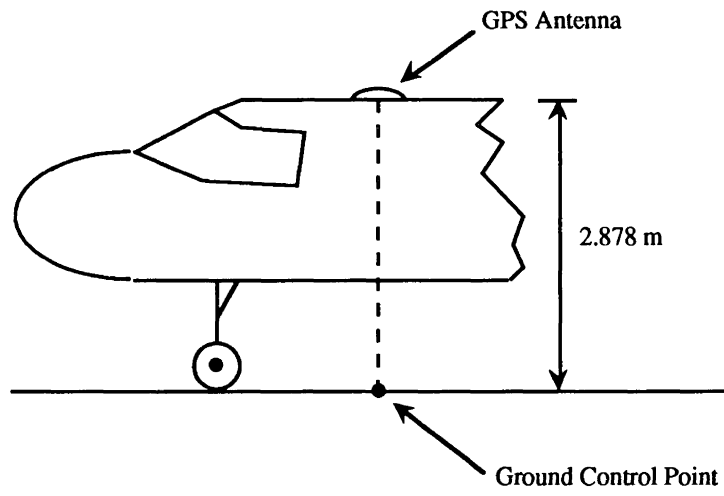


Figure 6.2 Location of the GPS antenna on the aircraft

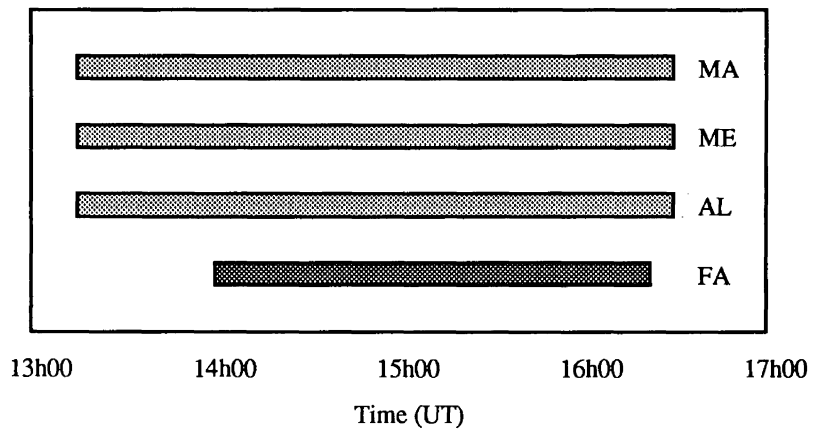


Figure 6.3 Observation sessions at all receivers

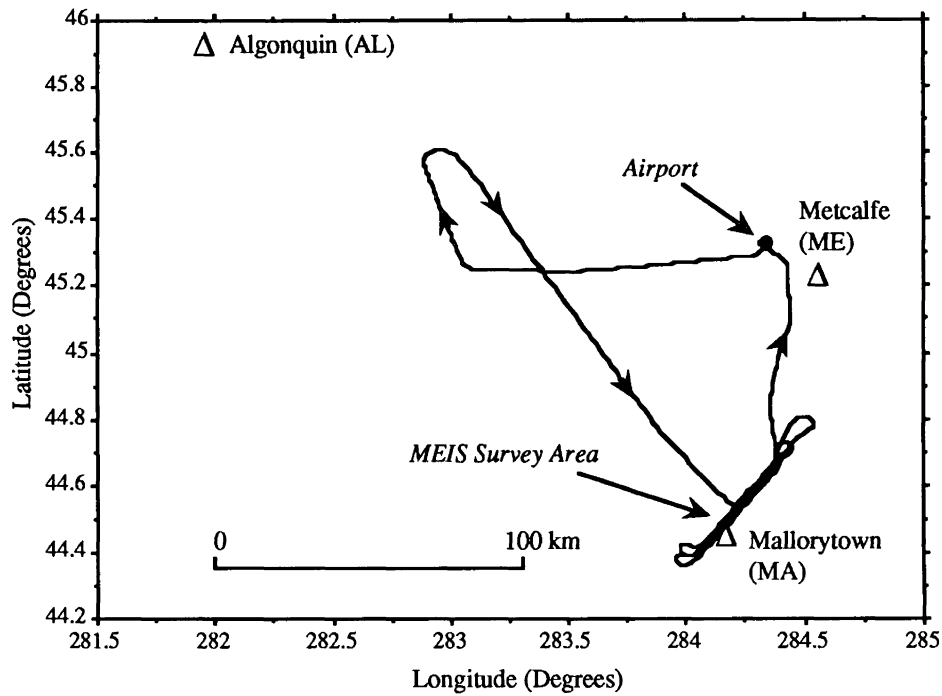


Figure 6.4 Trajectory of the aircraft and the locations of the monitor stations

6.2 Problems with the Data

Due to several factors which are outlined below much preprocessing of the data was necessary before the model could be implemented.

6.2.1 Data Volume

Due to the small measurement interval of 0.5 s, each data file occupied about 10 Mbytes of disk space. Although this was not a problem in itself, handling such large and unwieldy files was quite inconvenient, mainly because it took a long time read and write the entire file even if only a small change was made. In addition, it was obvious from processing a 15 s subset of the data that using the 0.5 s data for the same purpose would have required many hours. To avoid this, the beginnings of the files from the ground stations were deleted up to the epoch when the aircraft receiver was switched on. Furthermore, while the 0.5 s data were used to detect and remove cycle slips and

calculate the ionospheric phase delay for the monitor stations, 15 s data were used for computing the positions of the aircraft.

6.2.2 Data Quality

The Ashtech MD–XII receivers used in the experiment cannot extract the P–code from the received signals. Therefore, in order to get two signals at different frequencies to obtain a value for the phase delay, it is necessary to square the received L2 carrier signal. This results in an L2 signal with twice the frequency of the original, while also destroying any code or message on the carrier. Although we now have a means of calculating the ionospheric delay on the L1 carrier, the noise on the L2 signal is also squared, giving a smaller signal to noise ratio (SNR). This ratio is a measure of the relative strengths of the received signal, and the noise at the frequency of the signal. Obviously a smaller ratio indicates noisy, and therefore poorer quality data. This disadvantage is compounded by the fact that the L2 signal is transmitted at a lower power than the L1 [Melbourne, 1989]. Only fractional phases are recorded in this particular type of receiver for the L2 data, while the integer number of cycles is calculated for this frequency when the data is decoded using the whole cycle count for L1. Assuming the differences in the biases between the frequencies is small over the measurement interval, the change in the integer number of L2 cycles over this period is directly related to the change in cycles on L1.

The data used in this research were collected using Ashtech MD-XII receivers. Unfortunately, the firmware installed in these receivers at the time of collection (October 1990) could cause a deterioration in the SNR of the signal at high data collection rates, as is the case in this dataset. The reason for this is that the value obtained for an observation includes information obtained during the whole time interval since the last observation, i.e., the observation is not an instantaneous measurement of the phase of the carrier signal, but a figure that is the result of this information being passed through a filter to reduce the noise level, and the more observations included in this filtering process, the

more the noise will be decreased [Kleusberg and Georgiadou, 1991a]. This could be illustrated by plotting a graph of SNR vs. collection rate, but unfortunately a receiver with an old enough version of the firmware could not be obtained. Since the receiver firmware and hardware have been improved considerably since then, collecting data for illustration of this phenomena now would not give valid results [private communication, Sergei Gourevitch, Ashtech, Inc., 1993]. An indication the SNR for one of the satellites observed during the experiment is shown in Figure 6.5. The quality indicator on the vertical axis is directly proportional to the true SNR [ibid.].

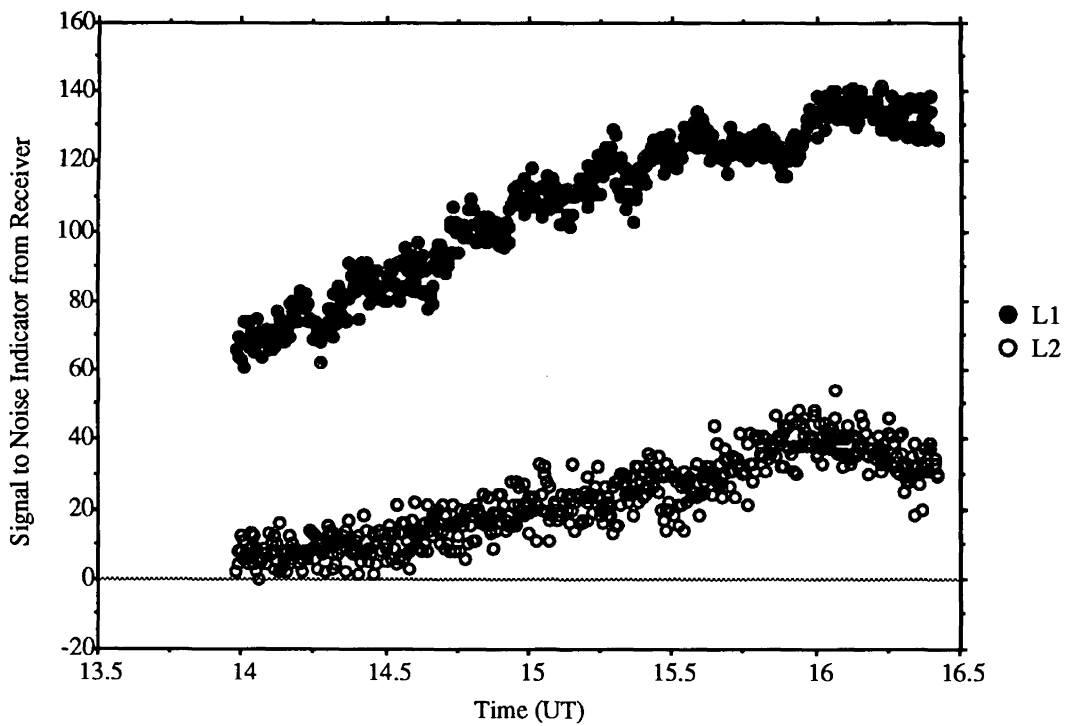


Figure 6.5 Indication of signal to noise ratio of phase observations for SV 13 at station Metcalfe

6.2.3 Incorrect Ephemeris Data

Once it was felt that all cycle slips had been corrected (described in section 6.3), the L3 solution (which is free of first order ionospheric delay) was computed for each baseline to

provide a check and to see if there were any other problems with the data. It was found that the residual plots for the double differences using SV 13 showed a periodic variation in the form of a sine wave with an amplitude of up to 20 cm; obviously, this would adversely affect the evaluation of the model if not corrected. After examining the ephemeris data, it was found that two of the records for SV 13 had reference time tags that were 496 s different from the hourly reference times (multiples of 3600 s). After removing the suspect records and recomputing the baselines the oscillation disappeared. It is not clear why these erroneous records were present, but the author has seen instances of this in other datasets, both from Ashtech and Texas Instruments TI-4100 receivers.

6.3 Data Pre-processing

It has been common practice in previous investigations to pass the raw data through a filter to remove all measurements below a certain SNR threshold. However, when this procedure was carried out on the above data, so many of the observations were eliminated as to render the dataset of little use. After experimenting with more tolerant thresholds and achieving only marginal improvements, it was decided to simply accept all of the data and delete sections which seemed to be more noisy as a whole. However, despite this, much time was still spent removing cycle slips from the data, all of which were on the L2 signal. The data was passed through a very elementary pre-processor, which simply calculated the satellite coordinates and formed double-differences of the ranges for the static baselines. No cycle slip detection was performed at this stage. Next, the L1 and L2 solutions for the baselines were computed using the DIPOP package [Kleusberg et al., 1989]. The residuals were inspected to detect cycle slips, which would appear as sharp jumps in the time series. These jumps can be either positive or negative and will be close to an integer number of wavelengths in magnitude.

With knowledge of the time tag, the number of cycles, and frequency of the cycle slip, it was possible to track down the satellite-receiver pair for which the slip had occurred.

This was done by looking for discontinuities in the time series of the phase delays for all four satellite–receiver combinations of the double–difference; error–free phase delays appear to change smoothly over time, and this would certainly be the case with data at a collection rate of 0.5 s. It would be very unusual to see changes in the delay of the magnitude of one cycle over such a short time period, and it is therefore unlikely that a real change in the data would be mistaken for a cycle slip. Computing the L3 ionosphere–free solutions allowed a check to see if any slips had escaped detection by being masked by the ionospheric contribution to the residuals.

This turned out to be an iterative process, since some cycle slips were not evident until others around them had been corrected. One of the more tedious aspects of this stage of the project was ensuring that there were dual frequency data for four satellites from the time the aircraft receiver was switched on until the aircraft landed. As chance would dictate, initially only three satellites with clean data were visible for each of the first and last half–hours of the session (SVs 2, 6, 9 and 12, 13, 14 respectively). After much editing, the data for SV 13 were extended to the beginning, and those for SV 9 to the end, ensuring a minimum of four satellites for the whole session.

6.4 Static Baseline Computation

The main purpose of computing the baselines between the ground–based stations was to check and correct any errors in the data, as outlined above. However, this undertaking also provided an opportunity to see if there was any correlation between the residuals from the L1 and L2 adjustments, and the variation in phase delays computed from the same data. Figure 6.6 is one example of this — the correlation between the variations in the delay and the residuals is obvious. The linear trend apparent in the curve of the delay has been absorbed by the coordinates in the baseline adjustment, and therefore does not show up in the residuals. On the premise that since the correlation between the ionospheric delay and the residuals of the static adjustments was so high, then the same

would be true for the mobile data, it was felt that validation of the model could proceed, i.e., most of the error in the positions could be attributed to the ionosphere.

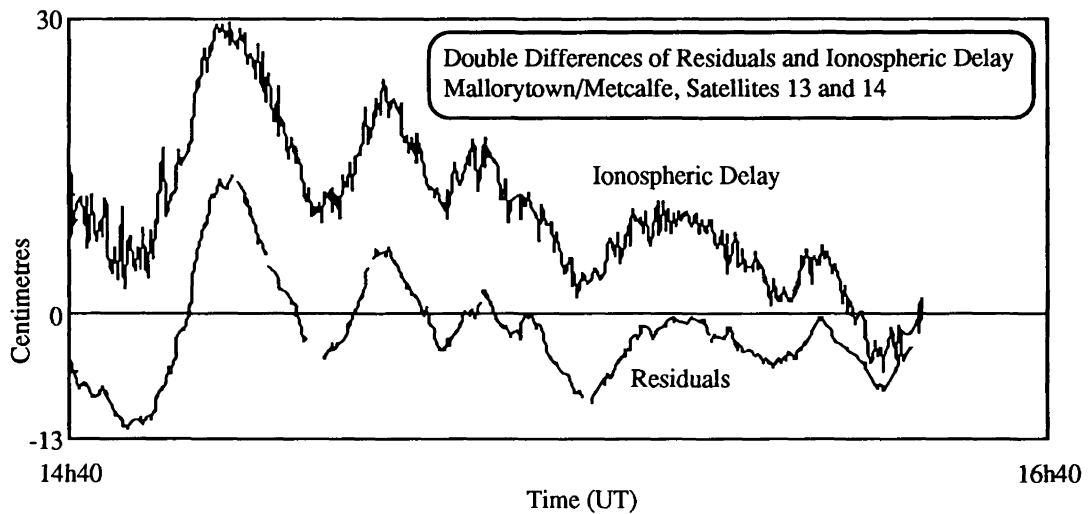


Figure 6.6 Example of the correlation between the residuals and the ionospheric delay

6.5 Computation of the Aircraft Trajectory and Model Validation

The trajectory of the aircraft was computed with the GPS kinematic positioning software HIPPOS using all three measurement types indicated above. Obviously, the best method of checking the validity of the model would be to compare the results with those from a dual frequency receiver on the aircraft. However, since only single frequency data were available from the aircraft this was not possible. Also, the data from the LTN-51 inertial navigation system proved to be useless for the purposes of this investigation since the resolution of the measurements was 0.00137° , or about 140 m in latitude and 100 m in longitude, these figures being too large by far to check the results.

To evaluate the performance of the model, three separate solutions were computed for the aircraft at each epoch, with respect to each of the monitor stations, Mallorytown (MA), Metcalfe (ME), and Algonquin (AL) using the original, uncorrected L1 data. The next

best alternative for evaluation of the performance of the model was thought to be to difference the solutions to see the amount of agreement (or lack thereof) between them. After running the model and applying the results to aircraft data, three new solutions could be calculated. These were then differenced to see if the degree of agreement had increased; this should be so if the reasoning behind the model is correct.

Several figures will be referred to in the following discussion of the results. It should be noted that these figures, showing the time series of the differences between various solutions, are arranged so that one component of the position occupies a whole page, with the difference from the uncorrected data at the top, and that from the ionosphere-corrected data at the bottom. It is felt that this is the best arrangement to facilitate direct comparison of the results.

6.5.1 Difference Between the MA/FA and ME/FA Solutions

From the upper plots of Figures 6.7, 6.8 and 6.9 it can be seen that all three position components exhibit systematic variations using the uncorrected data. The range of the variations (disregarding extremes caused by data spikes) is 53 cm in latitude, 35 cm in longitude and 2.27 m in height, and are particularly noticeable between 14h30 and 15h30. Obviously these are the result of some systematic error in the observations. If these errors are due to the ionosphere, the variations should be reduced after application of corrections derived from the model, depending on how close an approximation the model is to reality. The height is affected more due to the geometry of the situation; since all the satellites are above the stations, the solution for the vertical component of an estimated position is weaker than that for the horizontal components, since satellites will be generally more evenly spread in azimuth, i.e., the vertical dilution of precision (VDOP) is greater than the horizontal dilution of precision (HDOP).

The mean, standard deviation and range (computed without spikes) of the three components are given in Table 6.2. The spikes are all caused by a change in the visible constellation of satellites, i.e., a measurement from one satellite is not recorded at that particular epoch for some reason, perhaps because the signal path is momentarily obstructed.

	Latitude (m)		Longitude (m)		Height (m)	
	Uncorrected	Corrected	Uncorrected	Corrected	Uncorrected	Corrected
Mean	0.100	-0.049	0.063	-0.049	0.294	0.183
Standard Deviation	0.096	0.040	0.072	0.021	0.450	0.090
Range	0.525	0.216	0.345	0.110	2.271	0.428

Table 6.2 Statistics before and after using the model; solutions using MA & ME

The lower plots in each of Figures 6.7, 6.8 and 6.9 show differences using the corrected data. Immediately obvious is that the larger fluctuations seen previously have largely disappeared. Consequently, the range in the discrepancies for all three components is greatly reduced, but especially so for height, which is to be expected if, as is suspected, the cause of the large variations using the uncorrected data are due to the ionosphere. The discrepancies are now generally 10 cm or below for latitude and longitude, and 40 cm for height. Over a distance of 100 km, 10 cm represents a relative error of one ppm.

From Table 6.2, it can be seen that in all cases, the mean is closer to zero, indicating better overall agreement between the solutions, the standard deviations have decreased, indicating less variation in the differences, and the maxima and minima have become less extreme, again a sign of closer overall agreement.

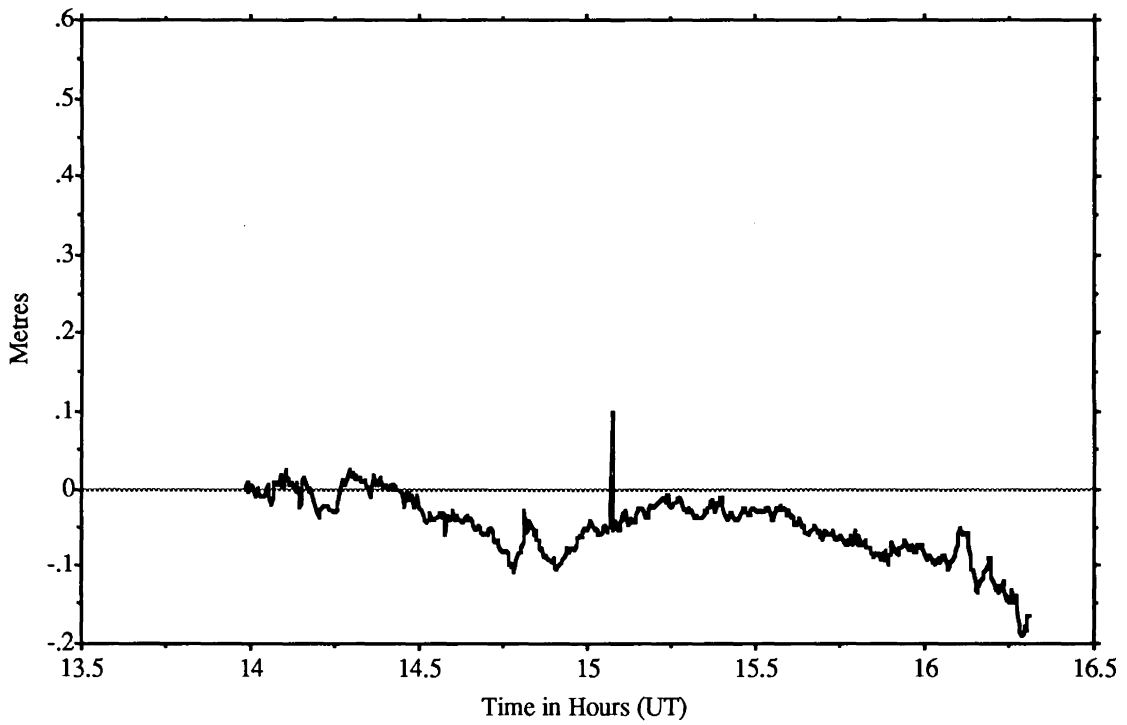
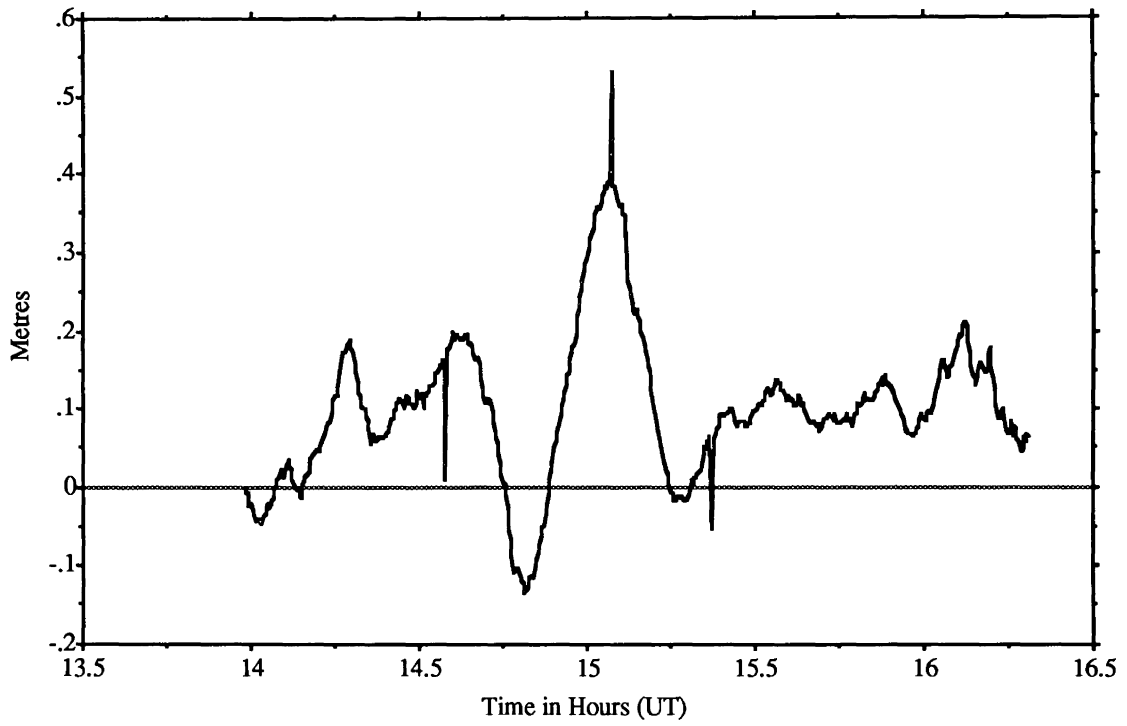


Figure 6.7 Latitude differences between MA/FA and ME/FA solutions

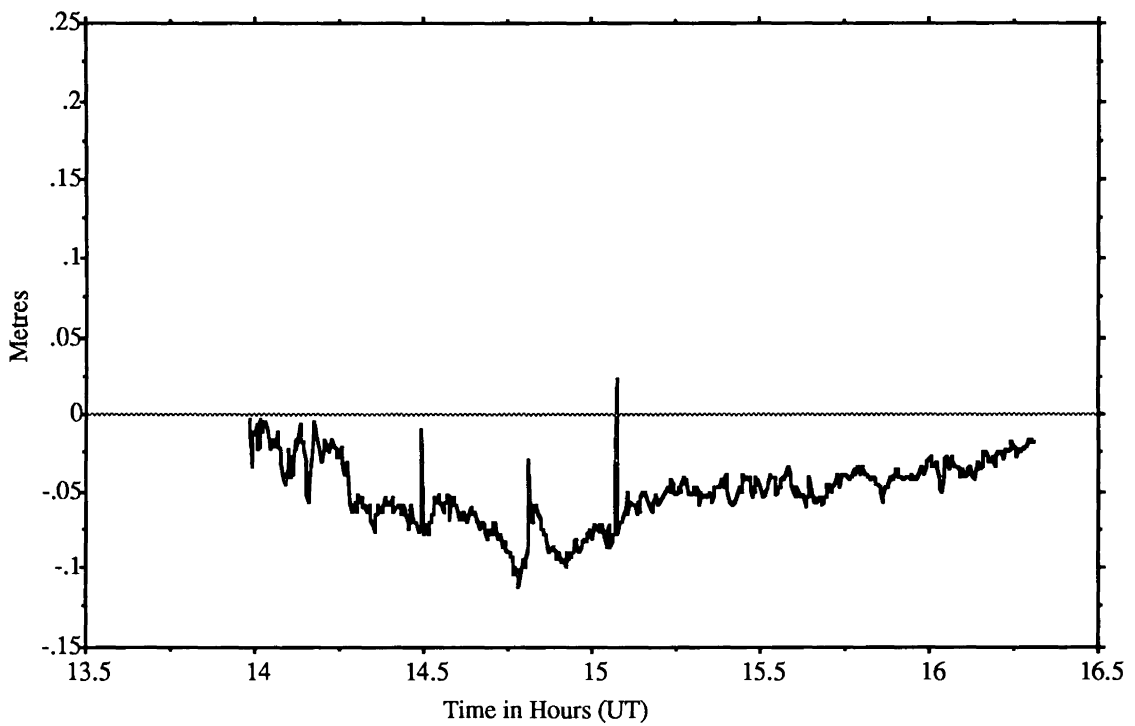
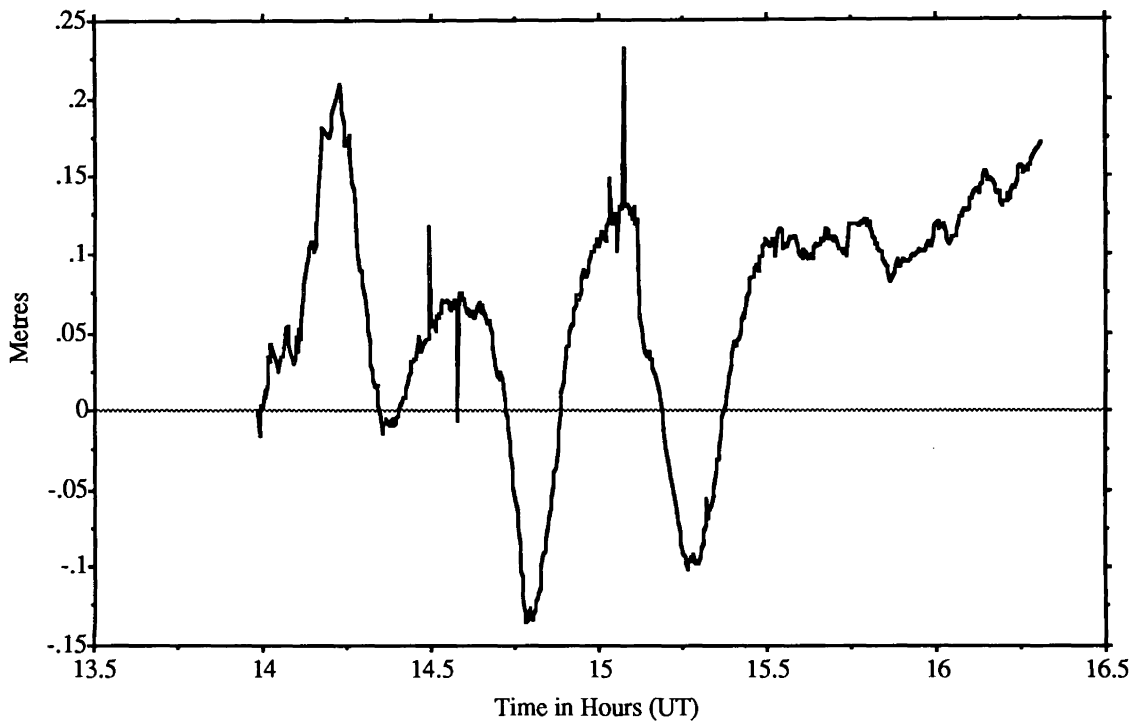


Figure 6.8 Longitude differences between MA/FA and ME/FA solutions

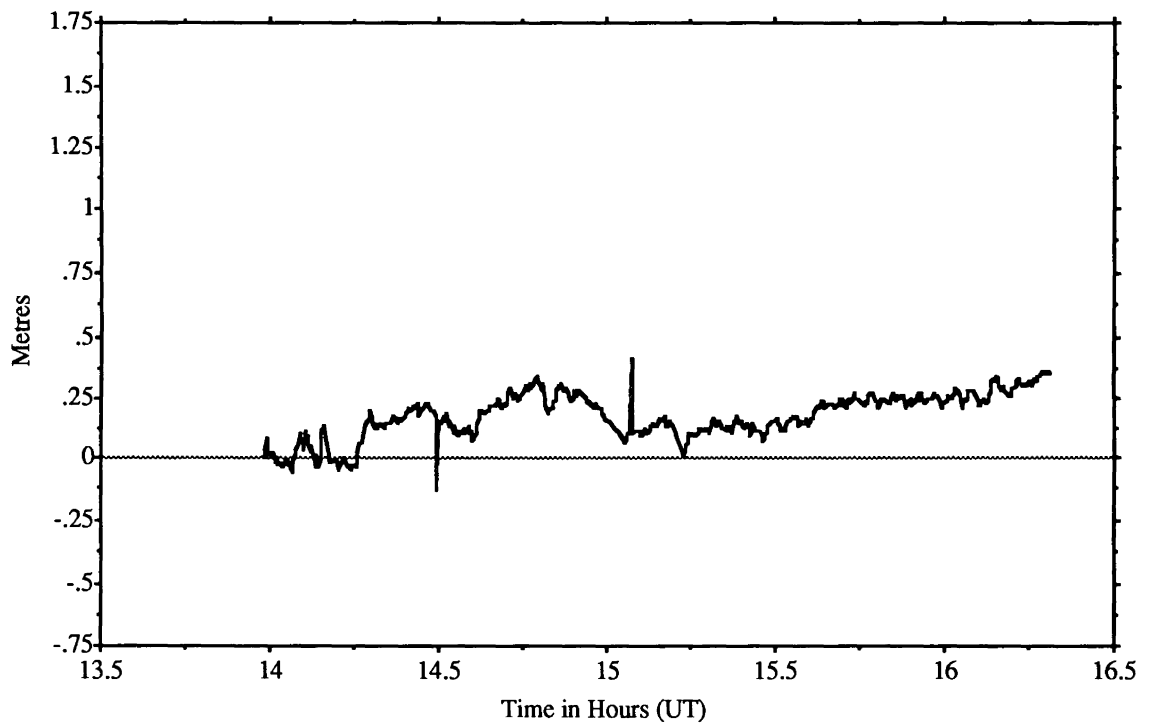
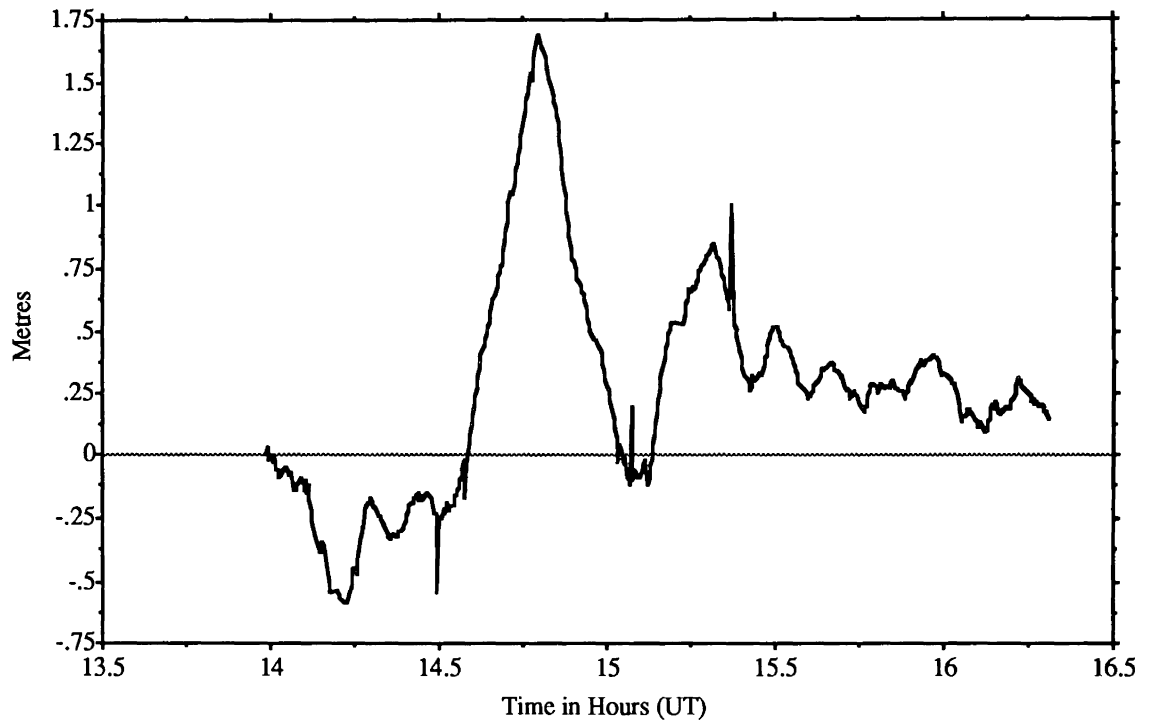


Figure 6.9 Height differences between MA/FA and ME/FA solutions

6.5.2 Difference Between the MA/FA and AL/FA Solutions

The third solution for the aircraft was calculated with respect to the Algonquin receiver and was differenced with the solution using Mallorytown as the base station. Since Algonquin was relatively far from both MA and ME (about 220 km) and the aircraft was generally closer to the other two stations it was expected that the differences would be bigger, due to the greater disparities in ionospheric delay between the signals received at different stations.

	Latitude (m)		Longitude (m)		Height (m)	
	Uncorrected	Corrected	Uncorrected	Corrected	Uncorrected	Corrected
Mean	-0.667	0.199	-0.325	0.021	2.243	0.150
Standard Deviation	0.894	0.143	0.410	0.043	2.678	0.397
Range	3.268	0.451	1.240	0.186	7.499	1.604

Table 6.3 Statistics before and after using the model; solutions using MA & AL

The upper plots in Figures 6.10, 6.11 and 6.12 show this to be the case. The differences in latitude reach extremes of ± 0.5 m until 15h15, when the solutions start to diverge, until at the end of the session they differ by 2.7 m (see Table 6.3 for statistics). Longitude again shows the least difference between solutions, but as before systematic variations are obvious, and are greater than those for the MA/ME difference.

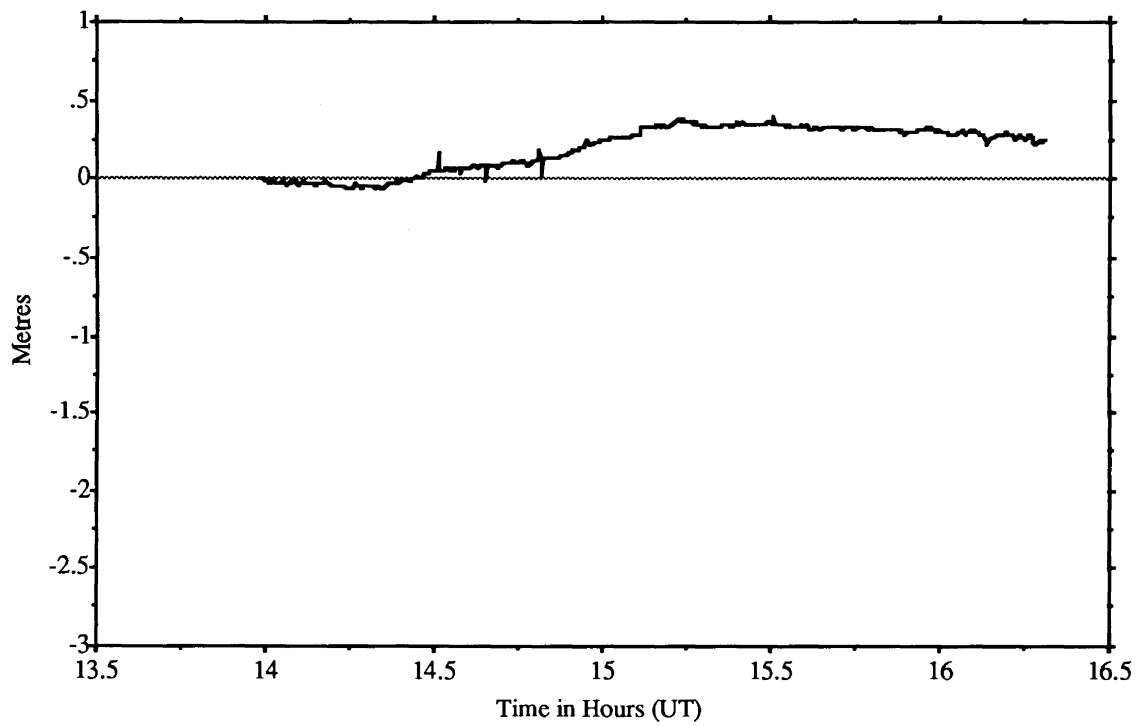
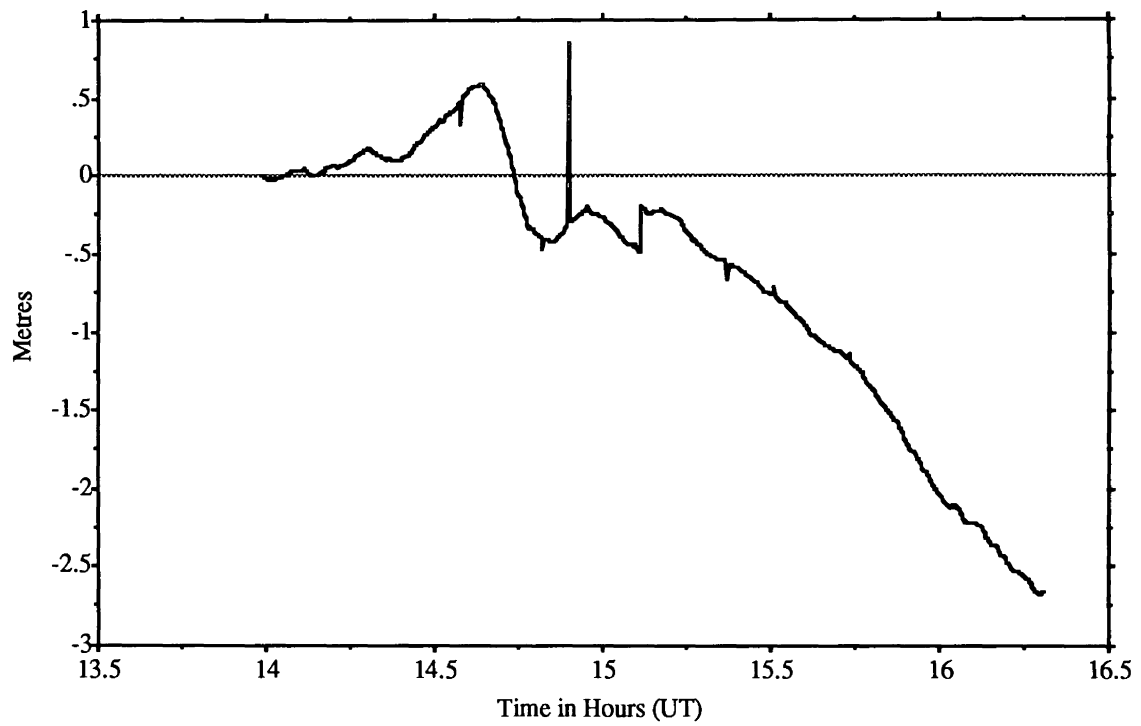


Figure 6.10 Latitude differences between MA/FA and AL/FA solutions

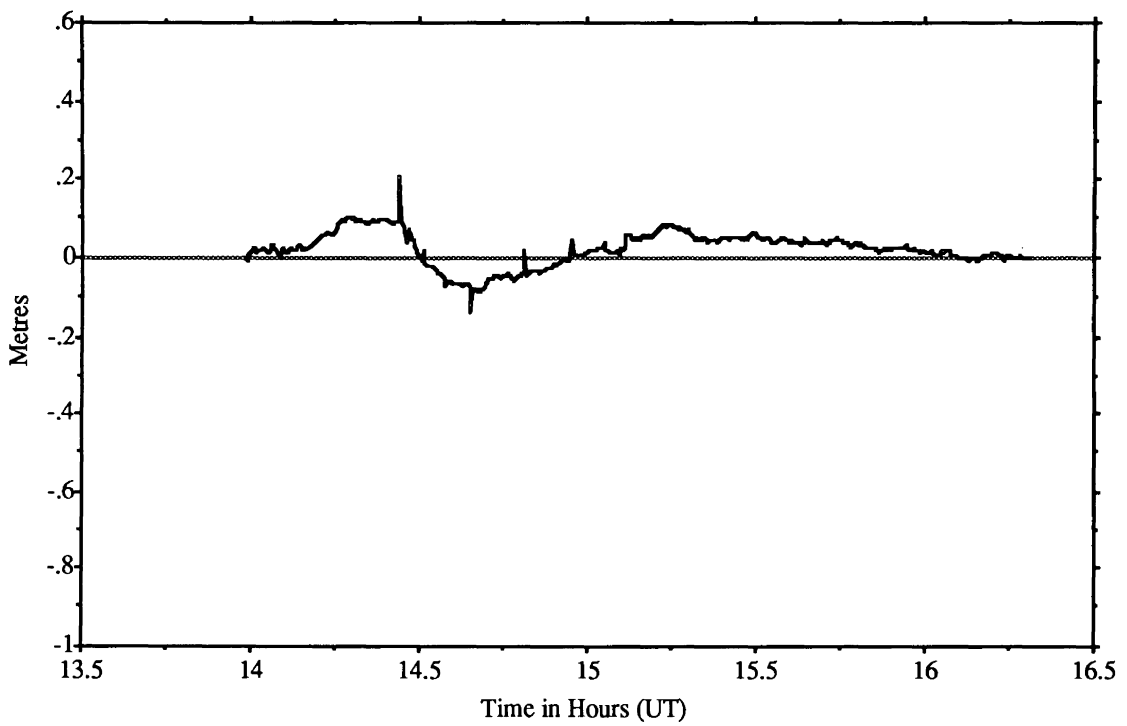
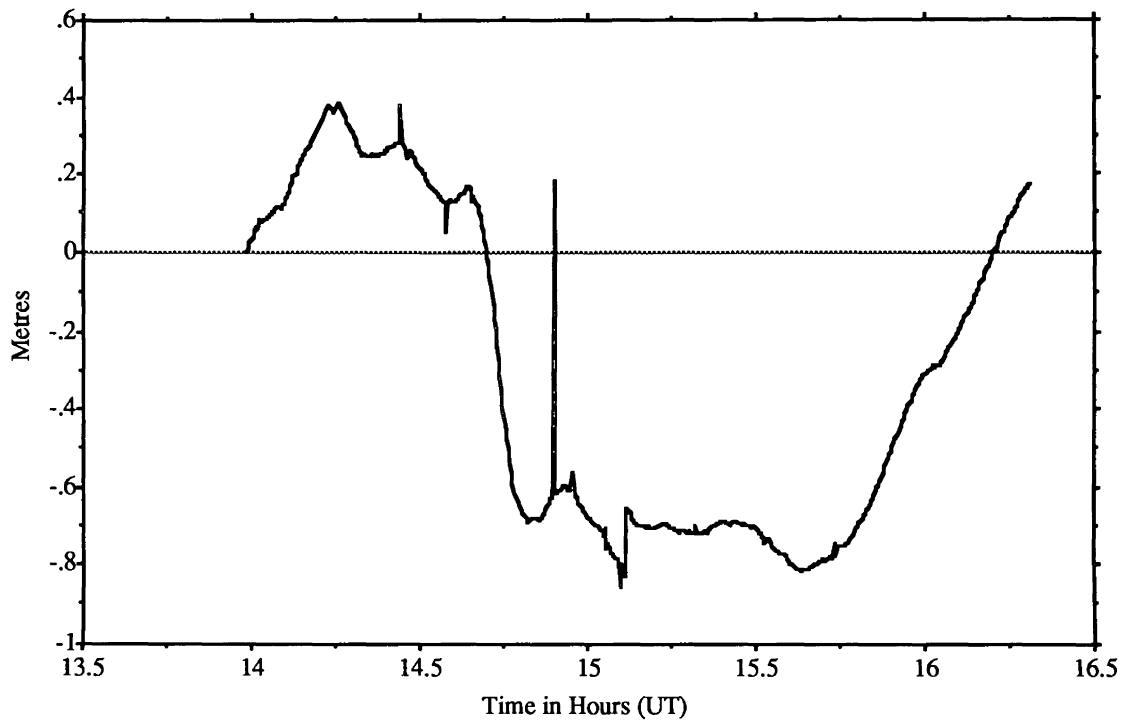


Figure 6.11 Longitude differences between MA/FA and AL/FA solutions

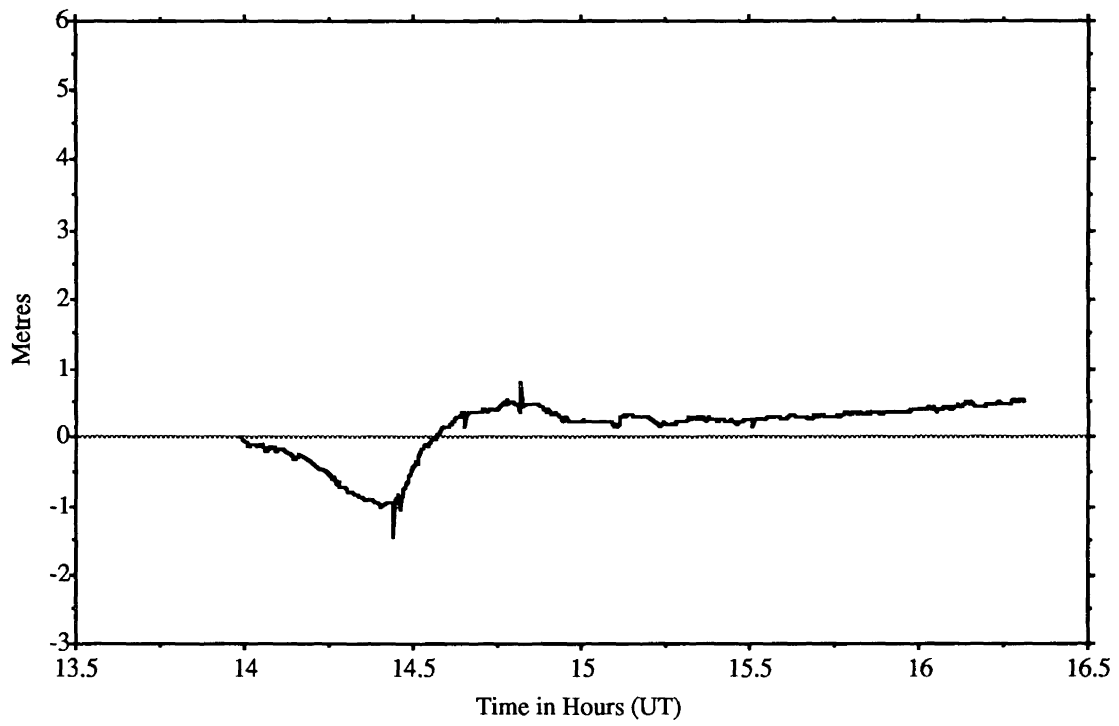
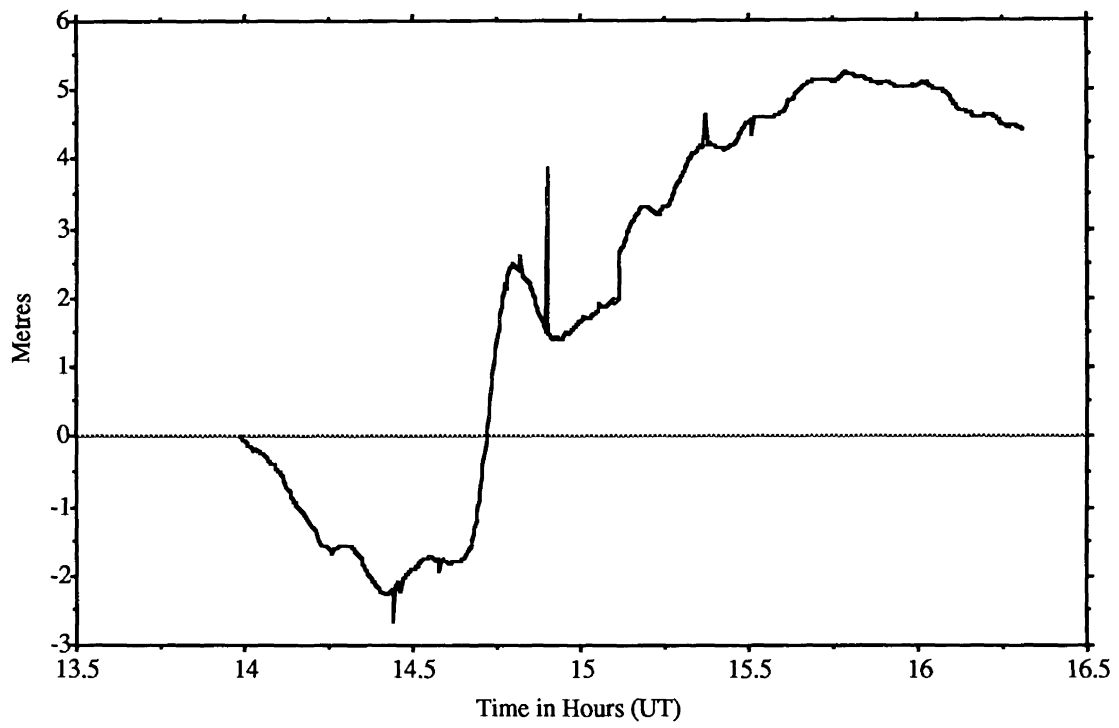


Figure 6.12 Height differences between MA/FA and AL/FA solutions

The height component is again the worst of the three, and now shows differences of up to 5.25 m. Indeed, after 15h00 the discrepancy is never below 2.0 m and is generally much greater. The corrected solutions again show greater accord. The divergence in latitude towards the end of the session has been eliminated and the large discrepancies in latitude and longitude have disappeared. As before, the means are closer to zero (especially that for height), and the standard deviation and ranges have decreased as well. In general, the corrected differences between the MA and AL solutions show the same improvements as those between the MA and ME solutions, but to a greater degree in relative terms. In addition, the improvements in the height discrepancies for both the MA/ME and MA/AL solutions show the greatest absolute changes.

6.5.3 General Remarks

A noticeable feature on all three of the uncorrected plots of Figures 6.10, 6.11 and 6.12 is a sudden jump just after 15h00, which evidently disappears when the corrected data is used. In fact, a similar jump at exactly the same epoch is present in the uncorrected plots of Figures 6.7, 6.8 and 6.9, but is not so discernable. Again, the corrected plots show no sign of the jump. Initially, the cause of this was thought to be a cycle slip in the L1 data, since it was visible when L1 data alone were used, but not so when L2 was included. However, no cycle slips could be found in any of the 24 satellite/receiver combinations possible at the epoch indicated. The cause was finally found to be the disappearance of SV 6 below the horizon; this is exactly the same as for the data spikes, except the satellite does not reappear. In both cases, the solution is responding to a sudden change in the information available; results given by Greenspan et al. [1991] also show a jump in the GPS-derived positions due to a change in the visible constellation. The spikes and the discontinuity serve to show the inconsistency of the measurements, i.e., a different solution will generally be found for every different subset of four satellites used.

It is interesting to note that after application of the corrections to the data, the magnitude of some of the data spikes remains virtually unchanged whereas others disappear. In the latter case it seems the measurements are now in greater agreement, and it is conjectured that the amount by which the spike decreases depends on the geometry of the situation and the influence of other biases at those epochs. Note also that the discontinuity disappears.

If nothing else, these results generally indicate a greater degree of agreement between the solutions.

Chapter 7

Summary, Conclusions and Recommendations

7.1 Summary of the Research

It was stated in Chapter One that the objective of this research has been the mitigation of potentially the largest factor in the error budget of GPS users, namely refraction of signals caused by free electrons in the atmosphere. Range errors due to this effect of up to 150 m are possible. Since the errors will propagate into any solution for parameters, many groups of users need to use methods to reduce or eliminate their effects. This thesis has presented one such method which can be employed in a post-processing mode for either static or kinematic data. It computes corrections to satellite-receiver double differences of phase measurements which are then used as input to positioning software, which in turn estimates differential positions and velocities for a remote receiver. The model which has been demonstrated here estimates ionospheric delays at the frequency of the L1 signal for the remote receiver, based on dual frequency GPS measurements at a number of monitor stations; the receivers at these stations may be either code-correlating or codeless. A surface, in the form of a bivariate algebraic polynomial, is then used to describe the spatial variation in ionospheric delay at L1, based upon the delays from the monitor stations. Temporal variations in the delay are catered for by the estimation of a different surface for each epoch. This thesis has therefore presented a deterministic approach to modelling ionospheric delay errors in GPS carrier phase measurements.

To evaluate the model, test data were used from three dual frequency monitor stations and an airborne single frequency receiver. Although this scenario fulfilled the minimum requirements of the model (three monitor stations are required to form a plane, the most basic surface), the lack of either ionospheric delays, or sufficiently accurate ionosphere-free positional information for the remote receiver meant that a complete verification of the model was not possible; i.e., a comparison between the solutions for the position of the aircraft after correction by the model and ionosphere-free, reference solutions for the same, could not be made. Therefore, in order to be able to draw some conclusions, three separate solutions were obtained for the position of the remote receiver, one with respect to each monitor station, and the discrepancies between these were examined before and after application of the model to the L1 data. The conclusions obtained from an analysis of the results are presented below.

7.2 Conclusions

It was shown in the previous chapter that after application of the model, the systematic variations in the discrepancies between solutions were generally reduced, in some cases by as much as an order of magnitude. However, this does not necessarily mean that the corrected solutions are better than the original ones and merely indicates that the solutions proved to be in greater agreement after the model was applied. Of course, if the two solutions in each comparison were correct, there would be no discrepancies. Without a reference solution for the remote receiver, it is not possible to state without reservation that the model did improve the single frequency solutions. However, since all three solutions were in good agreement, unless they are all biased by some common error, roughly equal in magnitude in all cases, it is felt that this development is a qualified success.

The remaining differences are due to residual atmospheric refraction, both tropospheric and ionospheric in nature, orbital errors and random measurement errors. Incorrect

coordinates for the monitor stations will also have an adverse effect on the results. In addition, if the initial position of the aircraft is given a high weight, as was the case in this research, any error in these coordinates will be apparent in the difference of the solutions.

Although the data were collected at a time of maximum solar activity, they are from sites located under the mid-latitude region of the ionosphere, which is generally regarded as being relatively quiet, at least compared to other regions such as the polar and equatorial ionospheric regions; in other words, the model was not tested in an extreme area, in terms of variations in ionospheric delay, either temporal or spatial. However, it should be noted that signals from satellites at low elevation angles can pass through several regions of differing ionospheric characteristics [Bishop et al., 1991].

As was stated in the introduction, the limiting factor with regard to the effectiveness of the model is how closely the interpolated surface resembles the true spatial variation in ionospheric delay over the area. Since temporal variations are taken into account by the estimation of a new surface at every epoch, it is how well the spatial variation of the surface responds to spatial variations in ionospheric delay that determines the accuracy of the estimated delays; this is dependent on the location and number of monitor stations used in the experiment. In areas where the horizontal gradient of ionospheric delay is less predictable, it is wiser to employ monitor stations at closer intervals than would be the case in, say, the mid-latitude regions. The consequence of this would be the ability to more accurately model the higher frequency spatial changes in the delay by constructing a patchwork of adjacent surfaces using sets of monitor stations. It would be interesting to see the effect of varying the spacing of monitor stations on the accuracy of the estimated delays.

From the results of one data set it is impossible to give recommendations concerning the spacing of stations for all regions. However, the data used here show that for mid-latitude regions inter-station spacing can exceed 200 km and still give sub-metre

accuracy both horizontally and vertically for single-frequency remote receivers. For many applications this level of accuracy is quite adequate. In polar and auroral regions it is debatable whether any attempt to model the ionosphere is worthwhile, not only because of the general difficulty in predicting the delay in these areas, but also because of the low number of users. Those that do wish to use GPS in these areas might be best to use dual frequency receivers, although even these may have problems maintaining lock during severe ionospheric storms [Langley et al., 1991]. Furthermore, attempts to use the broadcast model above and below 75° will be frustrated by the fact that the user's latitude will automatically be set to 75° [Newby, 1992]

7.3 Recommendations for Related Future Research

The research undertaken in this thesis is a development of a previous model. Further developments which could be included in future work are:

- Instead of assuming that any constant part of the double difference delay is absorbed by the ambiguities and residuals, a better approach would be to gather information on the absolute delay for each satellite/monitor station pair, perhaps using dual frequency P-code receivers with the carrier phase being used to smooth the delays. Although the delays obtained by this method would not be as precise as those derived solely from carrier phase measurements, it would at least be known that the constant part of the delays was not influencing the solution for the parameters. Another advantage of this approach would be that the assumption that the average inter-station offset for each satellite is zero would not be necessary (the validity of this assumption is increasingly dubious with increasing baseline length). For many users the chance of implementing this idea depends largely on whether the Y-code is being transmitted. This code is the modulo 2 sum of the P-code and the W-code; the generating functions of the latter will remain unknown outside authorised circles. Switching this code on is called

Anti-Spoofing, or A/S, and has been implemented on a periodic basis since 1 August 1992. In this situation, these users would have to revert to using receivers which square the incoming L2 signal. However, recent developments have indicated that it is still possible to monitor absolute delay even when A/S is active. Several so called "Y-busting" methods have been proposed including cross-correlation of the carrier signals as implemented in the TurboRogue receiver [Meehan et al., 1992] and by Trimble Navigation; this method relies on the fact that the same version of the P-code is superimposed on both L1 and L2; therefore, cross-correlating these signals can provide information on the difference in propagation delay between them. Yet another method of avoiding the effects of A/S is "P-W" tracking which breaks the Y-code into the original P-code and the encrypting W-code [Ashtech, n.d.]. It is claimed that this method offers superior SNR figures to straight cross-correlation.

- With the use of more monitor stations, more complex surfaces could be used to describe the variation in delay. Alternatively, the surfaces could be fitted in a least-squares sense, and the residuals used in a stochastic improvement to the deterministic model; indeed, these methods could be used in conjunction with each other, given enough monitor stations.
- Extending this idea even further, a network of automatic, dual frequency receivers spaced in a regular fashion and equipped to relay information to users, would undoubtedly prove to be a great asset to single frequency users equipped to receive the information. With this approach, a series of surfaces could be interpolated over the area in question, similar to the technique of patchwise interpolation found in digital terrain modelling. For example, if sets of three monitor stations were used, a patchwork of triangular surfaces could be built up, similar to a conventional triangulation network in surveying. Of course, some method of

enforcing a degree of continuity between adjacent surfaces would have to be developed, otherwise users may experience sharp changes in the interpolated delay as the ray path to a particular satellite crosses a boundary between two patches; indeed, the delay may jump unpredictably at this junction if the surfaces were estimated in a redundant fashion (there would be no requirement for them to meet along common boundaries).

Undoubtedly, developments on this scale are some way off in terms of time, due mainly to the massive organizational and financial requirements needed to implement such a system. However, once in place, information could be collected and transmitted at little cost or effort for a variety of functions besides modelling ionospheric delays, e.g., orbit computations and crustal movement studies. An ongoing study towards goals of this nature is the Canadian Active Control System (ACS), which consists of a number of dual frequency stations, including Rogue receivers, spread over the country. Developments in this area certainly seem promising.

REFERENCES

- Ackroyd, N. and R. Lorimer (1990). *Global Navigation. A GPS User's Guide*. Lloyd's of London Press, London, U.K.
- ARINC (1991). "NAVSTAR GPS space segment/navigation user interfaces (Public Release Version)." Interface Control Document ICD-GPS-200, ARINC Research Corporation, CA., U.S.A.
- Ashtech (n.d.) Publicity Brochure, Ashtech, Inc., 1170 Kifer Rd. Sunnyvale, CA 94086., U.S.A.
- Bagley, B.C. and J.W. Lamons (1992). "NAVSTAR Joint Program Office and a Status Report on the GPS Program." *Proceedings of the Sixth International Geodetic Symposium on Satellite Positioning, Columbus, OH, U.S.A., 17 – 20 March, pp. 21 – 30.*
- Baker, R.M.L. (1967). *Astrodynamics: Applications and Advanced Topics*. Academic Press, New York, NY, U.S.A.
- Beutler, G., D. Davidson, R. Langley, R. Santerre, P. Vaníček and D. Wells (1984). "Some theoretical and Practical aspects of geodetic positioning using carrier beat phase difference observations of GPS satellites." Department of Surveying Engineering Technical Report No. 109, University of New Brunswick, Fredericton, N.B., Canada.
- Bishop, G.J., D.S. Coco and C. Coker (1991). "Variations in Ionospheric Range Error with GPS Look Direction." Paper presented at the Institute of Navigation Satellite Division's Fourth International Technical Meeting, Albuquerque, NM, U.S.A.
- Brunner, F.K. and M. Gu (1991). "An Improved Model for the Dual Frequency Ionospheric Correction of GPS Observations." *Manuscripta Geodætica*, Vol. 16, pp. 205 – 214.
- Brunner, F.K. and W.M. Welsch (1993). "Effect of the Troposphere on GPS Measurements." *GPS World*, Vol. 4, No. 1, pp. 42 – 51.
- Bugoslavskaya, N.Y. (1962). *Solar Activity and the Ionosphere*. Translated from Russian by G.O. Harding, Pergamon Press, New York, NY, U.S.A.
- Clynch, J.R., D.S. Coco and C. Coker (1989). "A Versatile GPS Ionospheric Monitor: High Latitude Measurements of TEC and Scintillation." *Proceedings of ION GPS-89*, Colorado Springs, CO, U.S.A., pp. 445 – 450.
- Considine, D.M. (Ed.)(1983). *Van Nostrand's Scientific Encyclopedia*. 6th Ed., van Nostrand Reinhold, New York, NY, U.S.A.
- Cross, P.A. (1983). "Advanced Least Squares Applied to Position-Fixing." Working Paper No. 6, Department of Land Surveying, North East London Polytechnic, 205 pp.

- Elgered, G. (1992). "Refraction in the Troposphere." *Proceedings of the Symposium on Refraction of Transatmospheric Signals in Geodesy*, The Hague, Netherlands, 19 – 22 March, pp. 13 – 19.
- Feess, W.A. and S.G. Stephens (1986). "Evaluation of GPS Ionospheric Time Delay Algorithm for Single Frequency Users." *Proceedings of the IEEE PLANS '86 Position Location and Navigation Symposium*, Las Vegas, NV, U.S.A., pp. 206 – 213.
- Georgiadou, Y. and A. Kleusberg (1988a). "On the Effect of Ionospheric Delay on Geodetic Relative GPS Positioning." *Manuscripta Geodætica*, Vol. 13, pp. 1 – 8.
- Georgiadou, Y. and A. Kleusberg (1988b). "On carrier signal multipath effects in relative GPS Positioning." *Manuscripta Geodætica*, Vol. 13, pp. 172 – 179.
- Georgiadou, Y. and K.D. Doucet (1990). "The Issue of Selective Availability." *GPS World*, Vol. 1, No. 5, pp. 53 – 56.
- Greenspan, R.L., A.K. Tetewsky, J.I. Donna and J.A. Klobuchar (1991). "The Effects of Ionospheric Errors on Single-Frequency GPS Users." *Proceedings of ION GPS-91*, Albuquerque, NM, U.S.A., pp. 291-297.
- Gu, M. and Brunner, F.K. (1990). "Theory of the Two Frequency Dispersive Range Correction." *Manuscripta Geodætica*, Vol. 15, pp. 357 – 361.
- Henson, D.J. and E.A. Collier (1986). "Effects of the Ionosphere on GPS Relative Geodesy." *Proceedings of the IEEE PLANS '86 Position Location and Navigation Symposium*, Las Vegas, NV, U.S.A., pp. 230 – 237.
- Héroux, P. (1988). "GPS and the Ionosphere in Auroral Regions." Unpublished seminar report as part of graduate degree requirements at the Department of Surveying Engineering, University of New Brunswick, Fredericton, N.B., Canada.
- Héroux, P., and A. Kleusberg (1989). "GPS Precise Relative Positioning and Ionosphere in Auroral Regions." *Proceedings of the Fifth International Geodetic Symposium on Satellite Positioning*. Las Cruces, NM, U.S.A., 13 – 17 March, Vol I, pp. 475 – 486.
- Hopfield, H.S. (1971). "Tropospheric effect on electromagnetically measured range: Prediction from surface weather data." *Radio Science*, Vol. 6, No. 3, pp. 357 – 367.
- Jones, T. (1989). "NAVSTAR Global Positioning System – Status and Update." *Proceedings of the Fifth International Geodetic Symposium on Satellite Positioning*. Las Cruces, NM, U.S.A., 13 – 17 March, Vol II, pp. 789 – 798.
- Kindle, J.H. (1950). *Analytic Geometry*. In series "Schaum's Outline Series", McGraw-Hill, New York, NY., U.S.A.
- Kleusberg, A. (n.d.). Unpublished lecture notes for undergraduate course in GPS Positioning, Department of Surveying Engineering, University of New Brunswick, Fredericton, N.B., Canada.

- Kleusberg, A. (1986a). "Kinematic Relative Positioning Using GPS Code and Carrier Beat Phase Observations." *Marine Geodesy*, Vol. 10, pp. 257 – 254.
- Kleusberg, A. (1986b). "Ionospheric Propagation Effects in Geodetic Relative GPS Positioning." *Manuscripta Geodætica*, Vol. 11, pp. 256 – 261.
- Kleusberg, A., Y. Georgiadou and H. Dragert (1988). "Establishment of Crustal Deformation Networks Using GPS: A Case Study." *CISM Journal*, Vol. 42, No. 4, pp. 341 – 351.
- Kleusberg, A., Y. Georgiadou, F. van Heuvel and P. Héroux (1989). *Single and Dual Frequency GPS Data Processing with DIPOP 2.1*. Department of Surveying Engineering Technical Memorandum TM-21, University of New Brunswick, Fredericton, N.B., Canada.
- Kleusberg, A., and Y. Georgiadou (1991a). "Analysis of Airborne and Ground GPS Data." Final contract report prepared for the Canada Centre for Surveying, Surveys, Mapping and Remote Sensing Branch, Ottawa, Ont., Canada, 28 March, 48 pp.
- Kleusberg, A., and Y. Georgiadou (1991b). "Algorithms and Results of Kinematic GPS Positioning." *CISM Journal*, Vol. 45, No. 4, pp. 569 – 575.
- Klobuchar, J.A. (1986). "Design and Characteristics of the GPS Ionospheric Time Delay Algorithm for Single Frequency Users". *Proceedings of the IEEE PLANS '86 Position Location and Navigation Symposium*, Las Vegas, NV, U.S.A., pp. 280 – 286.
- Langley, R.B. (1990). "Why is the GPS Signal so Complex?" *GPS World*, Vol. 1, No. 3, pp. 56 – 59.
- Langley, R.B., K. Doucet and A. Kleusberg (1991). "The Testing of Global Positioning System Receivers Under Ionospheric Influences". Final contract report prepared for the Canada Centre for Surveying, Geodetic Survey Division, Ottawa, Ont., Canada, October, 73 pp.
- Langley, R.B. (1991). "The GPS Receiver: An Introduction." *GPS World*, Vol. 2, No. 1, pp. 50 – 53.
- Langley, R.B. (1992a). "The Federal Radionavigation Plan." *GPS World*, Vol. 3, No. 3, pp. 50 – 53.
- Langley, R.B. (1992b). "The Effect of the Ionosphere and Troposphere on Satellite Positioning Systems." Paper presented at the Symposium on Refraction of Transatmospheric Signals in Geodesy, The Hague, Netherlands, 19 – 22 March.
- Leick, A. (1990). *GPS Satellite Surveying*. John Wiley, New York, NY, U.S.A.
- Lichtenegger, H., and B. Hofmann-Wellenhof (1989). "GPS-Data Preprocessing for Cycle-slip Detection." In *Global Positioning System: An Overview*, IAG Symposium, Edinburgh, U.K., August, pp. 57 – 67.

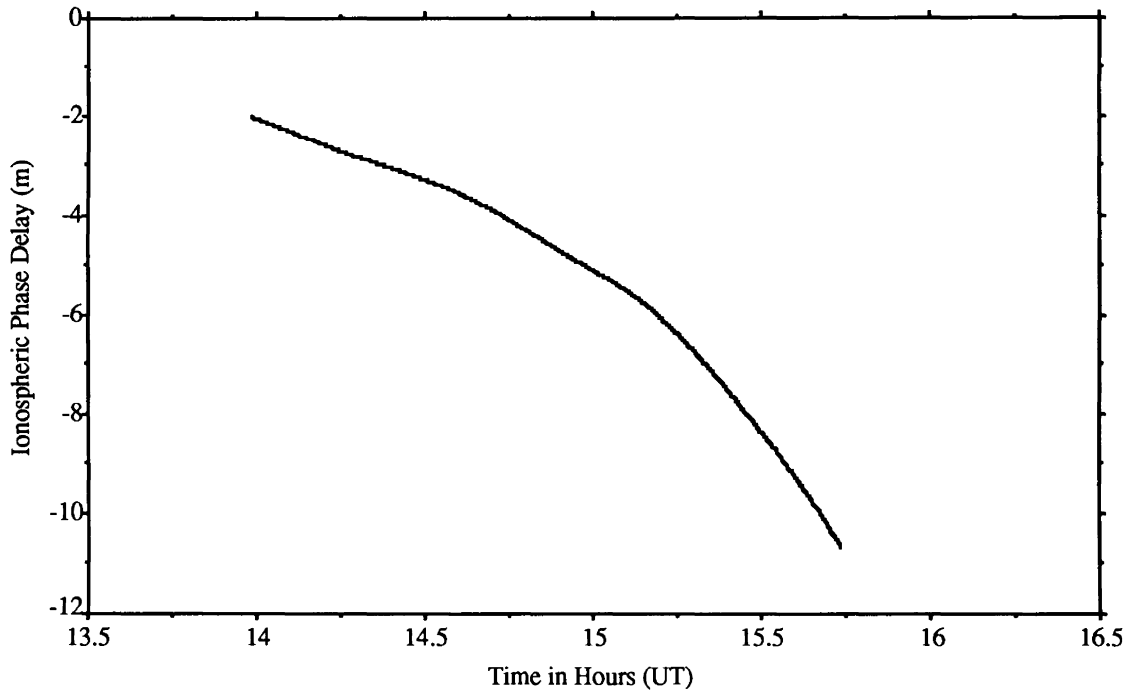
- McNamara, L.F. (1991). *The Ionosphere: Communications, Surveillance, and Direction Finding*. In series "ORBIT, A Foundation Series", Ed. E.F. Strother, Krieger Publishing Company, Malabar, FL, U.S.A.
- Meehan, T.K., J.M. Srinivasan, D.J. Spitzmesser, C.E. Dunn, J.Y. Ten, J.B. Thomas, T.N. Munson and C.B. Duncan (1992). "The TurboRogue GPS Receiver. *Proceedings of the Sixth International Geodetic Symposium on Satellite Positioning, Columbus, OH, U.S.A., 17 – 20 March, pp. 209 – 218.*
- Melbourne, W.G. (1989). "The Global Positioning System for Study of the Ionosphere — Overview." Paper presented at the fall meeting of the American Geophysical Union, San Francisco, CA, U.S.A., 4 – 7 December.
- Newby, S.P. (1992). *An Assessment of Empirical Models for the Prediction of the Transionospheric Propagation Delay of Radio Signals*. M.Sc.E. thesis, Department of Surveying Engineering Technical Report No. 160, University of New Brunswick, Fredericton, New Brunswick, Canada, 212 pp.
- Ratcliffe, J.A. (1970). *Sun, Earth and Radio*. McGraw-Hill, New York, NY, U.S.A.
- Rishbeth, O. and O.K. Garriot (1969). *Introduction to Ionospheric Physics*. In series "International Geophysics Series", Ed. J. van Mieghem, Academic Press, New York, NY, U.S.A.
- Santerre, R. (1989). *GPS Satellite Sky Distribution: Impact on the Propagation of Some Important Errors in Precise Relative Positioning*. Department of Surveying Engineering Technical Report No. 145, University of New Brunswick, Fredericton, N.B., Canada.
- Spilker, J.J. (1980). "GPS Signal Structure and Performance Characteristics." In: *Global Positioning System*. Papers published in *Navigation*, reprinted by the (U.S.) Institute of Navigation, Vol. I, pp. 29 – 54.
- Spofford, P.R., W.G. Kass and R.L. Dulaney (1992). "National Geodetic Survey Precise GPS Orbit Computations: Status, Availability, Accuracy". *Proceedings of the Sixth International Geodetic Symposium on Satellite Positioning, Columbus, OH, U.S.A., 17 – 20 March, pp. 89 – 97.*
- van Dierendonck, A.J., S.S. Russel, E.R. Kopitzke and M. Birnbaum (1980). "The GPS Navigation Message." In: *Global Positioning System*. Papers published in *Navigation*, reprinted by the (U.S.) Institute of Navigation, Vol. I, pp. 55 – 73.
- Vaniček, P. and E. Krakiwsky (1987). *Geodesy: The Concepts*. 2nd ed., 2nd printing, North Holland, Amsterdam, Netherlands.
- Wells, D.E., N. Beck, D. Delikaraoglou, A. Kleusberg, E.J. Krakiwsky, G. Lachapelle, R.B. Langley, M. Nakiboglu, K.P. Schwarz, J.M. Tranquilla and P. Vaniček (1987). *Guide to GPS Positioning*. Second printing with corrections, Canadian GPS Associates, Fredericton, N.B., Canada.
- Wells, D.E. and A. Kleusberg (1989). "Kinematic Differential Global Positioning System." Contract report for the U.S. Army Engineer Topographic Laboratories, Fort Belvoir, VA, U.S.A., March, 36pp.

- Wild, U., G. Beutler, W. Gurtner and M. Rothacher (1989). "Estimating the Ionosphere Using one or more Dual Frequency GPS Receivers." *Proceedings of the Fifth International Geodetic Symposium on Satellite Positioning*, Las Cruces, NM, U.S.A., pp. 724 – 736.
- Wild, U., G. Beutler, S. Fankhauser, and W. Gurtner (1990). "Stochastic Properties of the Ionosphere Estimated from GPS Observations." *Proceedings of the Second International Symposium on Precise Positioning with the Global Positioning System*, Ottawa, Ont., Canada, pp. 411 – 428.

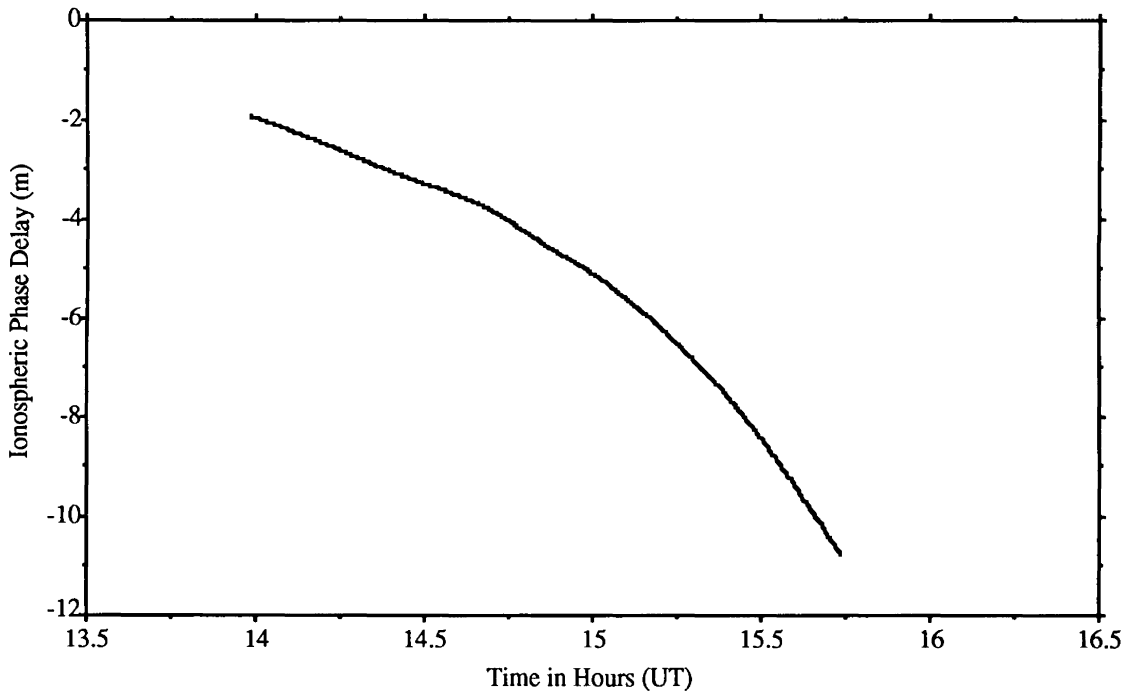
APPENDIX I

Plots of Phase Ionospheric Delays

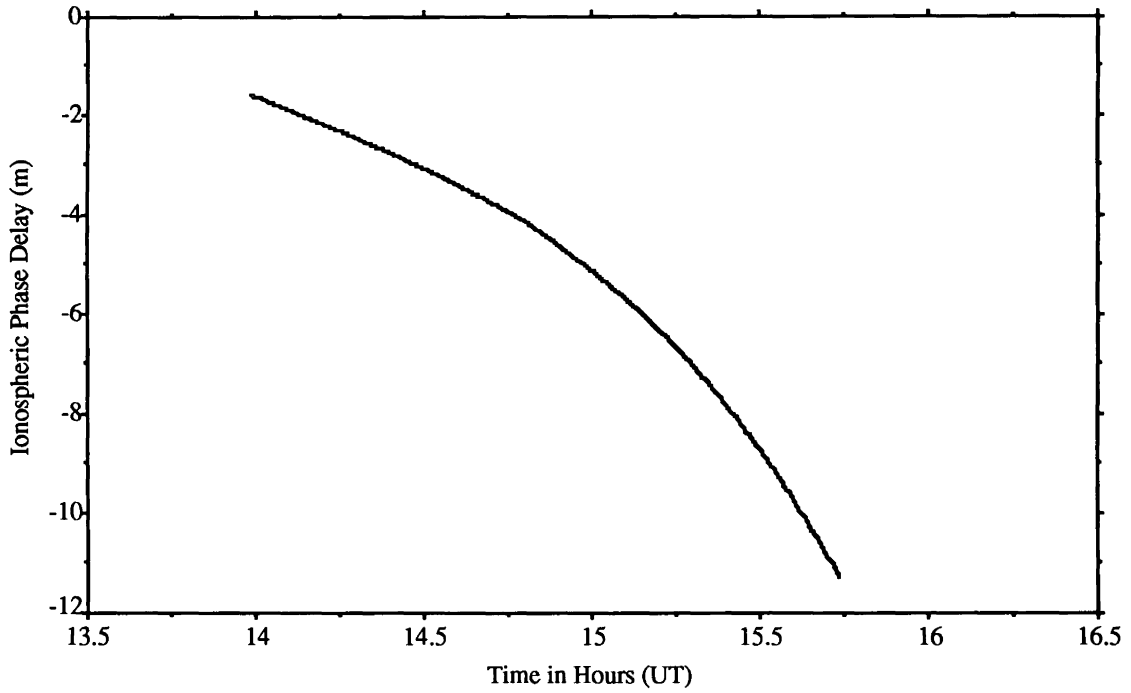
Note: These plots represent the change in ionospheric delay over time and contain an unmodelled constant bias; therefore the values for the delays should be treated as relative, not absolute.



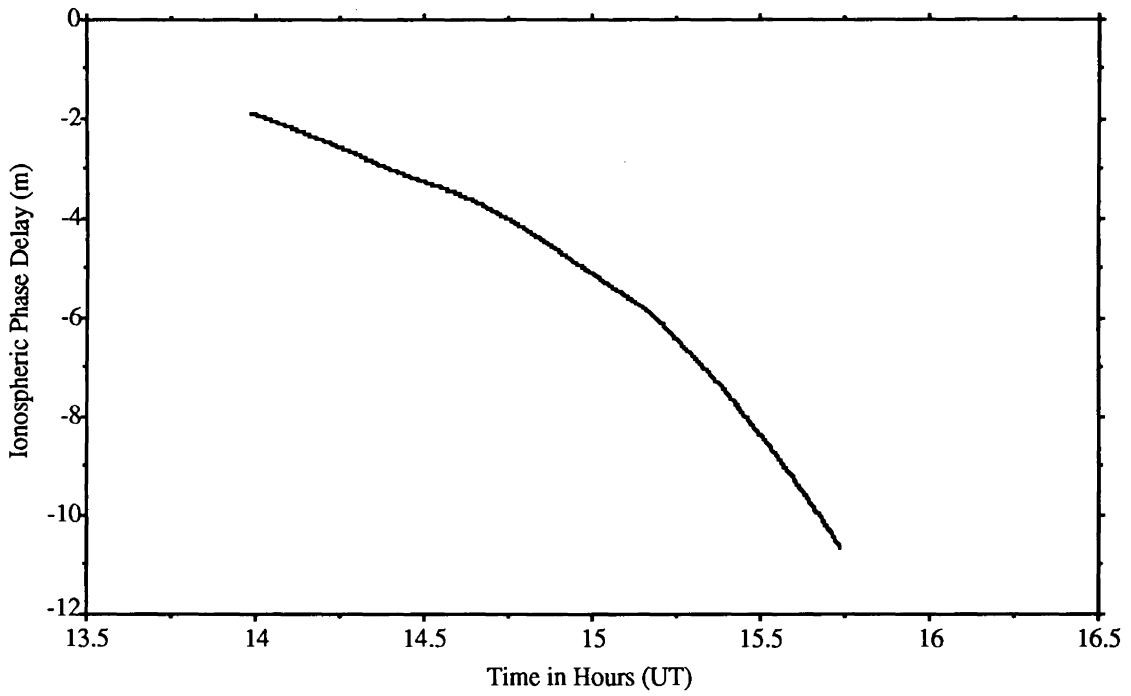
Ionospheric Phase Delay — SV 2, Mallorytown



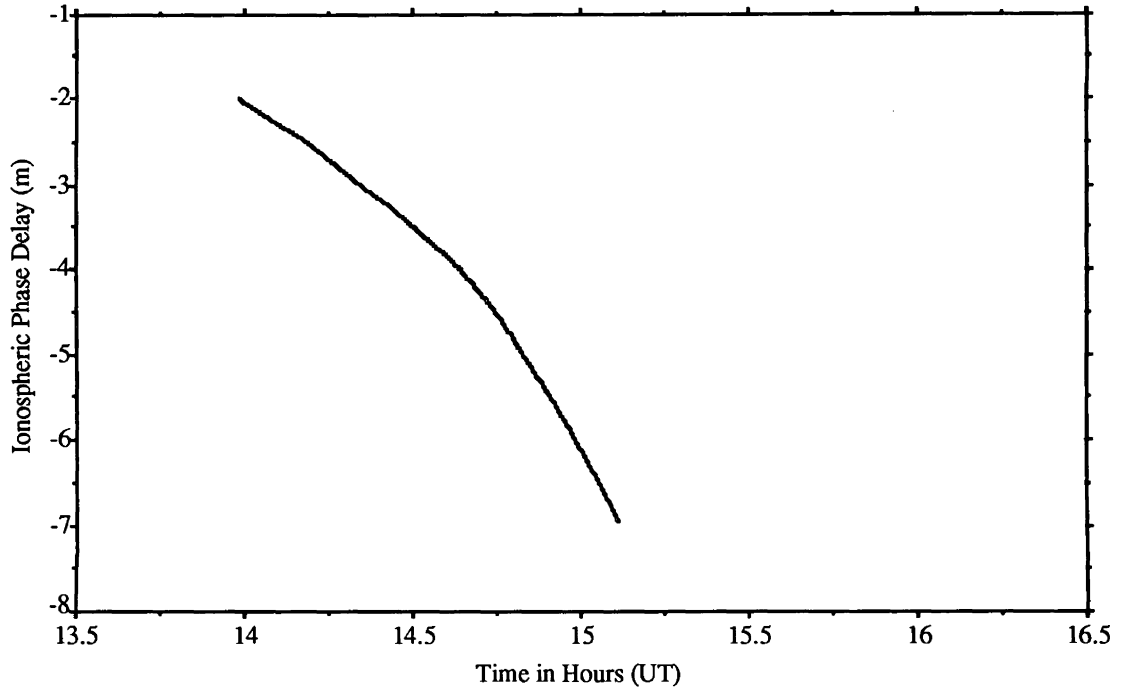
Ionospheric Phase Delay — SV 2, Metcalfe



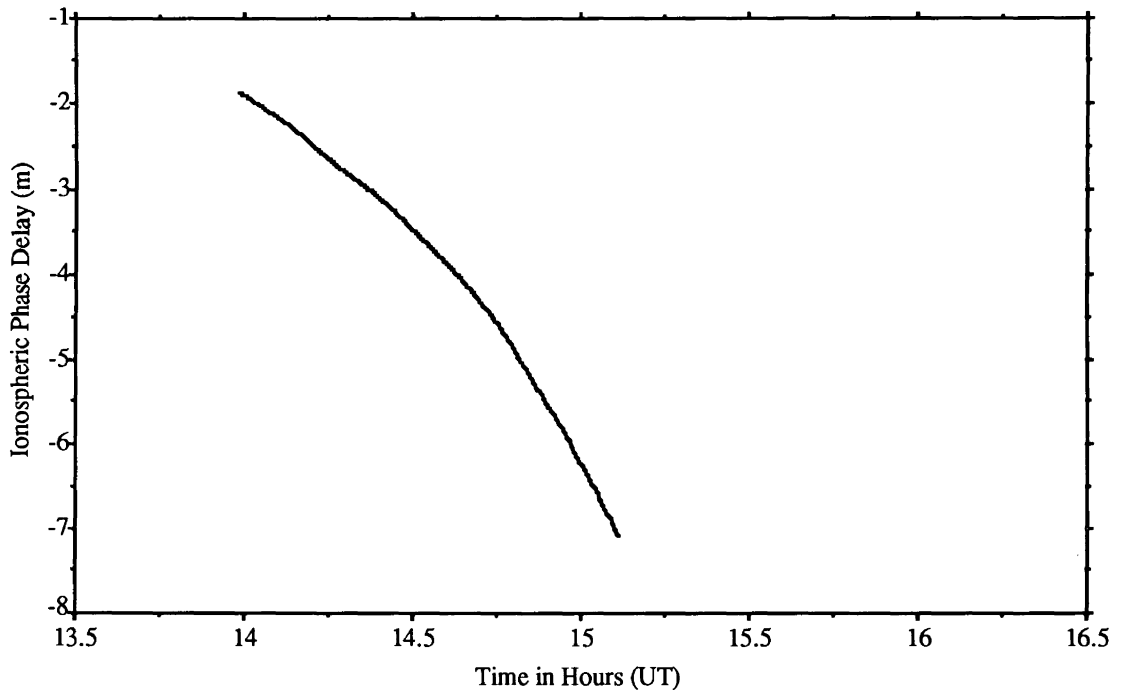
Ionospheric Phase Delay — SV 2, Algonquin



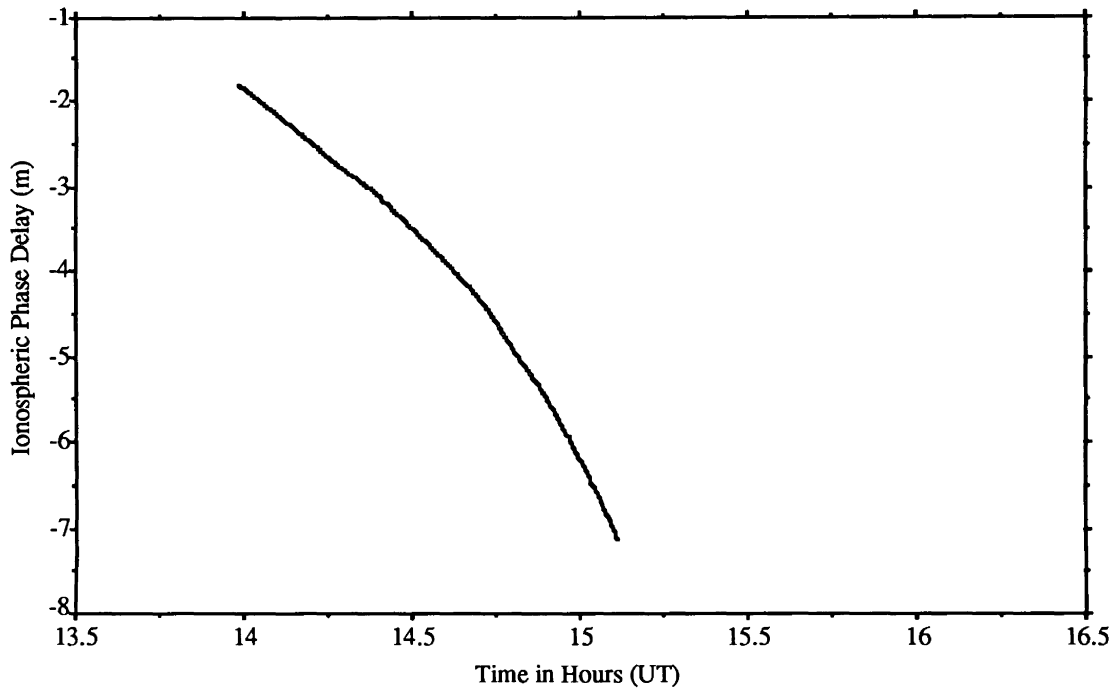
Ionospheric Phase Delay — SV 2, Falcon



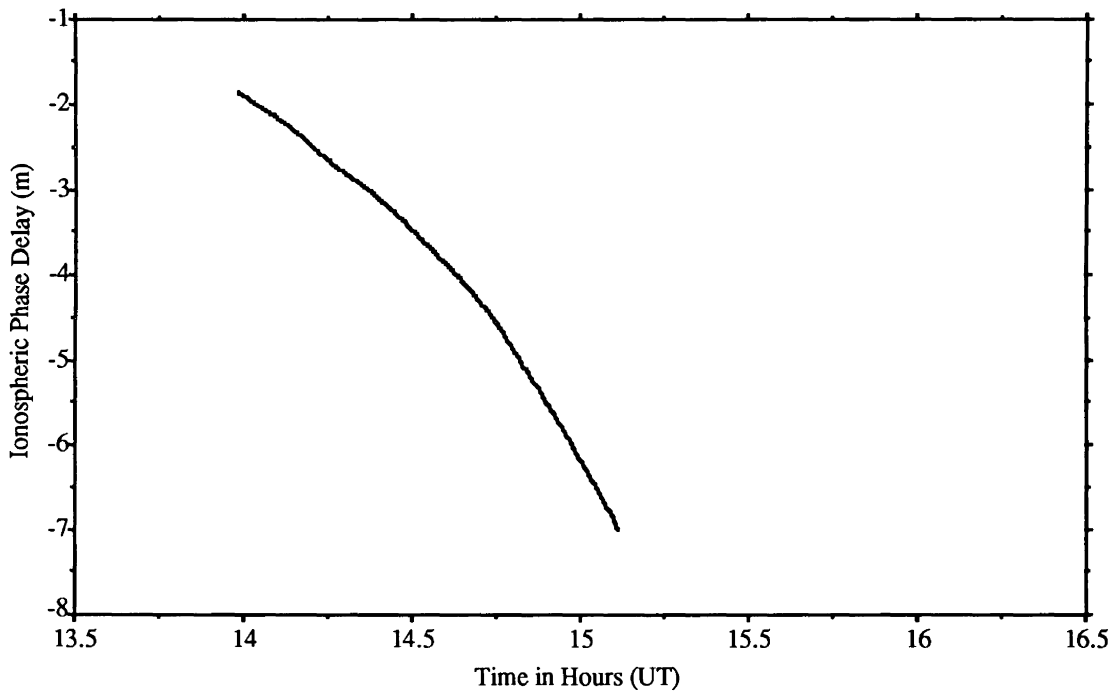
Ionospheric Phase Delay — SV 6, Mallorytown



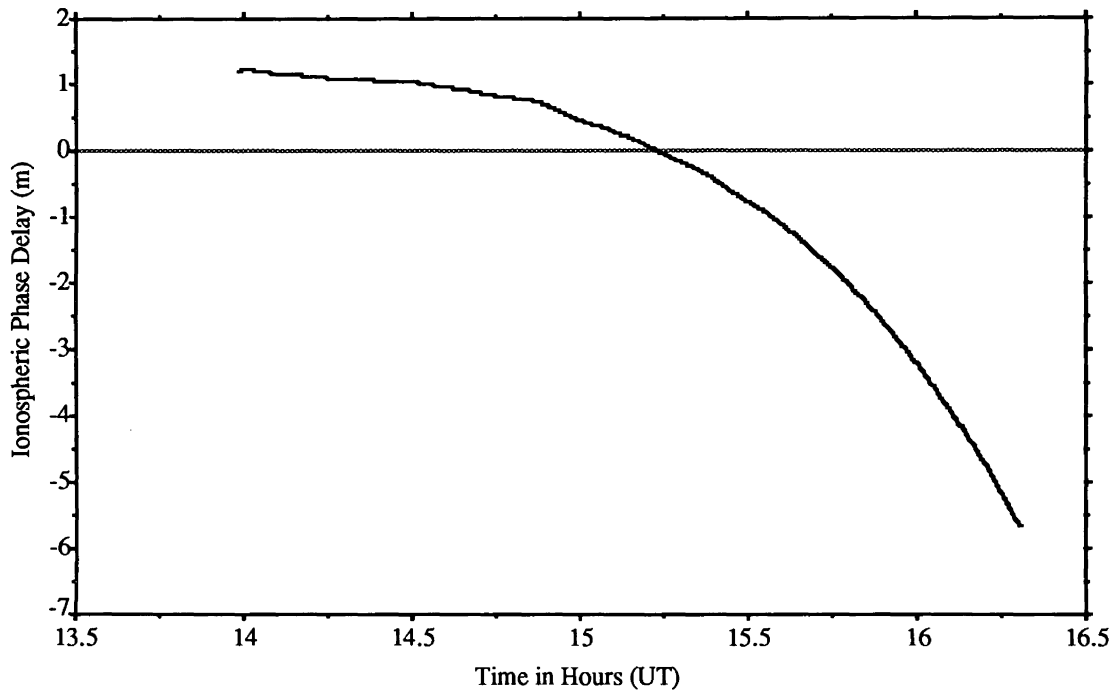
Ionospheric Phase Delay — SV 6, Metcalfe



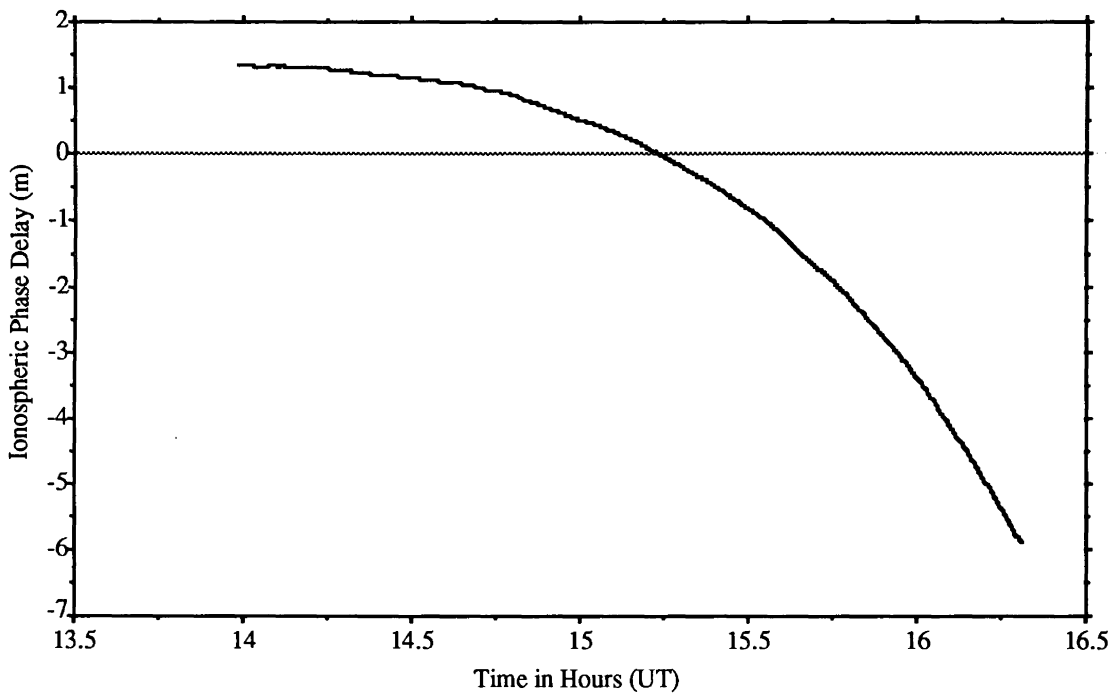
Ionospheric Phase Delay — SV 6, Algonquin



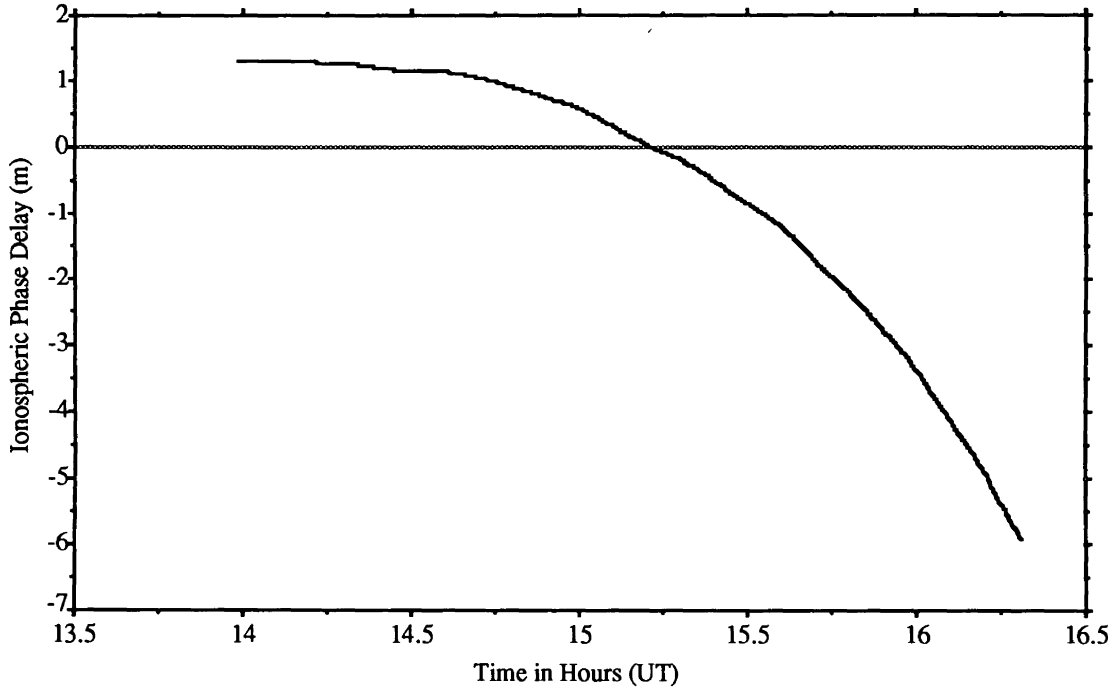
Ionospheric Phase Delay — SV 6, Falcon



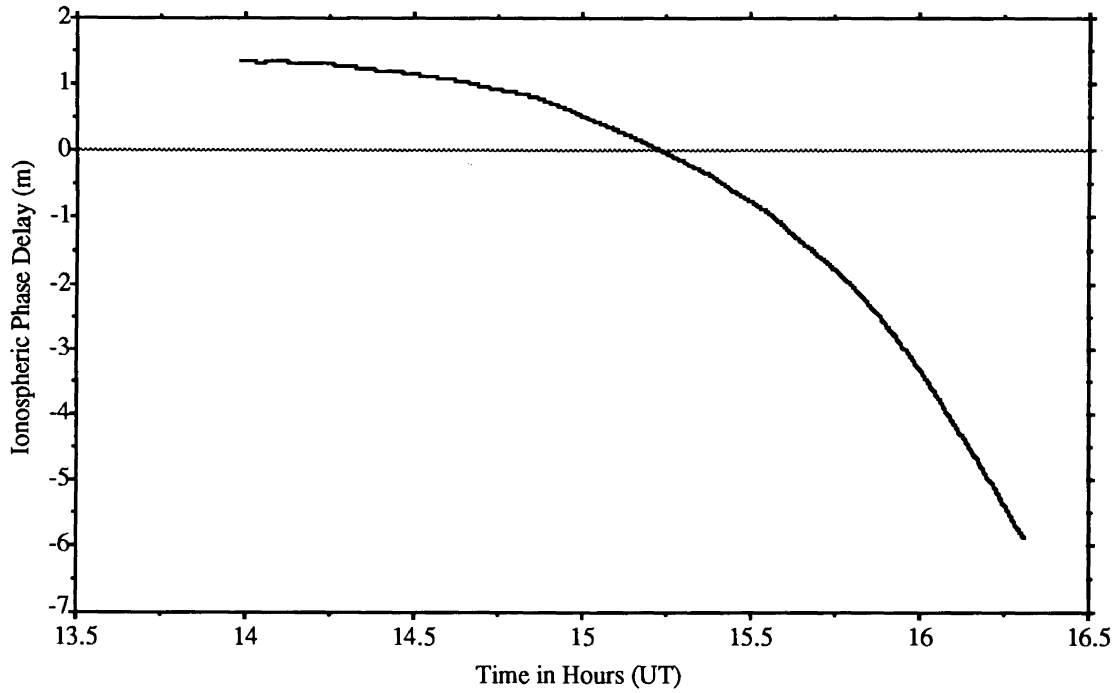
Ionospheric Phase Delay — SV 9, Mallorytown



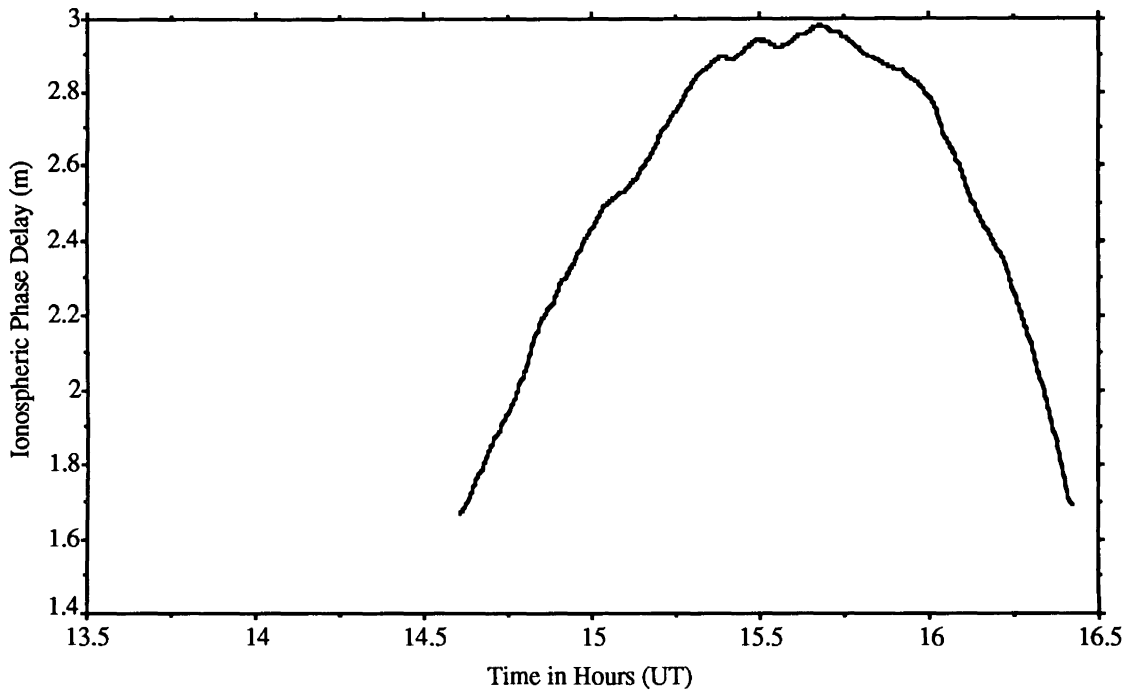
Ionospheric Phase Delay — SV 9, Metcalfe



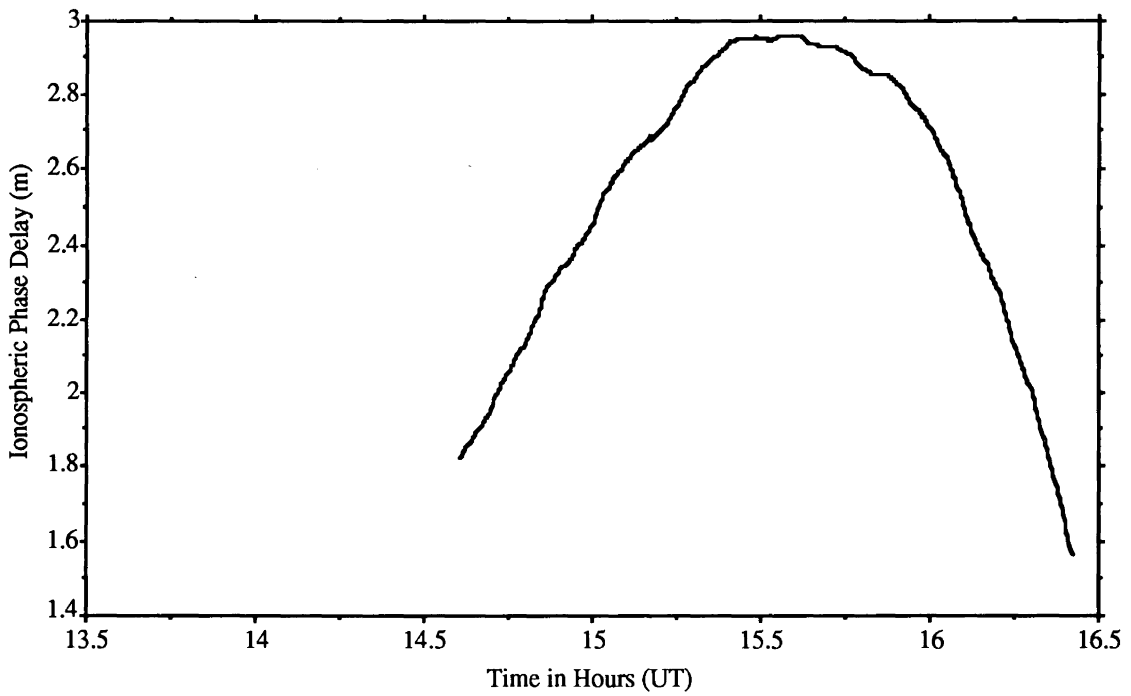
Ionospheric Phase Delay — SV 9, Algonquin



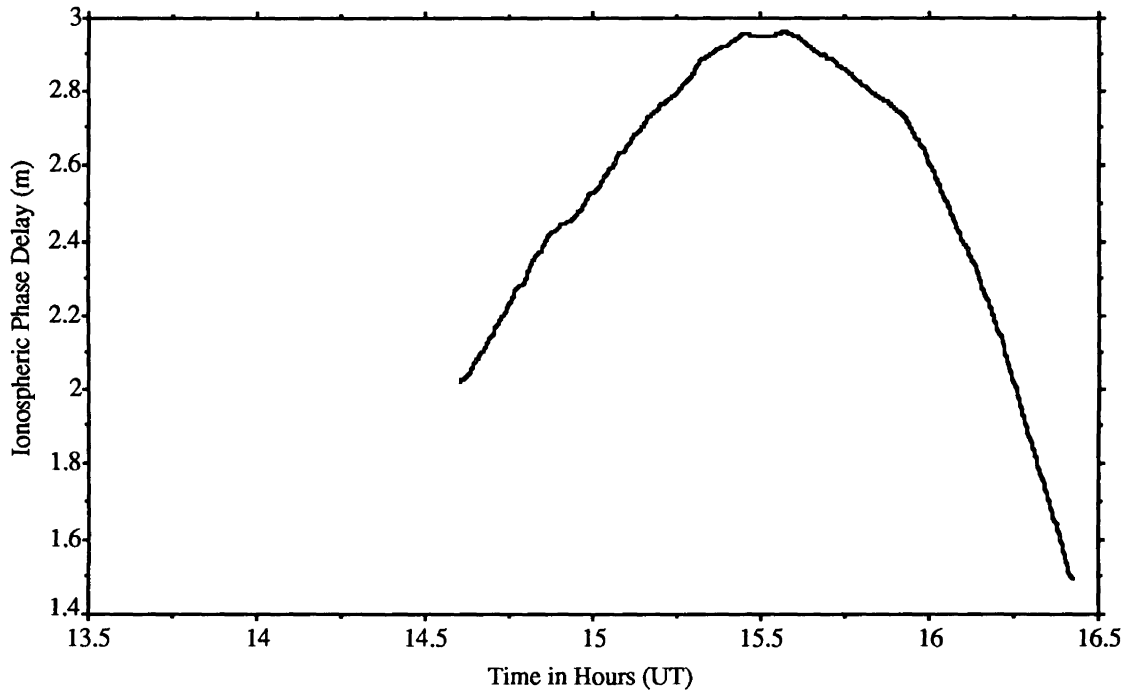
Ionospheric Phase Delay — SV 9, Falcon



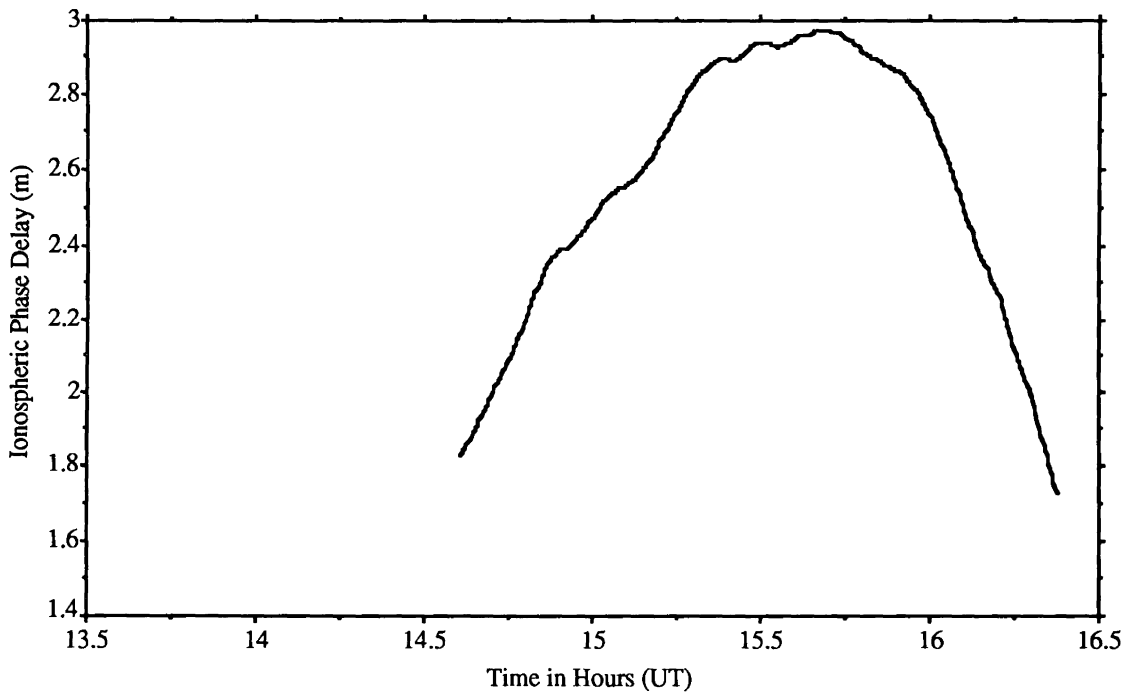
Ionospheric Phase Delay — SV 12, Mallorytown



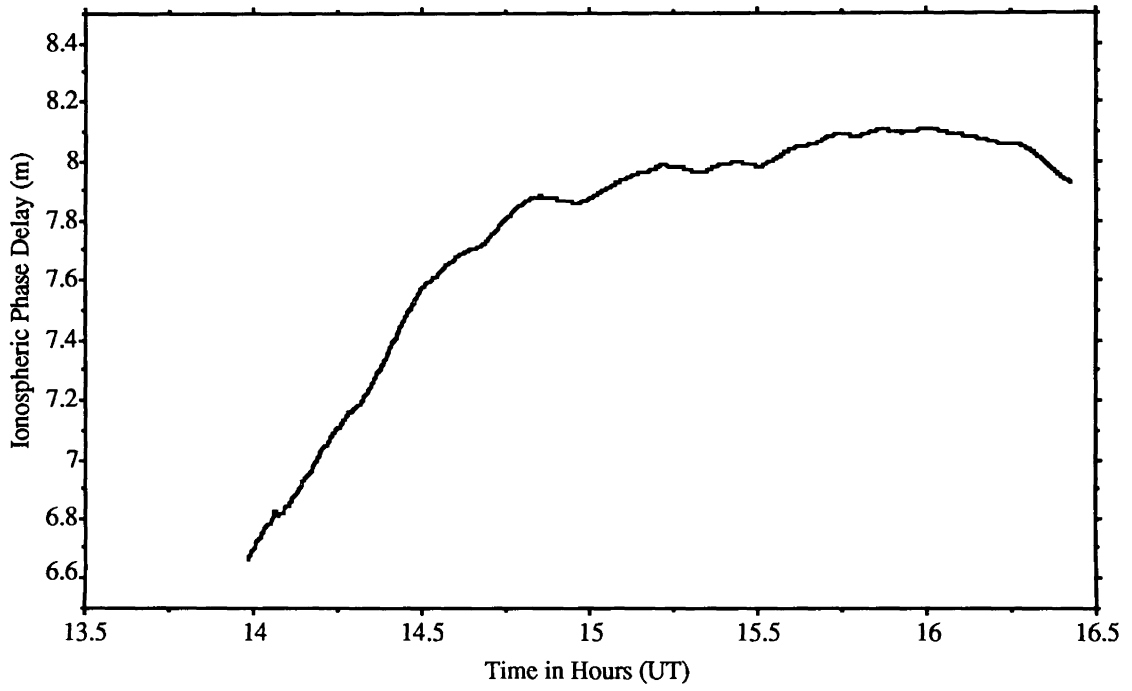
Ionospheric Phase Delay — SV 12, Metcalfe



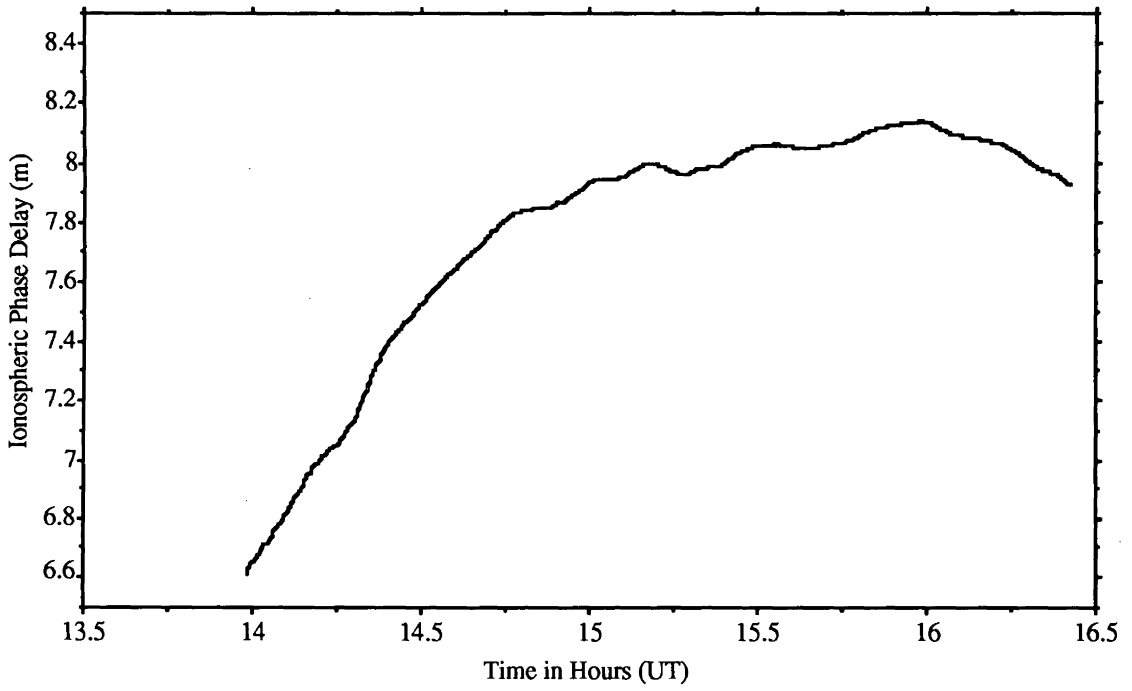
Ionospheric Phase Delay — SV 12, Algonquin



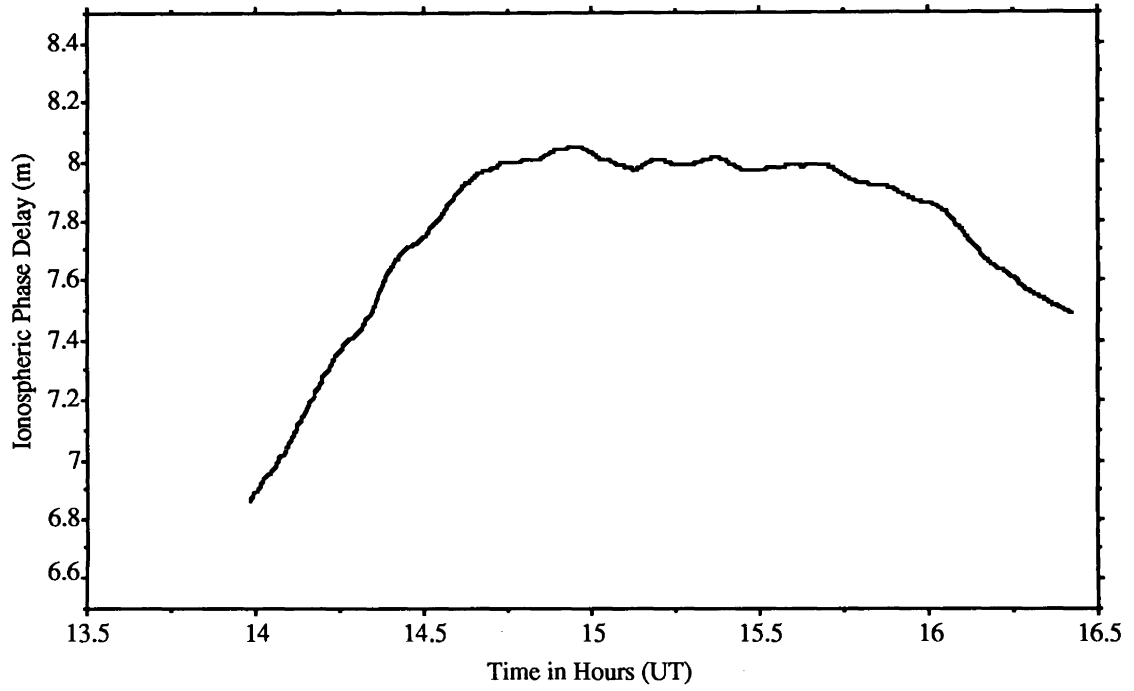
Ionospheric Phase Delay — SV 12, Falcon



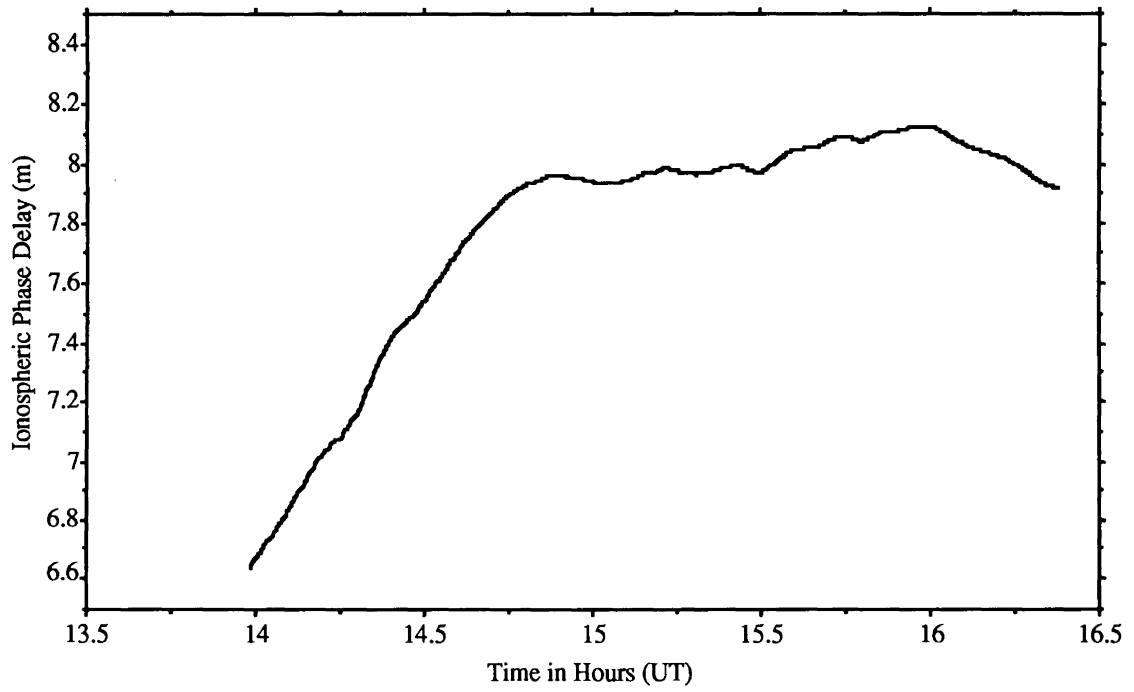
Ionospheric Phase Delay — SV 13, Mallorytown



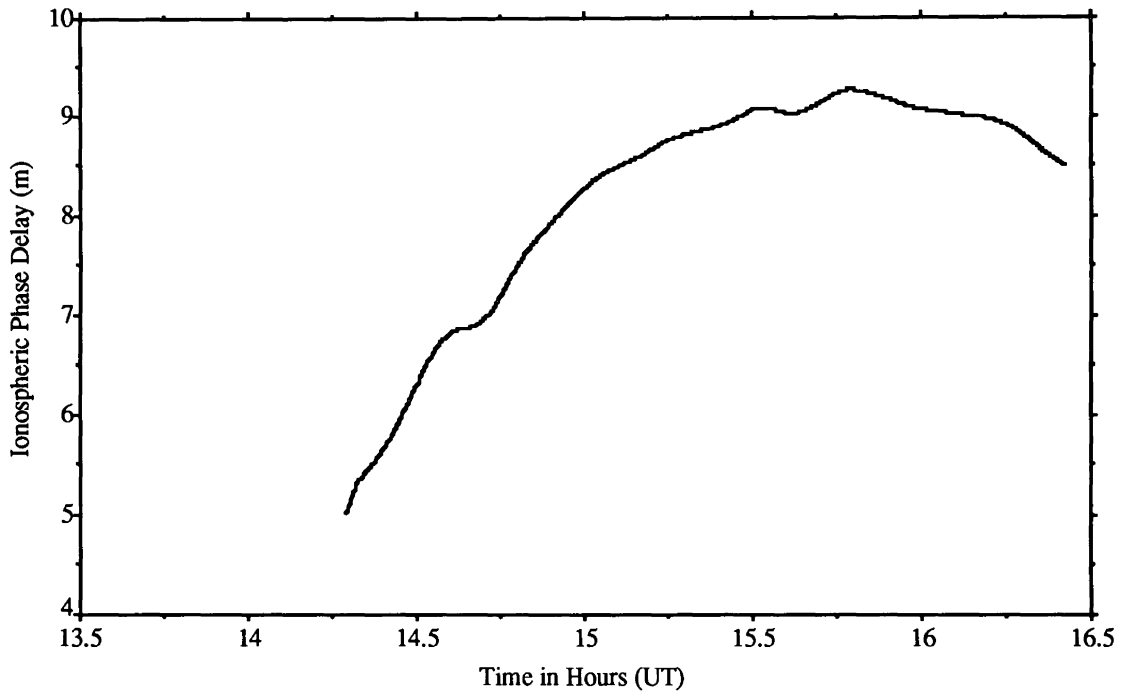
Ionospheric Phase Delay — SV 13, Metcalfe



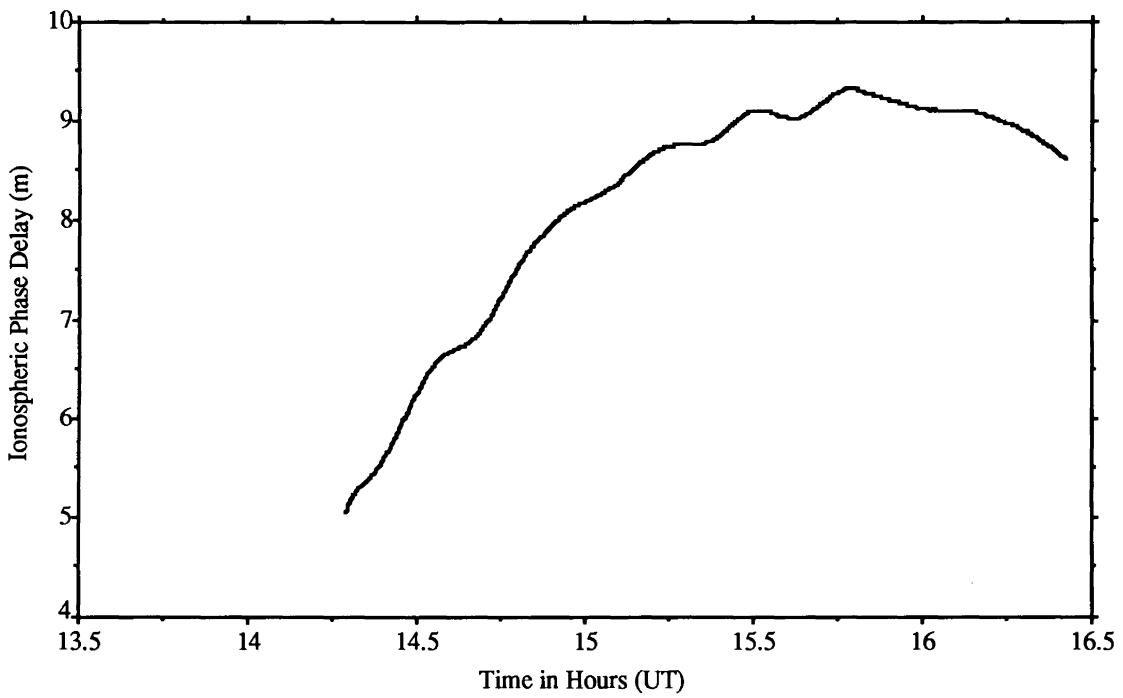
Ionospheric Phase Delay — SV 13, Algonquin



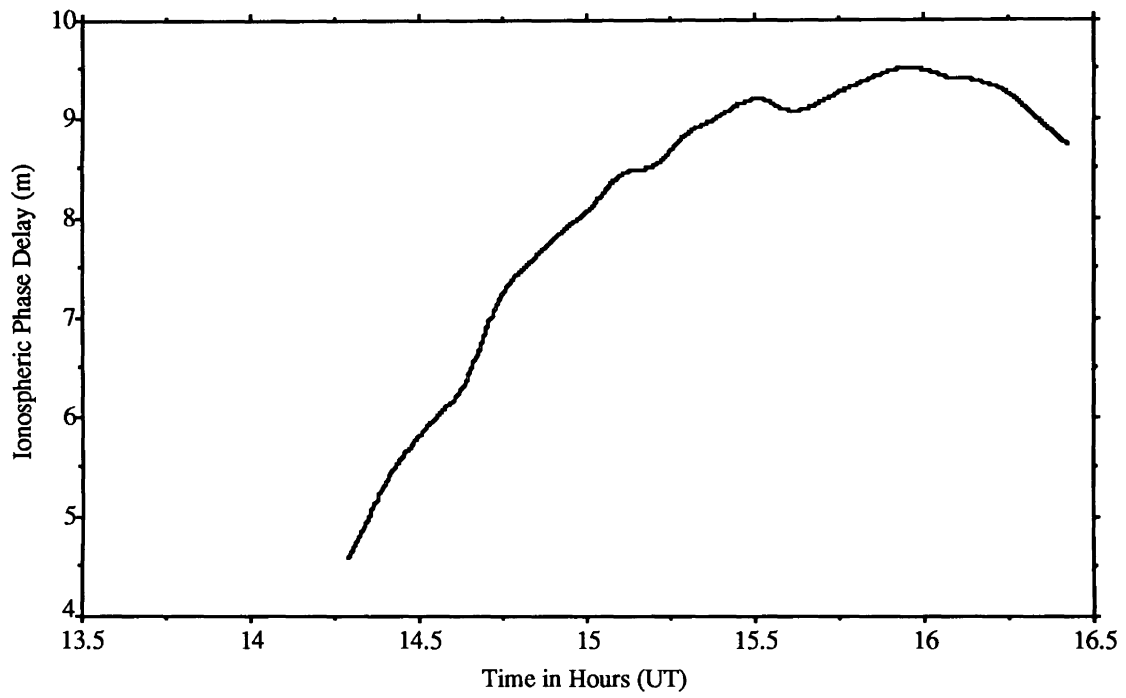
Ionospheric Phase Delay — SV 13, Falcon



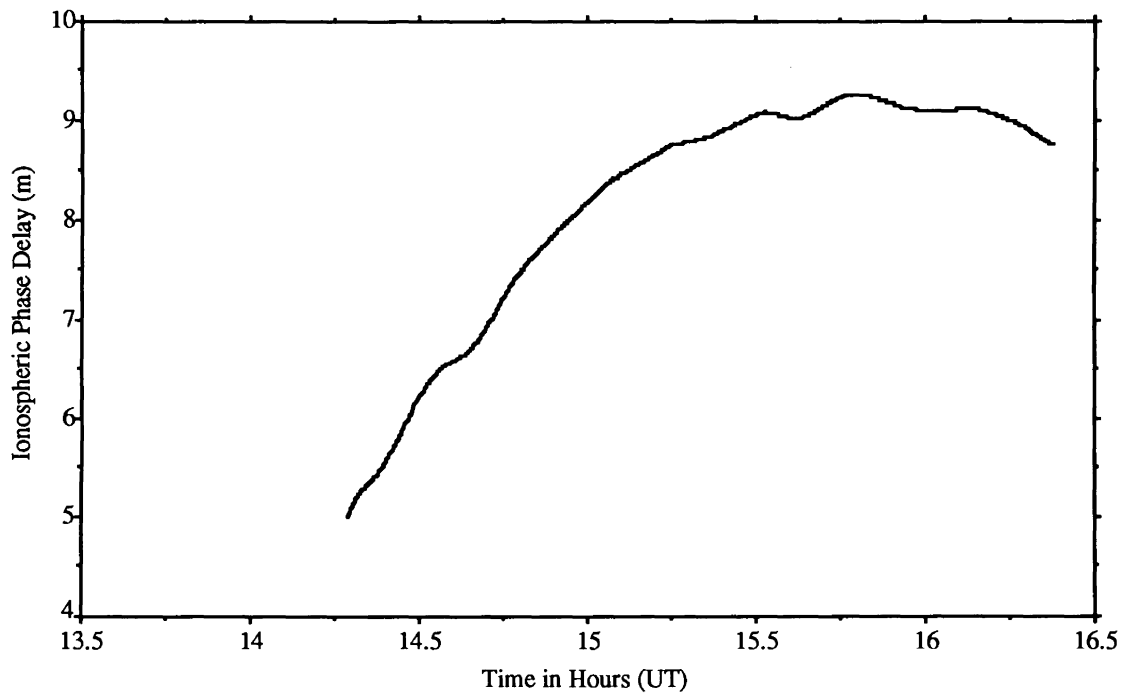
Ionospheric Phase Delay — SV 14, Mallorytown



Ionospheric Phase Delay — SV 14, Metcalfe



Ionospheric Phase Delay — SV 14, Algonquin

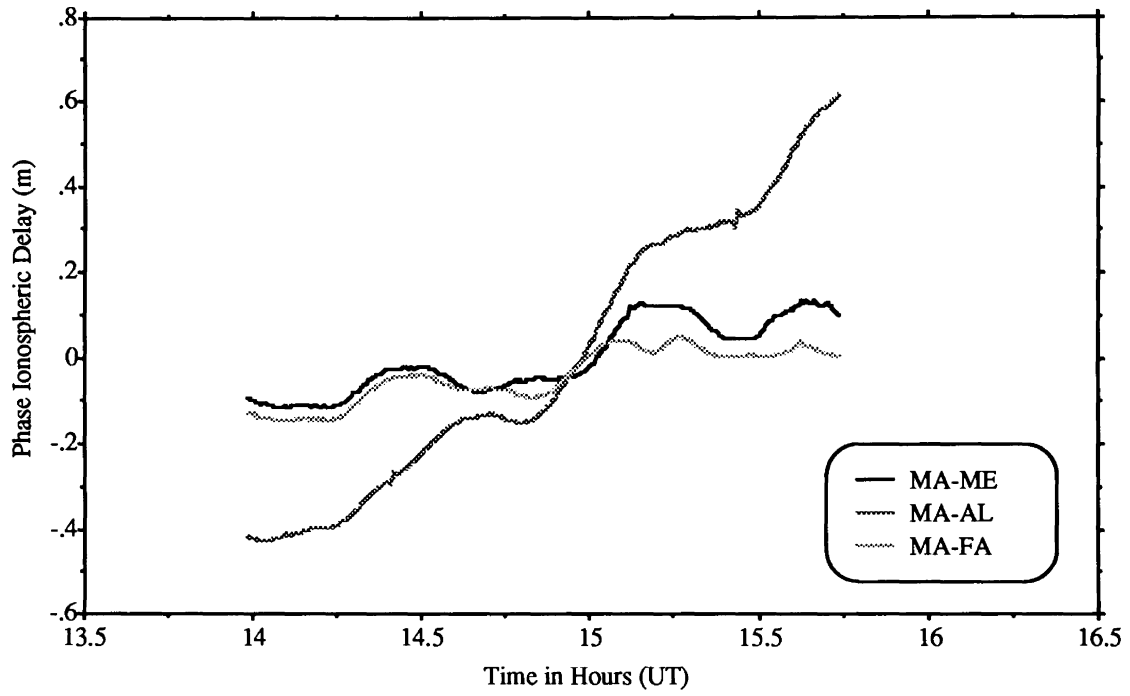


Ionospheric Phase Delay — SV 14, Falcon

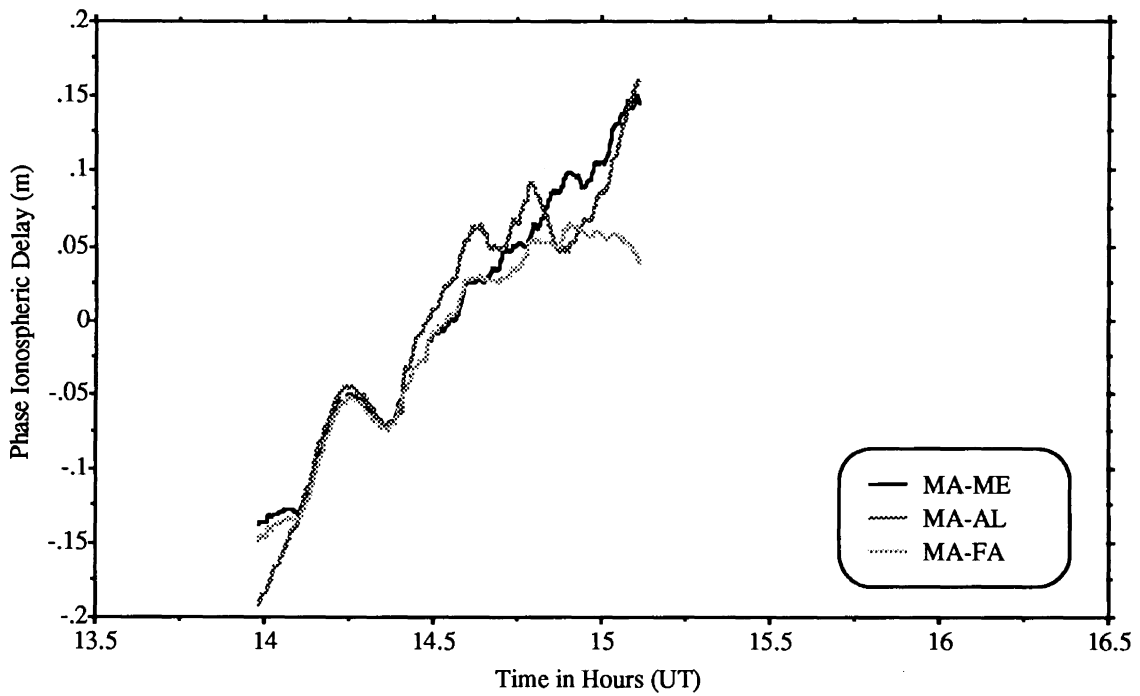
APPENDIX II

Plots of Between-station Differences of Phase Ionospheric Delays

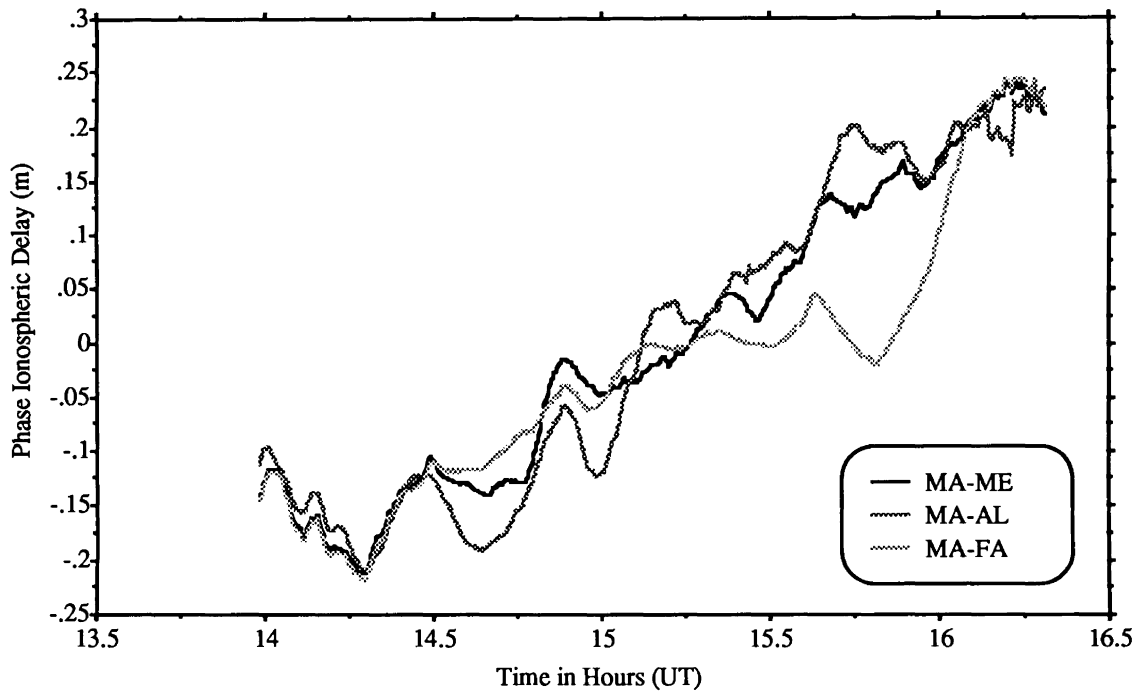
Note: Each graph shows the difference of the phase ionospheric delays of each of ME, AL and FA with MA for one satellite.



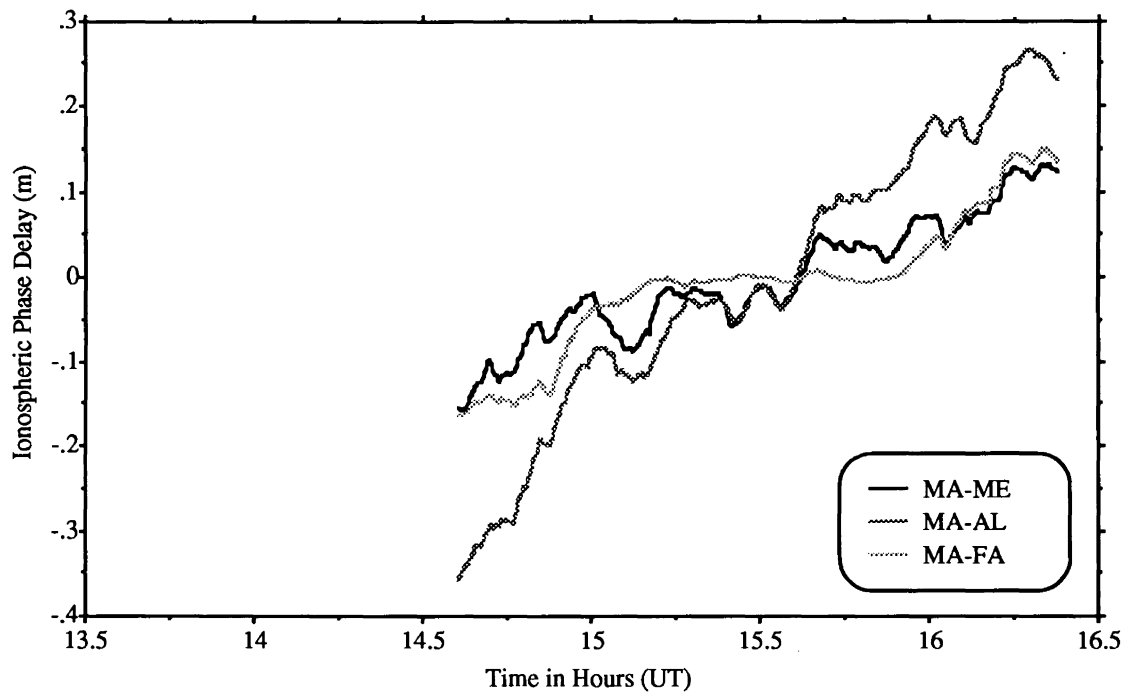
Single Differences of Ionospheric Phase Delay — SV 2



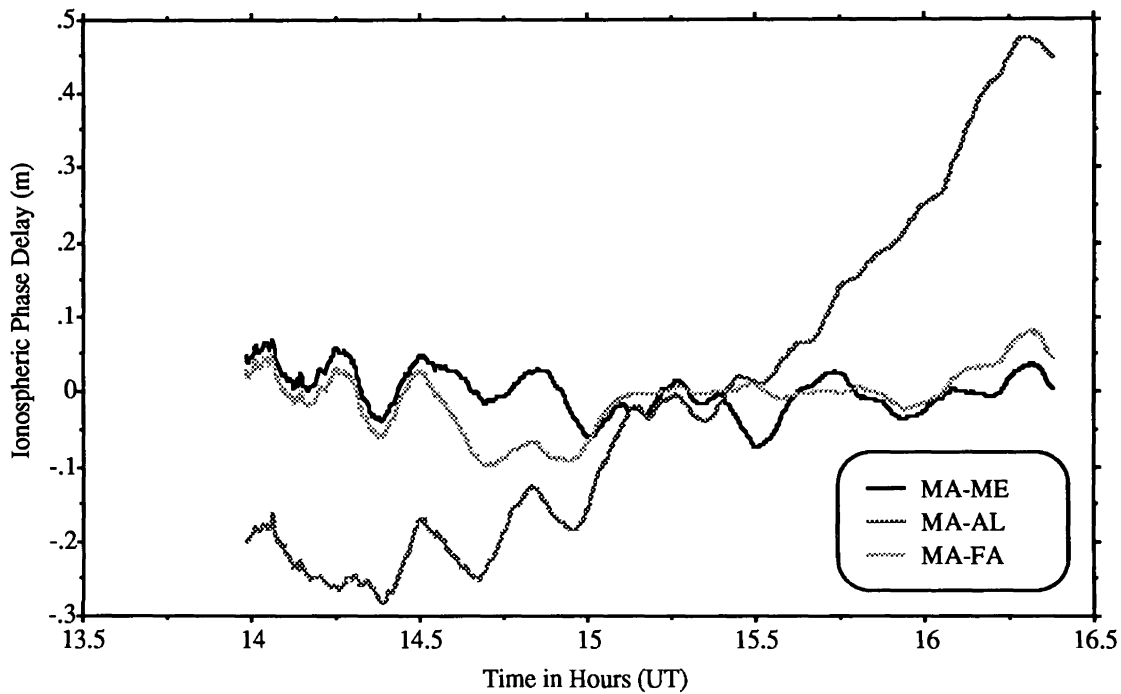
Single Differences of Ionospheric Phase Delay — SV 6



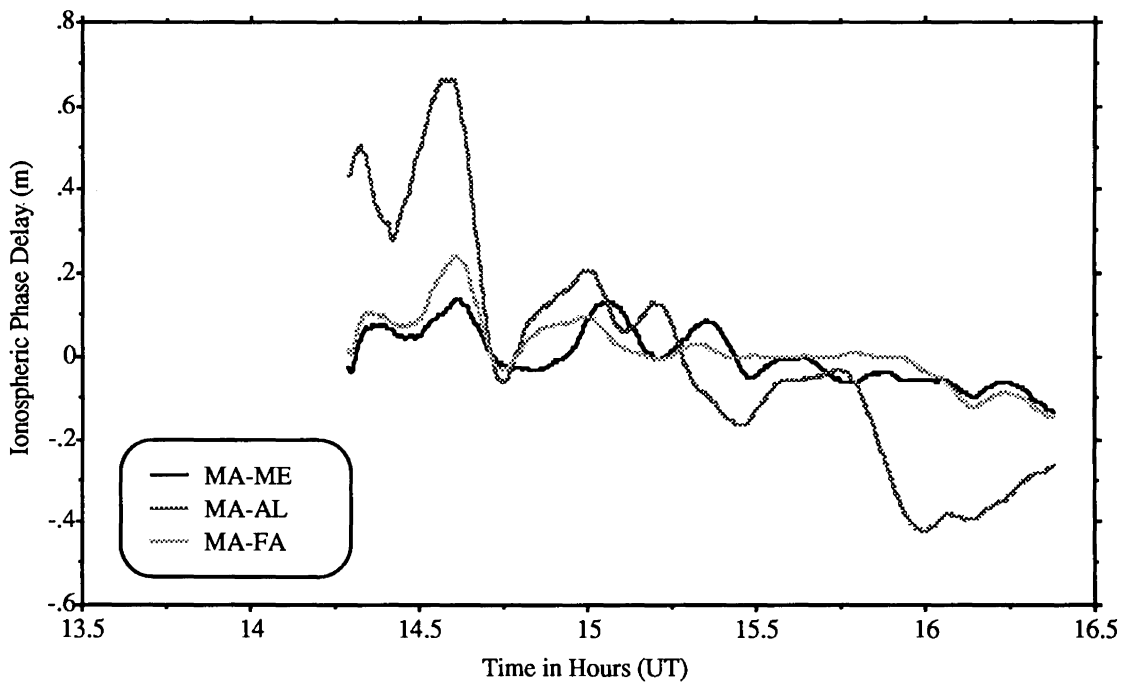
Single Differences of Ionospheric Phase Delay — SV 9



Single Differences of Ionospheric Phase Delay — SV 12



Single Differences of Ionospheric Phase Delay — SV 13

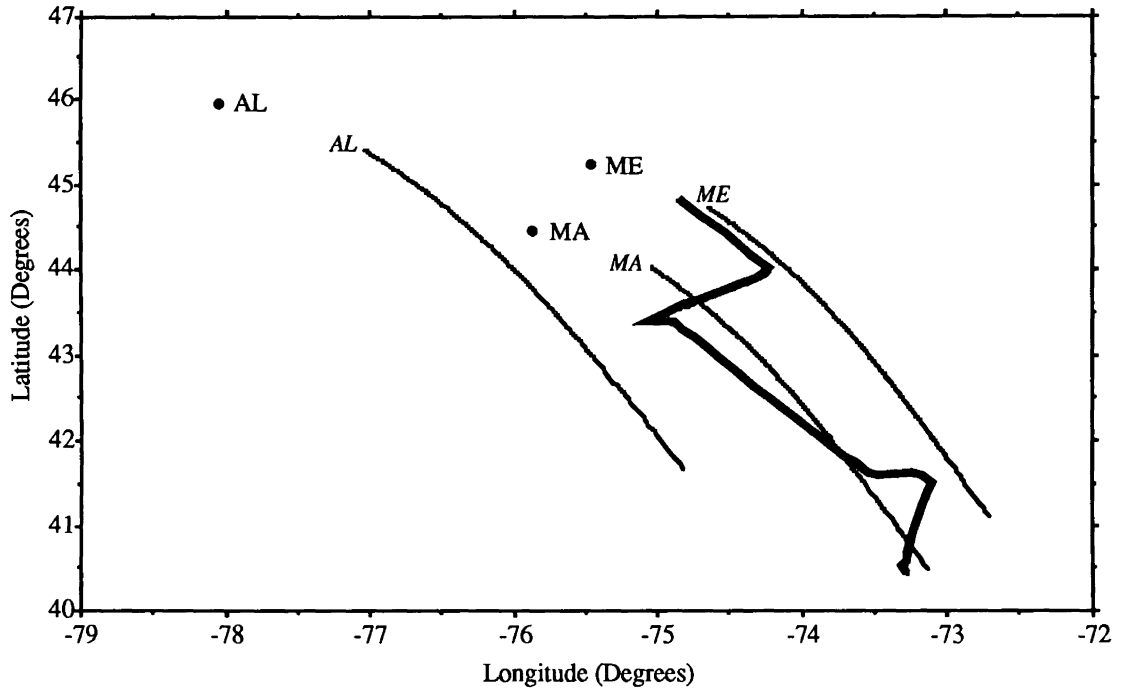


Single Differences of Ionospheric Phase Delay — SV 14

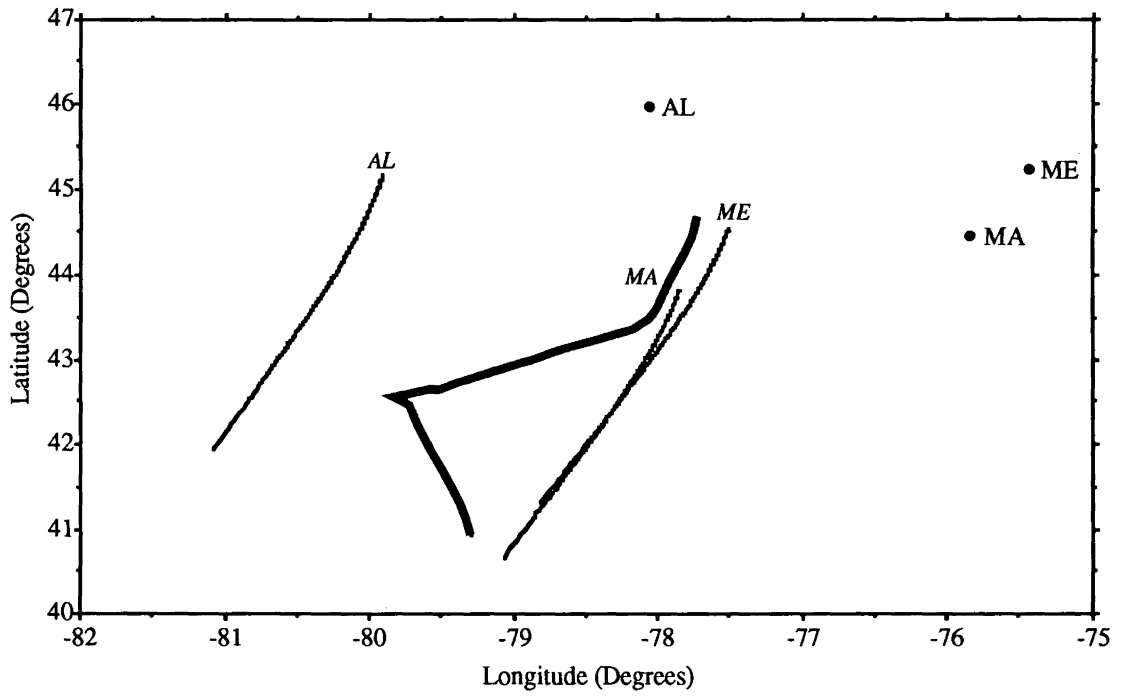
APPENDIX III

Plots of the Tracks of Sub-ionospheric Points for Each Satellite

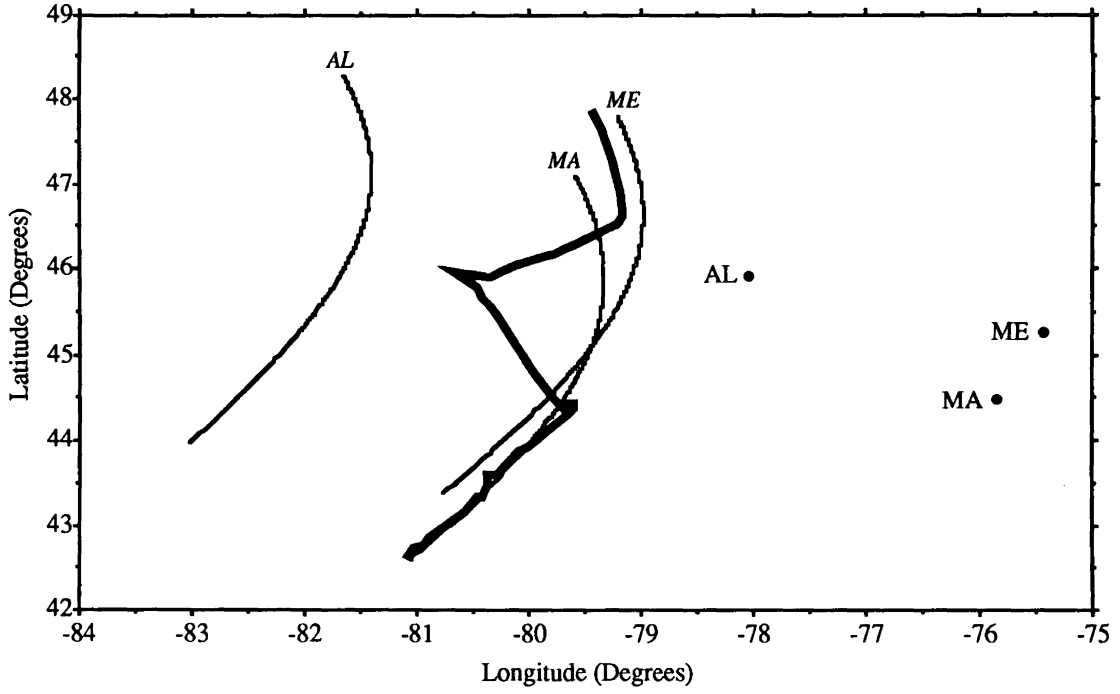
- Notes:
- 1) Longitude is reckoned positive east of Greenwich, negative west.
 - 2) The tracks for Falcon are in bold.
 - 3) The sub-ionospheric points for each station at initial lock-on are at the beginning of the tracks indicated by the station's name in italics.



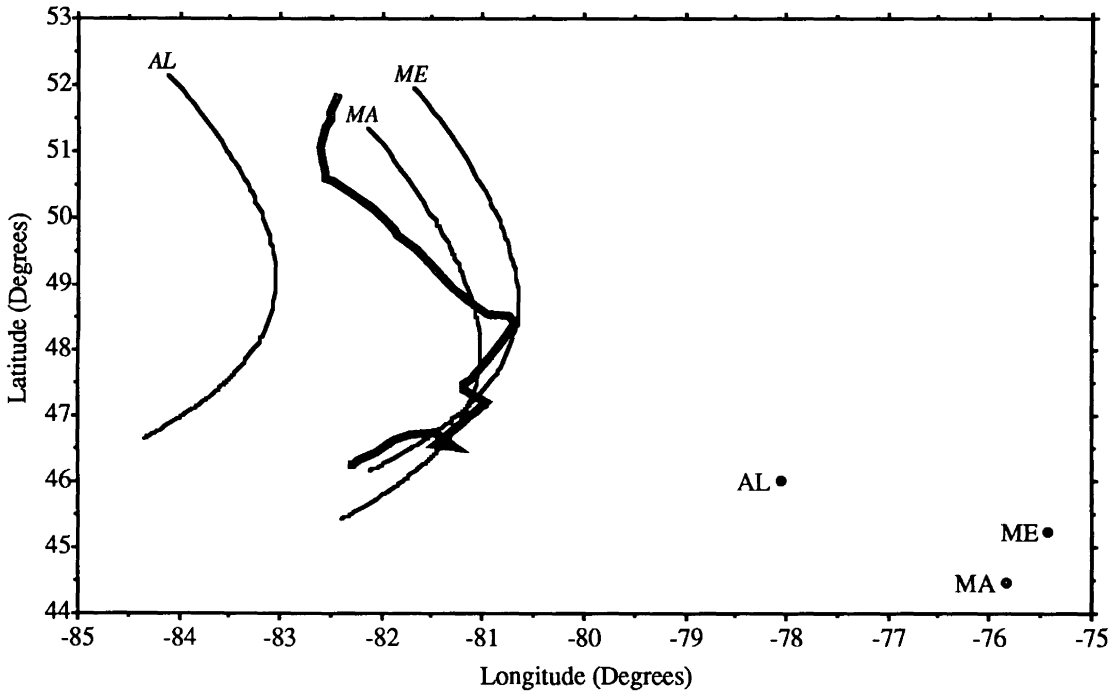
Tracks of Sub-ionospheric Points for SV 2



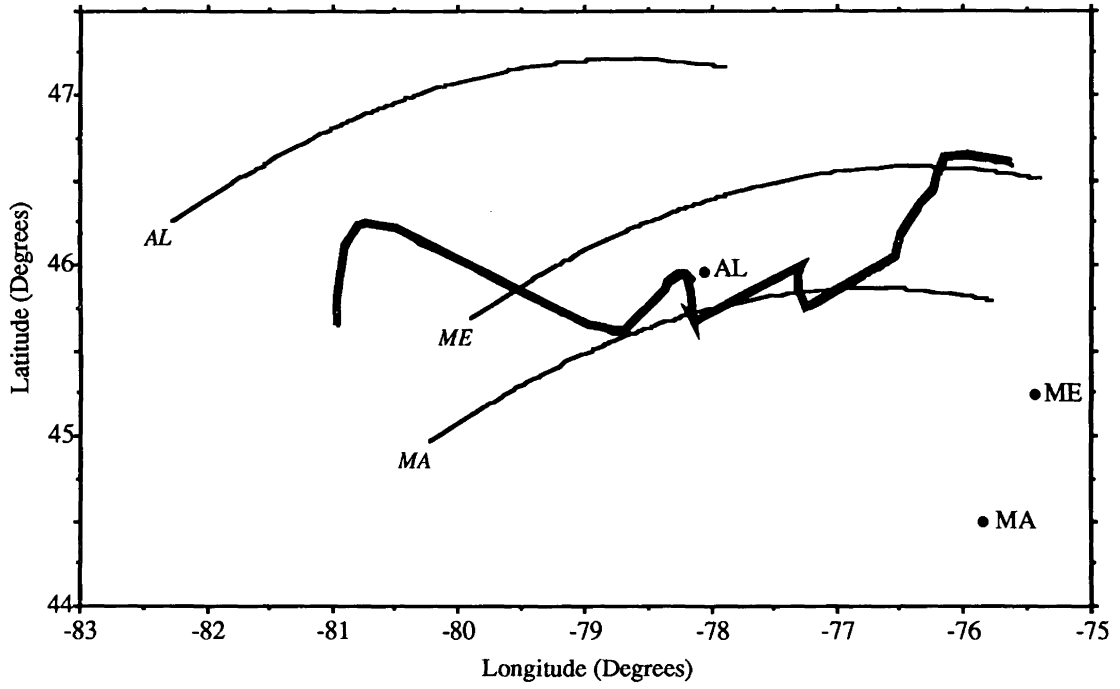
Tracks of Sub-ionospheric Points for SV 6



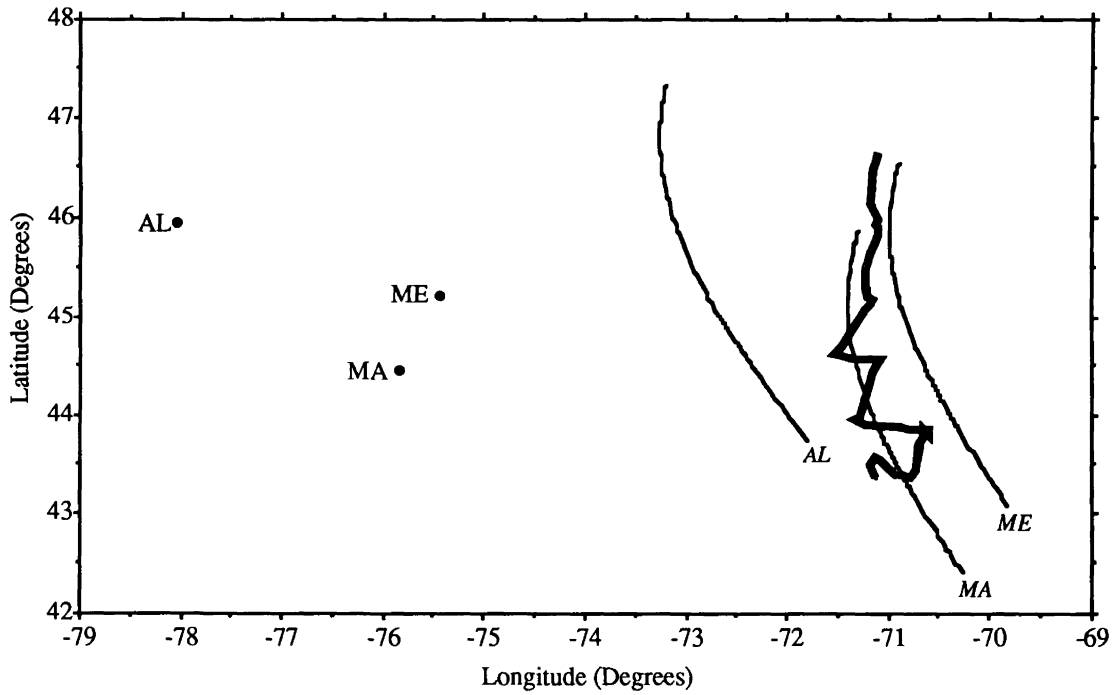
Tracks of Sub-ionospheric Points for SV 9



Tracks of Sub-ionospheric Points for SV 12



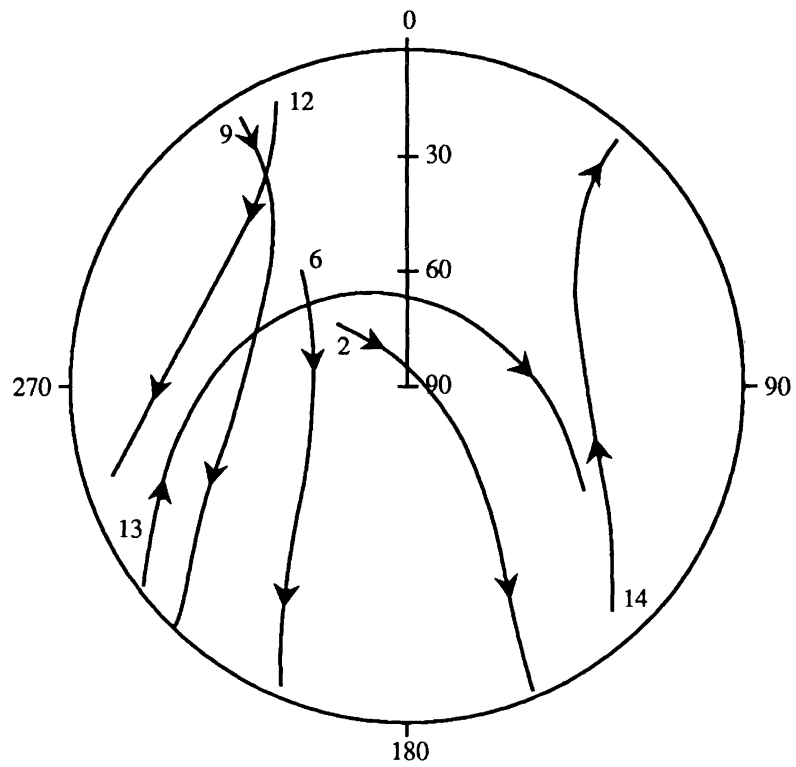
Tracks of Sub-ionospheric Points for SV 13



Tracks of Sub-ionospheric Points for SV 14

APPENDIX IV

Polar Plot of Satellite Visibility



Figures at the start of the satellite tracks are the SV numbers.

North is to the top and units in azimuth and elevation are degrees.

VITA

- Full Name** : Iain Robert Webster
- Place and Date of Birth** : Blairgowrie, Scotland, U.K. 22nd January 1967.
- Permanent Address** : 150 Claremont
Alloa
Central Region
SCOTLAND FK10 2EG
U.K.
- Schools Attended** : Dollar Academy
Dollar
Central Region
SCOTLAND
U.K.
- Universities Attended** : Department of Geography and Topographic Science
University of Glasgow
University Avenue
Glasgow
SCOTLAND G12 8QQ
U.K.
1985-1989, B.Sc (Hons) Topographic Science.

Publications

- Georgiadou, Y., I. Webster, A. El-Rabbany, and A. Kleusberg (1990). "Analysis of the 1989 Vancouver Island GPS survey data." Final contract report for the Pacific Geoscience Centre, Sidney, B.C., Canada, May.
- Webster, I. and A. Kleusberg (1992). "Regional Ionospheric Modelling for Single Frequency Users of the Global Positioning System." *Proceedings of the Sixth International Geodetic Symposium on Satellite Positioning*, Columbus, OH, U.S.A., 16-20 March, pp. 230 - 239.